

184-33535

NASA TECHNICAL MEMORANDUM

NASA TM- 77414

RESEARCH ON OXIDATION BY AIR AND TEMPERING  
OF RANEY NICKEL ELECTROCATALYSTS FOR THE H<sub>2</sub> ANODES OF  
ALKALI COMBUSTION MATERIALS CELLS :

H.-J. Selbach

Translation of "Untersuchungen zur Luftoxidation und  
Temperung von Raney-Nickel Elektrokatalysatoren für die  
H<sub>2</sub>-Anoden von Alkalischen Brennstoffzellen," Braunschweig,  
Technische Universitaet, Naturwissenschaftliche Fakultaet,  
Dissertation, 1982, pp. 1-152.

NATIONAL AERONAUTICS AND SPACE ADMINISTRATION  
WASHINGTON, D.C. 20546

AUGUST 1984

## STANDARD TITLE PAGE

1. Report No. NASA TM-77414	2. Government Accession No.	3. Recipient's Catalog No.	
4. Title and Subtitle RESEARCH ON OXIDATION BY AIR AND TEMPERING OF RANEY NICKEL ELECTROCATALYSTS FOR THE H <sub>2</sub> ANODES OF ALKALI COMBUSTION MATERIALS CELLS		5. Report Date August 1984	6. Performing Organization Code
7. Author(s) H.-J. Selbach		8. Performing Organization Report No.	10. Work Unit No.
9. Performing Organization Name and Address Leo Kanner Associates Redwood City California 94063		11. Contract or Grant No. NASW-3541	13. Type of Report and Period Covered Translation
12. Sponsoring Agency Name and Address National Aeronautics and Space Adminis- tration, Washington, D.C. 20546		14. Sponsoring Agency Code	
15. Supplementary Notes  Translation of "Untersuchungen zur Luftoxidation und Temperung von Raney-Nickel-Elektrokatalysatoren für die H <sub>2</sub> -Anoden von Alkalischen Brennstoffzellen," Braunschweig, Technische Universität, Naturwissenschaftliche Fakultät, Dissertation, 1982, pp. 1-152. (A83-18494)			
16. Abstract The controlled oxidation in air of Raney nickel electrocata- lysts was studied with special attention paid to the quan- titative analysis of nickel hydroxide. The content of the latter was determined through X-ray studies, thermogravi- metric measurements and spectral photometric examinations. The dependence of the content on drying of activated cata- lysts was determined. The effect of nickel hydroxide on electrochemical parameters of the catalysts, such as diffu- sion polarization, is studied, including a measurement of the exchange current density using the potential drop method. Conservation by oxidation in air with ancillary stabilization of the oxide in an H <sub>2</sub> flow at 300° C is explored, including reduction by H <sub>2</sub> , the influence of tem- pering time, and structural studies on conserved and stabilized catalyst. Long-term research with effect of aging and results of impedance measurements are presented.			
17. Key Words (Selected by Author(s))		18. Distribution Statement  Unclassified-Unlimited	
19. Security Classif. (of this report)  Unclassified	20. Security Classif. (of this page)  Unclassified	21. No. of Pages  101	22. Price



## Table of Contents

1.	Introduction and Subject	1
2.	Depyrophorization of NiTi <sub>2</sub> Catalysts through Air Oxidation	2
2.1.	Theoretical Considerations on the Course of Air Oxidation	2
2.2.	Equipment Arrangement	3
2.2.1.	Function of the Equipment for Oxidation and Practical Execution of Depyrophorization	4
2.3.	Determination of the Ni(OH) <sub>2</sub> Content	5
2.3.1.	X-Ray Studies of Raney Nickel Catalysts and their Products of Oxidation	5
2.3.2.	Thermogravimetical Measurements with Raney Nickel Preserved in Air	8
2.3.3.	Quantitative Analysis of the Nickel Content through Spectral-Photometric Studies	10
2.3.4.	Relationship of the alpha-Ni(OH) <sub>2</sub> Content and Drying of the Active Catalyst	12
2.4.	Effect of the alpha-Nickel Hydroxide on the Electrochemical Parameters of Raney NiTi <sub>2</sub> Catalysts	13
2.4.1.	Production and Principle Structure of Supported Raney NiTi <sub>2</sub> Electrodes	13
2.4.2.	Current-Voltage Characteristic	15
2.4.3.	Measurement of the Exchange Current Density According to the Method of Potential Jump	18
2.4.4.	Estimation of the Effect of Nickel Hydroxide on Diffusion Polarization	24
2.4.5.	Discussion	29
2.5.	Behavior During Continuous Operations	30
3.	Preservation through Air Oxidation with Subsequent Stabilization of the Oxide in a H <sub>2</sub> Flow at 300° C	31
3.1.	Mechanisms of Reduction through Hydrogen and Experimental Studies of this Phenomenon	32
3.2.	Effect of Tempering Time of the η-i Characteristics and the Exchange Current Density	34
3.3.	Structural Studies with Preserved and Stabilized Raney NiTi <sub>2</sub> Catalysts	41
3.3.1.	Effect of Tempering on the alpha-Ni(OH) <sub>2</sub> Content	41
3.3.2.	Electron-Grid Microscope Exposures of Preserved Raney NiTi <sub>2</sub> Powders	44

## Table of Contents - continued

3.3.3.	BET Surface and Pore Structure of Raney NiTi <sub>2</sub> Catalysts as a Function of Tempering Time	50
3.3.3.1.	Fundamental on the BET Measurements of Surface Determination, Experimental Arrangement and Measurement Results	50
3.3.3.2.	Determination of Pore Distribution	55
3.3.4.	Discussion	59
4.	Long-Term Experiments with Air-Preserved and Hydrogen-Reduced Raney NiTi <sub>2</sub> Catalysts	61
4.1.	Long-Term Behavior of Raney NiTi <sub>2</sub> Catalysts as a Function of Operating Temperature	62
4.2.	Effect of Tempering Time on Long-Term Stability	64
4.3.	Relationship of Aging Rate and Polarization	65
4.3.1.	Effect of Occupation Density of the Electrodes on the Long-Term Behavior of Raney NiTi <sub>2</sub> Catalysts	68
4.4.	Discussion	69
5.	Preservation of Raney NiTi <sub>2</sub> Catalysts by Air Oxidation with Subsequent Tempering in a Nitrogen Atmosphere at 300° C	70
5.1.	Execution of the Studies	70
5.2.	Measurement Results	71
5.3.	Discussion	73
6.	Measurements of Impedance	73
6.1.	Fundamentals of Impedance Measurements	73
6.2.	Equivalent Circuit Diagram for Porous Raney NiTi <sub>2</sub> Electrodes	74
6.2.1.	The Impedance of the Supported Gas Diffusion Electrode	75
6.2.2.	Local Curve Representation	78
6.3.	Equivalent Circuit Diagram for Raney NiTi <sub>2</sub> Electrodes without Hydrogen Diffusion	79
6.4.	Description of the Experiment	81
6.4.1.	Arrangement of the Measurement Equipment for Alternating Current Measurements	81
6.4.2.	Evaluating the Measurement Results	83
6.5.	Effect of Tempering Time on the Network Parameters of Raney NiTi <sub>2</sub> Electrodes	85

Table of Contents - continued

6.6.	Discussion	89
7.	Summary	90
References		93 - 96

## 1. Introduction and Subject

/1\*

The suggestion presented more than a decade ago for introducing hydrogen as a universal energy carrier [1,2] was recently reintroduced and discussed [3-6]. With this background, the hydrogen-oxygen combustion element also gained in interest for terrestrial applications. This development was accelerated by the introduction of more inexpensive, non-noble and highly active catalysts, for example by the Raney nickel proposed in 1954 by Justi, Scheibe and Winsel [7], a frequently applied electro-catalyst on the hydrogen side of the  $H_2$ - $O_2$  fuel cells. The manufacture of this catalyst is carried out by removing the aluminum portion from the  $Al_5O - Ni_5O$  alloy in 6 n KOH. In this case, a highly porous nickel foam with defective structure from the pulverized ( $< 30 \mu m$ ) Raney alloy, exhibiting high catalytic activity on the basis of the large specific surface. This activity may be increased through controlled air oxidation and tempering of the material previously dried in a vacuum [8-10]. Simultaneously, the catalyst loses the pyrophoric property in oxidation and through the  $Ni(OH)_2$  and  $NiO$  produced on the surface so that storage and processing are substantially facilitated. By the production of an alloy with transition elements, such as Fe, Mo and Ti, further increases in activity are possible [11-14]. A Raney NiTi alloy with a weight ratio of 50 % Al, 48 % Ni and 2 % Ti has proven extremely productive. Within the framework of this report, an attempt will be made to improve the activity further through suitable measures, especially the long-term behavior of this catalyst. For this purpose, two different procedures will be applied, both based on the fundamental idea of precisely controlling the ratio of the two oxidation products created mainly in the depyrophorization,  $Ni(OH)_2$  and  $NiO$ , relative to the non-oxidized portion. The first possibility is based on the variation in water content of the material dried in a vacuum before air oxidation such that different amounts of  $Ni(OH)_2$  are produced during the oxidation phase according to the degree of drying or water content of the catalyst.

/2

Alternatively, an attempt will be made to alter the  $NiO/Ni(OH)_2$  ratio through a stabilization process undertaken after oxidation. For this purpose, the material oxidized and pre-treated as indicated above is subjected to tempering in an hydrogen flow at approximately  $300^\circ C$ . It is possible to affect the oxidation products during subsequent treatment through thermal decomposition of the  $Ni(OH)_2$  and partial surface reduction of the  $NiO$  crystal. Subsequently, it is necessary to repeat the controlled oxidation in order to depyrophorize the material once again. For quantitative determination of the nickel oxides, thermo-gravimetric measurements are undertaken, accompanying these studies.

Recently, various measurement procedures with alternating

---

\* Numbers in the margin indicate pagination in the foreign text.

current have gained in significance for the study of electrode kinetics. In this case, an attempt is made to gain information on the individual reaction mechanisms through the pure electrical impedance and phase frequency characteristic. Difficulties resulted for porous electrodes because of the low frequency of up to  $10^{-3}$  Hz required for this purpose; however, the possibility of the application of impedance measurements for highly porous supported electrodes was presented by the improved function generator with a lower frequency limit of  $10^{-3}$  to  $10^{-4}$  Hz, recently introduced on the market. In a further section of this report, the alternating current behavior of the individual differently treated catalysts will therefore be discussed.

## 2. Depyrophorization of $\text{NiTi}_2$ Catalysts through Air Oxidation

/3

The Raney nickel catalyst is employed exclusively in the present work and consists of an alloy of 50 % by weight of aluminium, 48 % by weight of nickel and 2 % of titanium. The aluminium portion is removed in 6 n KOH at  $80^\circ\text{C}$  in 24 hours to a residual aluminium content of 3 % [15]. The highly porous Ni foam produced in this manner is dried in a low vacuum after rinsing in distilled water. The dried catalyst powder is very pyrophorous and therefore not stable in air. With an uncontrolled addition of oxygen in air, the material suddenly burns almost completely such that it is useless for an application in fuel cells.

In various reports, several authors have described procedures for depyrophorizing Raney nickel, both through chemical and electrochemical oxidation, i.e. for preventing the addition of oxygen through special methods of conservation [8-11, 16-20]. The procedure described in the following for controlled air oxidation is based on reports by Wendtland, Jung and von Sturm et al. [8-10].

### 2.1. Theoretical Considerations on the Course of Air Oxidation

The removal of the aluminium contained in the Raney nickel is carried out with the volatile hydrogen. In this process, hydrogen is adsorbed at the nickel surface such that the surface exhibits a high coating of hydrogen after drying the catalyst. On the basis of the large catalytic activity of nickel, the adsorbed hydrogen is immediately oxidized with the addition of oxygen, first forming a film of water on the nickel surface. As a result of oxygen diffusion through the water film or its desorption through the heat of reaction, portion of the Ni surface are also oxidized to  $\text{NiO}$  in a further step or to  $\text{Ni(OH)}_2$  in the presence of  $\text{H}_2\text{O}$ . The kinetics of nickel oxidation are clearly dependent on the water film produced, as proven by brief suctioning of the reaction chamber and the accompanying desorption of  $\text{H}_2\text{O}$  [21]. In the subsequent reintroduction of air, the material reacts more vigorously. A situation critical for oxidation may occur, if the powder is heated locally in the case

/4

of excess oxygen such that the water suddenly evaporates at this location and the oxidation of nickel now proceeds very rapidly, leading to greater local heating and therefore to further desorption of the water. In this stage, it is almost no longer possible to stop this process similar to a chain reaction (for example through rapid evacuation of the reaction chamber), so the powder almost completely burns to non-reducible nickel oxides and therefore becomes useless.

It has proven advantageous for the depyrophorization of nickel with oxygen from the air to run the major portion of oxidation at a pressure around 25 mbar. In this case, slight amounts of the atmosphere with less oxygen are suctioned continuously at one side of the reaction chamber and the addition of fresh air is controlled simultaneously such that the desired pressure is established so that the nitrogen-oxygen ratio may be maintained almost constant and the oxygen diffusion is not subject to any uncontrolled changes because of the nitrogen atmosphere.

The lower limit of the pressure results from the requirement that it may not fall below the vapor pressure of water at room temperature so that the water film created in the oxidation does not evaporate immediately; the value of 25 mbar is still clearly removed from this limit. On the other hand, the pressure is so slight that even with a volume in the reaction chamber of about 0.5-1 liter, the entire volume of oxygen remains limited to a few  $\text{N cm}^3$ . Very precise regulation is therefore possible.

/5

## 2.2. Equipment Arrangement

The solution for the problems described in section 2.1. in the case of air oxidation requires continuous control of the powder temperature during oxidation as well as the addition of air into the reaction chamber controlled by the pressure, and, additionally, the possibility of rapid automatic evacuation of the chamber when a preselected powder temperature is exceeded.

Fig. 1 presents a diagram of the arrangement of the equipment, taking these requirements into consideration. The reaction chamber consists of a quartz tube, connected to the vacuum pump at one side through a ground glass plug via the two valves in a parallel circuit (magnetic valve 1 and needle valve 1). A NiCr-Ni thermoelement is guided through the glass plug with a vacuum seal for measuring temperature, thereby controlling the magnetic valves 1 and 2 without depending on temperature via a temperature measurement device with a 220 V circuit output (type: Ruhstat). The air may be added in doses through the needle valve 2 when the magnetic valve 2 is open. A U-shaped pipe manometer is connected between the inlet valves and the reaction chamber for measuring pressure, equipped with 2 contacts for regulation.

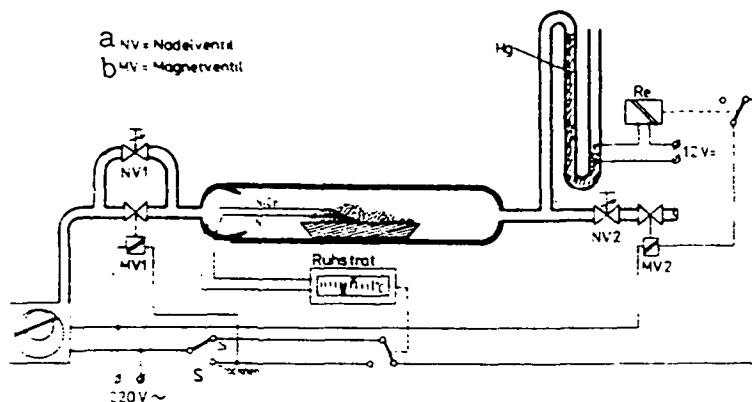


Fig. 1: Diagram of the Equipment for Controlled Air Oxidation of Raney Nickel Catalysts.

Key: a. needle valve  
b. magnetic valve

#### 2.2.1. Function of the Equipment for Oxidation and Practical Execution of Depyrophorization

The activated catalyst rinsed free of alkalis is introduced into the reaction chamber while still moist in a copper shuttle such that good heat contact to the thermal element is insured. After conclusion of the drying process in the vacuum, the maximum permissible temperature is preselected at the temperature measurement device and switch S is put in position for oxidation. Now air flows over the magnetic valve 2 and the needle valve 2 into the reaction chamber until the pressure of 25 mbar, determined by the two contacts at the U shaped pipe manometer, has been achieved and the magnetic valve 2 is closed. Since the pressure is slowly reduced via the needle valve 1, the magnetic valve 2 is reopened (after a period of time dependent on the setting of the needle valve). Through suitable precision adjustment of the two needle valves, it is possible in this manner to maintain a constant pressure in the reaction chamber at about  $\pm 0.5$  mbar and simultaneously to supplement the oxygen absorbed by the catalyst through fresh air so that the nitrogen cushion is never too large, interrupting further oxidation. When the maximum permissible temperature of approximately 60°C is exceeded, the reaction chamber is evacuated by magnetic valve 1, such that further oxidation of the powder is interrupted until the permissible temperature is again achieved. The entire process now begins again as described. The oxidation continues in this manner for several hours near the upper temperature limit. A reduction in powder temperature to room temperature is a sign that the oxidation is almost completed. The catalyst may now be slowly returned to a normal air atmosphere, although the

nickel in this stage still adsorbs considerable amounts of oxygen, but the heating effect is negligible. Thereafter, the oxidized material is inactive and may be stored with no problem or further processed to fuel cell electrodes.

### 2.3. Determination of the $\text{Ni}(\text{OH})_2$ Content

Since the air-oxidized nickel powder is not active as a catalyst, it must be reactivated before application as electrode catalyst, i.e. the oxides produced on the nickel surface must be reduced at least partially. For this purpose, the catalyst is retained in the customary electrode mounting (see section 2.4.1.) for approximately 10 hours in KOH at a temperature of  $80^\circ \text{C}$  at a hydrogen pressure of 1 bar. The catalyst then exhibits a considerably increased activity with respect to the non-oxidized material. It may be considered certain that the non-reduced  $\text{Ni}(\text{OH})_2$  and NiO are responsible for this result [15]. It is desirable for a more precise evaluation of this material to know the quantitative portion of the  $\text{Ni}(\text{OH})_2$  of the total amount of catalyst. The portion of  $\text{Ni}(\text{OH})_2$  may be calculated via the weight loss of the catalyst as a result of the thermal decomposition of the nickel hydroxide at temperatures above  $160^\circ \text{C}$  to NiO and water, if it is known to what extent the amount of water of crystallization must be taken into consideration. Nickel hydroxide may occur in two differing modifications:

- 1) as water-free stoichiometric  $\beta\text{-Ni}(\text{OH})_2$  and
- 2) as the  $\alpha\text{-3Ni}(\text{OH})_2 \cdot 2\text{H}_2\text{O}$  containing water of crystallization [22,23].

According to reports by Heuer [24],  $\alpha\text{-3Ni}(\text{OH})_2 \cdot 2\text{H}_2\text{O}$  is produced in the electrochemical oxidation of Raney nickel in an alkaline electrolyte. It must therefore be investigated whether the  $\alpha$  modification containing water or the  $\beta\text{-Ni}(\text{OH})_2$  is also produced in the controlled air oxidation of the Raney NiTi2.

#### 2.3.1. X-Ray Studies of Raney Nickel Catalysts and their Products of Oxidation

In order to determine which modification of the  $\text{Ni}(\text{OH})_2$  is present in the air-oxidized Raney nickel, various catalyst samples were examined in x-ray equipment (Philips PW 1010) with counting tube-interference Goniometer (Philips PW 1380) including a monochromator (AMR type: GVW 7190) according to the Debye-Scherrer procedure. Moreover, exposures of pure NiO, pure  $\beta\text{-Ni}(\text{OH})_2$  as well as electrolytically precipitated  $\alpha\text{-3Ni}(\text{OH})_2 \cdot 2\text{H}_2\text{O}$  powder were produced. The most important results of these measurements are presented in Figs. 2 and 3.

The upper curve in Fig. 2 shows the x-ray exposure of a Raney nickel Ti<sub>2</sub> sample, oxidized before measurements in 6n KOH at  $80^\circ \text{C}$  for 10 hours at 400 mV against hydrogen. The reflexes of the cubic central surface of nickel and that of the hexagonal



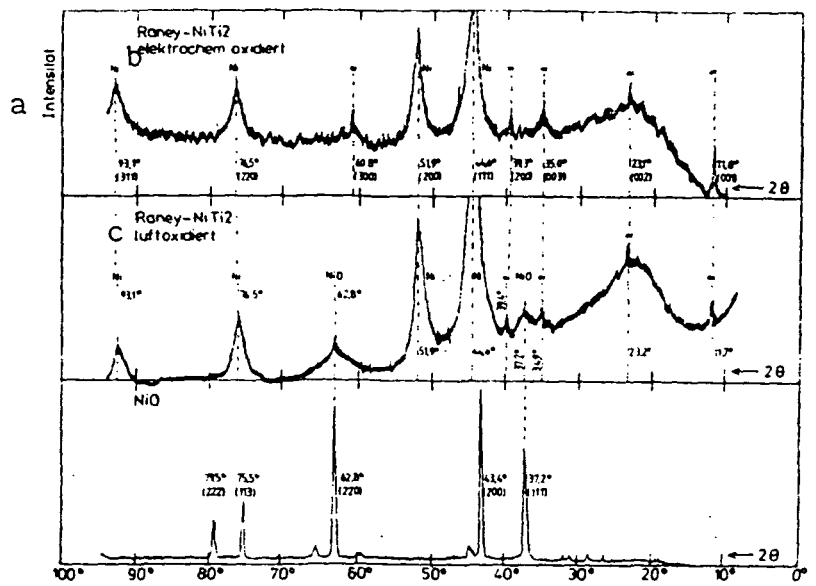


Fig. 2: X-Ray Spectra of Electrochemically (top) and Air-Oxidized (middle) Raney NiTi<sub>2</sub>, as well as Pure Nickel Oxide (bottom).

Key: a. intensity      b. electrochemically oxidized  
c. air-oxidized

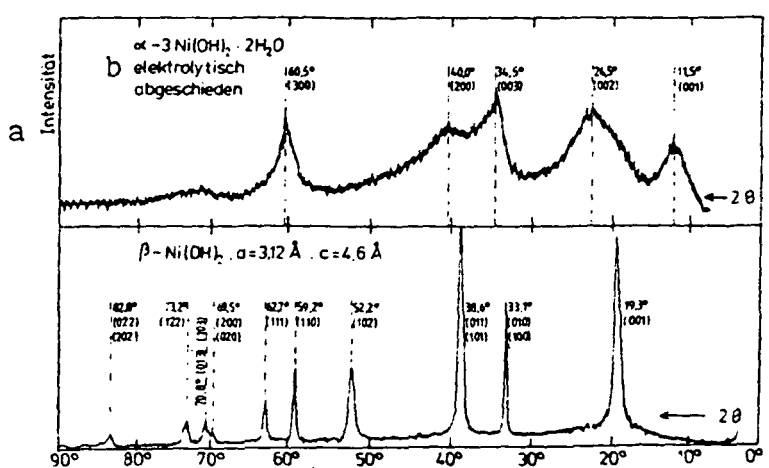


Fig. 3: X-Ray Spectra of α-3Ni(OH)<sub>2</sub> · 2 H<sub>2</sub>O (top) and Pure β-Ni(OH)<sub>2</sub> (bottom) Precipitated Electrolytically from Nickel Nitrate.

Key: a. intensity      b. precipitated electrolytically

$\alpha$ - $3\text{Ni}(\text{OH})_2 \cdot 2\text{H}_2\text{O}$  can be clearly recognized. From the (00 $l$ ) peaks ( $l = 1-4$ ) of the hydroxide, calculations according to the reflection condition for hexagonal crystal grids:

$$\sin^2 \theta = \frac{\lambda^2}{4a^2} \frac{4}{3} (h^2 + k^2 + hk) + \frac{a^2}{c^2} l^2, \quad \lambda = 1.54 \text{ \AA}$$

result in a grid constant  $c_0$  at 7.7 Å and from the reflex (hk0) the grid constant  $a$  at 5.3 Å. Since these values are in agreement with those found in the literature, this exposure was employed as a comparison measurement for further measurements with Raney nickel powders. For confirmation, an exposure of  $\alpha$ - $\text{Ni}(\text{OH})_2$  precipitated electrolytically from a nickel nitrate solution with a flow density of 1 mA/cm<sup>2</sup> may be employed (top curve in Fig. 3). The angles of the reflexes are almost identical to those of the  $\text{Ni}(\text{OH})_2$  generated electrochemically, although they are not as prominent. This may be attributed mainly to the formation of the  $\text{Ni}(\text{OH})_2$  crystals at room temperature. The central diagram of Fig. 2 presents the x-ray exposure of air-oxidized catalyst powder. The first three (00 $l$ ) reflexes and the (200) peak clearly demonstrate the presence of  $\alpha$ -nickel hydroxide in agreement with the upper diagram. Only the two reflexes at  $2\theta = 37.2^\circ$  and  $2\theta = 63.1^\circ$  cannot be correlated to  $\alpha$ - $\text{Ni}(\text{OH})_2$ . It is very probable that these are peaks of the  $\text{NiO}$  also produced in air oxidation. The lower curve in Fig. 2 confirms this assumption. The reflexes not indicated in the hexagonal grid of the  $\alpha$ - $\text{Ni}(\text{OH})_2$  are situated exactly at the angular values of the (111) and (220) peaks of  $\text{NiO}$  of great intensity, produced by annealing (approximately 1200° C) of nickel hydroxide powder in air [70]. These two reflexes of the  $\text{NiO}$  are also the only ones expected in a Raney nickel sample. The other maxima are either covered by the (111) and (220) peaks of nickel or their intensity is at least one order of magnitude smaller than those of the first reflexes. Furthermore, exposures of pure  $\beta$ - $\text{Ni}(\text{OH})_2$  powder were produced with the results presented in the lower curve of Fig. 3. It can be seen that none of the reflexes of the  $\beta$ -hydroxide may be identified with those of the air-oxidized Raney nickel.

It can therefore be concluded that in the air oxidation of Raney nickel in addition to the  $\text{NiO}$  as hydroxide only the  $\alpha$  modification  $3\text{Ni}(\text{OH})_2 \cdot 2\text{H}_2\text{O}$  is produced. Therefore, the weight loss of the sample because of cleavage in the water of crystallization must also be considered in thermogravimetical measurements for the quantitative determination of the  $\text{Ni}(\text{OH})_2$  contents, insofar as this process may not be separated from the decomposition of the  $\text{Ni}(\text{OH})_2$  by various temperature intervals. Fig. 4 demonstrates that this separation is not possible; it shows the results of a differential thermal analysis of air-oxidized Raney nickel. The dotted curve represents the zero line, recorded with an inert powder as reference. Endothermal reactions in the material examined cause deviations from the zero line to the negative values, exothermal reactions to positive

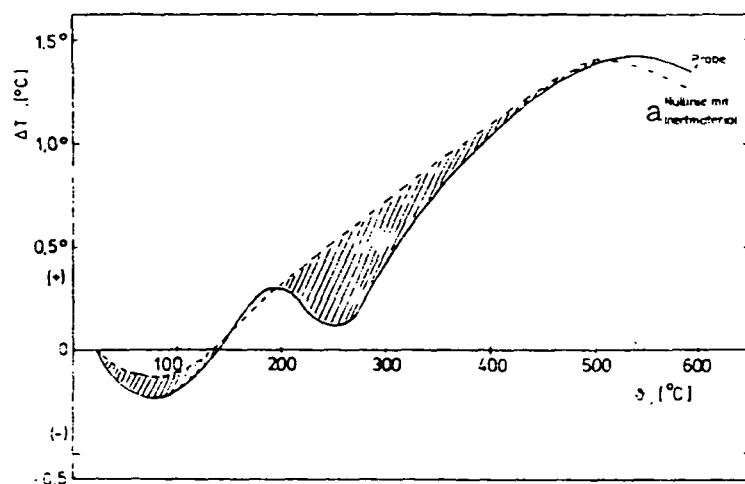


Fig. 4: Differential Thermal Analysis of 140 mg Air-Oxidized Raney NiTi<sub>2</sub>. Solid Line: Measurement Curve of the Sample. Dotted Line: Zero Line, Measured with Inert Material (NiO). Rate of Heating: 10 K/sec.

Key: zero line with inert material

$\Delta T$  values. It can be seen in Fig. 4 that only two endothermal reactions occur up to temperatures of 600° C, probably attributable to the production of water and the decomposition of the hydroxide is noticeable after approximately 200° C. It may be concluded that both the cleavage of the water of crystallization and the decomposition of Ni(OH)<sub>2</sub> occur in the same temperature interval. Therefore, no conversion of  $\alpha$ -3Ni(OH)<sub>2</sub> · 2 H<sub>2</sub>O into  $\beta$ -Ni(OH)<sub>2</sub> + 2/3 H<sub>2</sub>O↑ occurs preceding the decomposition of the hydroxide.

/12

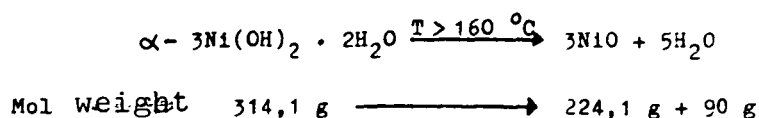
### 2.3.2. Thermogravimetric Measurements with Raney Nickel Preserved in Air

/13

The measurements for determination of the Ni(OH)<sub>2</sub> contents were carried out with the aid of an adsorptiongravimate of the Sartorius company, employed as thermal scale in the studies. Fig. 5 provides a diagram of the equipment employed for the measurements.

The sample to be examined was introduced into one of the two sides of the scale and dried in a vacuum up to 125° C until the weight remained constant. The temperature was then increased to 350° C and the loss in weight attributed to the thermal decomposition of the hydroxide [25] measured in accordance with:

/14



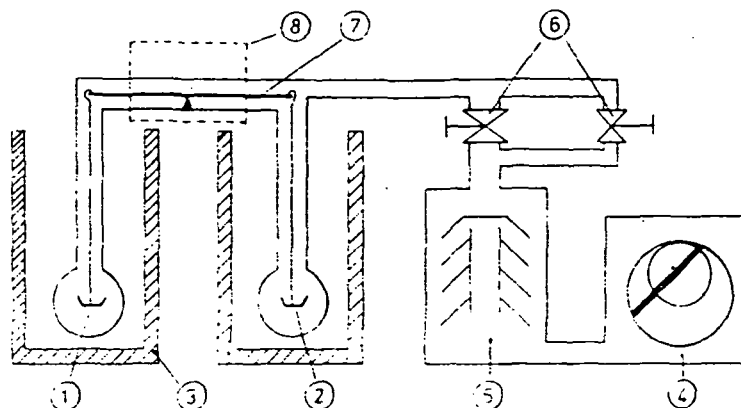


Fig. 5: Diagram of the Components of the Adsorption-gravimetric Employed for Determination of Hydroxide. 1) Balance Side for Counterweight; 2) Balance Side for the Sample; 3) Heater; 4) Preliminary Pump; 5) Oil Diffusion Pump; 6) Valves; 7) Scale Beam; 8) Electronic Measurement Value Pick-up for Weight Measurement.

Fig. 6 shows the typical weight development of an air-oxidized Raney NiTi<sub>2</sub> sample over time.

Curve a shows the behavior for non-reactivated material, curve b in contrast the same material after reactivation for 10 hours under a hydrogen pressure (1 bar) in 6 n KOH at 80° C. The change in weight is indicated in mg in relation to 1 g of catalyst material, previously having the absorbed water removed at 125° C. It can clearly be seen that approximately half of the nickel hydroxide produced in oxidation is again reduced during reactivation of the catalyst. The portion p of the nickel hydroxide in the entire amount of catalyst material is calculated, taking into consideration the water of crystallization, according to

$$p [\%] = \frac{M_1 \cdot m_2 \cdot 100 \cdot 3}{m_1 \cdot M_2 \cdot 5} = \frac{60 \cdot M_1 \cdot m_2}{M_2 \cdot m_1}$$

where

$M_1$  = weight loss through H<sub>2</sub>O in mg  
 $m_1$  = mol weight of the water = 18 g  
 $m_2$  = mol weight of nickel = 58.7 g  
 $M_2$  = total amount of nickel in mg.

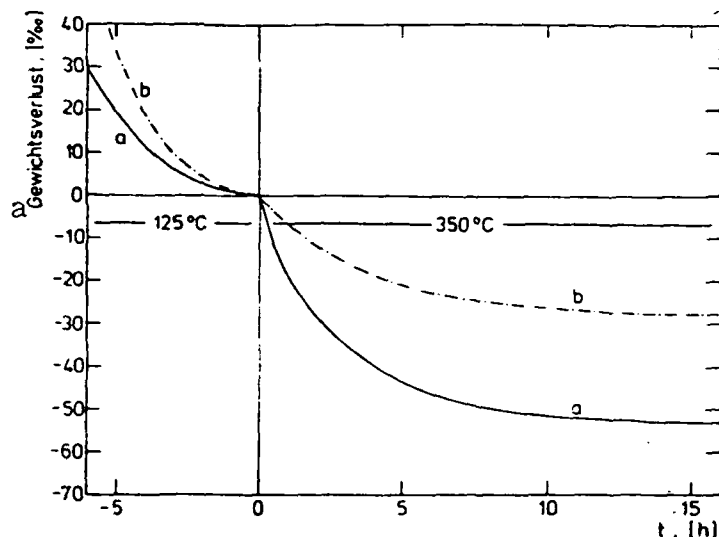


Fig. 6: Weight Loss of a Raney  $\text{NiTi}_2$  Sample through Reduction of Moisture at  $125^\circ\text{C}$  and Decomposition of the Hydroxide at  $350^\circ\text{C}$  over Time.

Curve a: Non-Reactivated Material,  
Curve b: Material Reactivated under Hydrogen Pressure in 6n KOH at  $80^\circ\text{C}$ .

Key: a. weight loss

The weight  $M_2$  of the nickel available in the sample may not be read directly from the thermogravimetical measurements, since the final weight at  $350^\circ\text{C}$  does not represent that of nickel, but a mixture of Ni, NiO and the alloy with titanium. In principle it would be possible to reduce the nickel oxide present to nickel with further increases in temperature (maximum possible temperature of the adsorptiongravimate about  $600^\circ\text{C}$ ) with hydrogen atmosphere, and thereby to calculate  $M_2$ , taking into consideration the titanium portion, but another procedure was selected for determining the nickel content for reasons of safety and greater accuracy.

### 2.3.3. Quantitative Analysis of the Nickel Content through Spectral-Photometric Studies

A linear relationship exists between the ion concentration of an element in a solvent and the light permeability in the spectrum of the solution down to transmission values of approximately 20 % [26]. This relationship is utilized to determine the concentration of an element in a solution. By applying monochromatic light of a suitable wave length, high selectivity is achieved for the element to be determined. The measurements of the nickel content were carried out with a Beckmann

spectral photometer (type B). The most advantageous wave length was determined for the transmission measurements in an preliminary experiment. For this purpose, a piece of nickel wire (356 mg) was dissolved in 100 ml of a 43 %  $H_2SO_4$  and the transmission of the solution measured as a function of wave length. Pure 43 %  $H_2SO_4$  was employed as reference liquid with a light permeability set at 100 % over the entire spectral range. The transmission spectrum of the nickel solution is presented in Fig. 7. The greatest adsorption corresponding to a transmission of 48 % is demonstrated by the curve at a wave length of 392 nm. Therefore, this value was selected for all further measurements. Interfering effects of titanium are not expected in this range, since the adsorption maximum of pure titanium ion solution is situated at approximately 500 nm and the concentration ratio between nickel and titanium ions amounts 25:1 in the Raney  $NiTi_2$  catalysts to be examined.

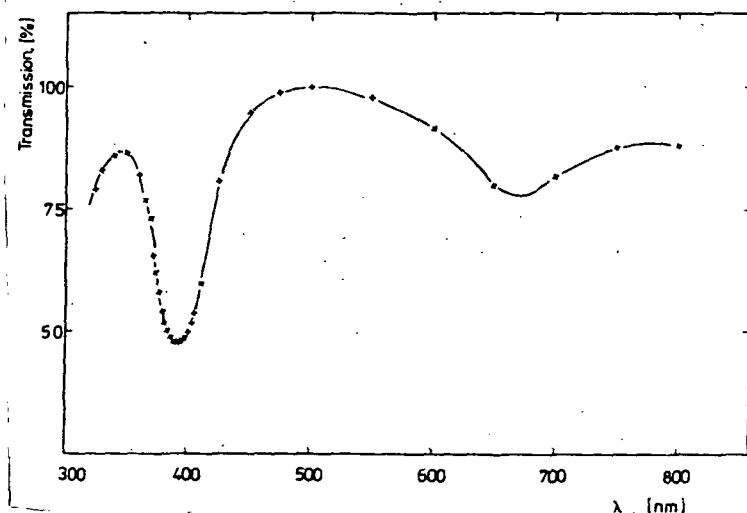


Fig. 7: Transmission Spectrum of a Solution of 100 ml 43 %  $H_2SO_4$  and 356 mg Ni. Reference: 43 %  $H_2SO_4$ .

A calibration curve (Fig. 8) was prepared for further measurements with several solutions of known nickel ion concentrations. The nickel content is related in each case to 50 ml of a 43 %  $H_2SO_4$  solution, while distilled water served as reference. Under this prerequisite, the regression line results for the determination of the nickel content  $M$  [mg] as a function of the transmission  $y$  [%]:

$$M \text{ [mg]} = \frac{89.8 - y \text{ [%]}}{0.2382}$$

It was only possible to determine the nickel portion of the catalysts samples easily with this curve (Fig. 8) by dissolving

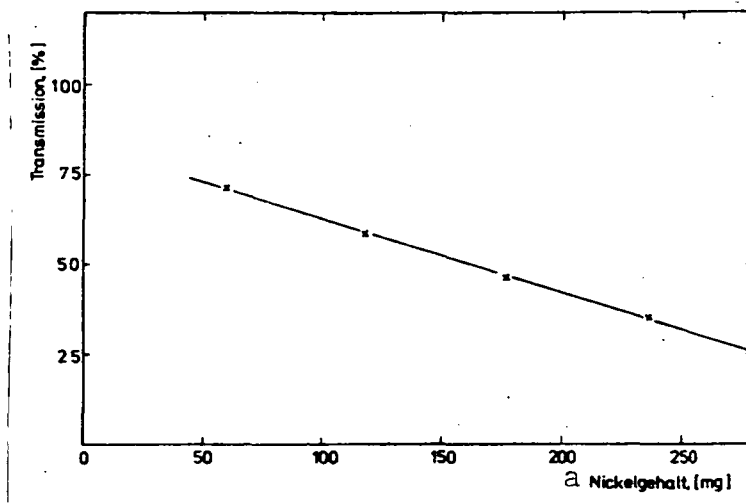


Fig. 8: Transmission of 43 %  $\text{H}_2\text{SO}_4$  as a Function of Nickel Contents at 392 nm with Distilled Water as Reference.

Key: a. nickel contents

the sample in a 50 ml 43 %  $\text{H}_2\text{SO}_4$  solution after each thermogravimetical measurement and by measuring the transmission of the solution in comparison to distilled water.

#### 2.3.4. Relationship of the $\alpha$ - $\text{Ni}(\text{OH})_2$ Content and Drying of the Active Catalyst

The  $\text{NiTi}_2$  catalyst dissolved in  $\text{KOH}$  at  $80^\circ \text{C}$  must be rinsed free of alkalis before the oxidation in air and dried in a vacuum. An attempt should be made through the degree of drying to influence the amount of the  $\alpha$ - $\text{Ni}(\text{OH})_2$  formed in this manner. Samples were dried in a vacuum for varying amounts of time before the air oxidation for this purpose. After subsequent depyrophorization, the nickel hydroxide contents of the samples were determined, partially in the depyrophorized state and after reactivation over 10 hours under hydrogen pressure (0.8 bar) in 6n  $\text{KOH}$  at  $80^\circ \text{C}$ . The results are presented in Table 2.1.

It can be seen that there is no clear relationship between the degree of drying and the yield of  $\alpha$ - $\text{Ni}(\text{OH})_2$ . There were different contents of hydroxide, but it is not possible to discover a logical correlation between the two parameters. It can therefore be concluded that the degree of drying of the powder is not the sole determinant quantity for the production of the hydroxide, but rather it appears to depend mainly on the manner of carrying out the air oxidation, especially the number of times the air had to be removed from the reaction chamber during oxidation as a result of increased temperature of the powder. In

Table 2.1.

/19

a Probe	b Trocknungszeit	c $\alpha$ -3Ni(OH) <sub>2</sub> Gehalt	d $\alpha$ -3Ni(OH) <sub>2</sub> nach Aktivierung
1	6 h	-	2,9 %
2	8 h	-	3,3 %
3	10 h	10 %	5,7 %
4	11 h	9,2 %	3,2 %
5	15 h	15,4 %	3,5 %
6	16 h	-	5,1 %
7	20 h	-	17 %
8	24 h	-	9,1 %
9	*	9,4 %	4,5 %

\* Sample was dried, until it has achieved room temperature again (about 15 hours).

Key: a. sample  
b. drying time  
c. content  
d. after activation

this case, moisture is then also withdrawn in an uncontrolled manner, especially the water film produced on the surface of the powder. It can be seen that statistically different amounts of  $\alpha$ -Ni(OH)<sub>2</sub> are produced through these processes, but attempts to produce electrodes with previously determined amounts of hydroxide with the available means are certain to fail. This difficulty is not important for further studies, however, because it is only important to have sufficient catalyst samples available with differing amounts of hydroxide in order to study the effect of the  $\alpha$ -3Ni(OH)<sub>2</sub> · 2 H<sub>2</sub>O on the electrical characteristics of the electrodes.

#### 2.4. Effect of the $\alpha$ -Nickel Hydroxide on the Electrochemical Parameters of Raney NiTi<sub>2</sub> Catalysts

/20

##### 2.4.1. Production and Principle Structure of Supported Raney NiTi<sub>2</sub> Electrodes

The best utilization of catalyst performance has been achieved up to now through the application of supported electrodes in fuel cells. The following electrochemical experiments with Raney NiTi<sub>2</sub> catalysts were therefore carried out exclusively with half cells of supported electrodes with a design based on a construction by v. Sturm, Weidlich and Nischik [27]. Fig. 9 shows the design in principle for this measurement cell.

The asbestos diaphragm is supported by a punctured sheet covered by a fine nickel net on the electrolyte side. The catalyst deposited on the diaphragm before construction of the

/21



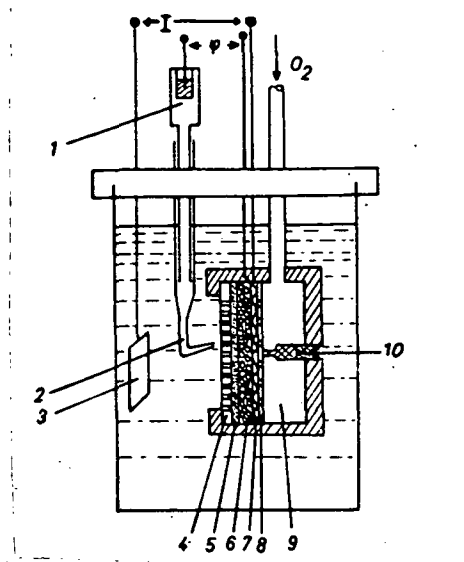


Fig. 9: Half Cell Arrangement for Supported Electrodes.

- 1) reference electrode (Hg/HgO)
- 2) Luggin capillary
- 3) opposite electrode
- 4) sheet with holes
- 5) asbestos diaphragm
- 6) catalyst powder
- 7) nickel net
- 8) pressure plate
- 9) gas chamber
- 10) setscrew.

measurement cell is pressed against the asbestos paper from the gas chamber via a further nickel net and the pressure plate. The pressure plate has two contact wires leading to the outside and gas tight for the power supply and measurement of potential. The gas for reaction is supplied to the catalyst from the back through the gas chamber via holes in the pressure plate.

A current can be supplied to the half cell via an opposing electrode of nickel sheet and an external voltage source, while the individual potential of the working electrode is determined against a Hg/HgO reference electrode with the aid of a Luggin capillary. All potential values supplied refer to the reversible hydrogen potential in the same electrolyte. 6n KOH serve as electrolyte. The voltage drop caused by the electrolyte resistance and contact resistances is taken into consideration through a separate measurement with a 30 kHz alternating current measurement bridge [28].

Since the attainable flow density with identical potential of the working electrode depends on the pressure exerted by the pressure plate on the catalyst filling [28], the setscrew

(Fig. 9) for varying mechanical pressure is tightened with the aid of a torque screw driver such that the same defined pressure on the catalyst layer is adjusted for all measurement cells. As Fig. 10 demonstrates for an electrode with  $50 \text{ mg/cm}^2$  depyrophorized Raney nickel ( $\text{Al}_{50} \text{Ni}_{50}$ ), the optimal pressure for nickel catalysts is situated between  $100 \text{ N/cm}^2$  and  $200 \text{ N/cm}^2$ . Therefore, an average value of  $150 \text{ N/cm}^2$  was selected for all electrodes, since slight scattering of the values has little effect on the flow density in this range.

/22

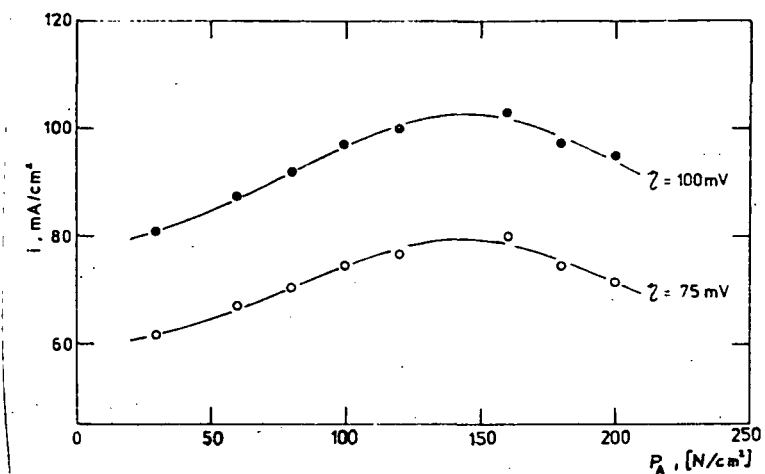


Fig. 10: Relationship of Current Density of a Supported Electrode with  $50 \text{ mg/cm}^2$  Depyrophorized Raney Nickel ( $\text{Al}_{50} \text{Ni}_{50}$ ) at  $60^\circ \text{C}$  in  $6\text{n KOH}$  and the Mechanical Pressure on the Catalyst Filling [28].

#### 2.4.2. Current-Voltage Characteristic

After constructing the measurement cell, the electrode was left in  $6\text{n KOH}$  for about 10 hours at a temperature of  $80^\circ \text{C}$  and a hydrogen pressure of 0.8 bar in order to reactivate the catalyst and to establish the same defined initial condition in all electrodes.

First, the different catalysts were examined with respect to their current-voltage characteristics.

For this purpose, the potential of the electrodes was measured for various current densities and corrected by the  $i$ - $R$  portion. Some results are presented in Fig. 11. All hydrogen anodes had a catalyst occupation of  $30 \text{ mg/cm}^2$  corresponding to  $375 \text{ mg NiTi}_2$  with the predetermined electrode surface of  $12.5 \text{ cm}^2$ . The electrolyte temperature amounts to  $80^\circ \text{C}$ . The content of the catalyst of  $\alpha\text{-3Ni(OH)}_2 \cdot 2 \text{H}_2\text{O}$  is given as parameter.

/23

It is noticeable in all  $\eta$ - $i$  characteristics that they can be represented with a very good approximation all the way to polarizations of  $100 - 130 \text{ mV}$  as straight lines. Therefore, no limitation in current density, as may occur for example through insufficient diffusion of the hydrogen to the reaction location, is noticeable in the range of interest up to approxi-

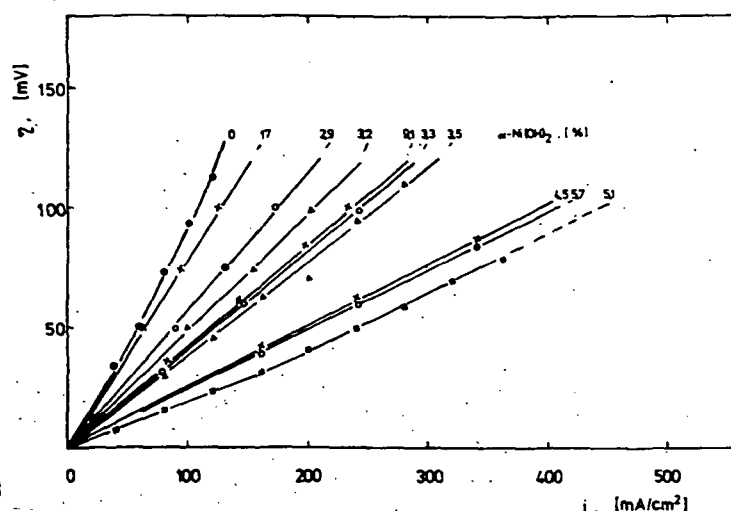


Fig. 11:  $i$ - $R$  Corrected  $\eta$ - $i$  Characteristics of Electrodes with  $30 \text{ mg/cm}^2$  Raney  $\text{NiTi}_2$  Catalysts of Different Hydroxide Content in  $6\text{N KOH}$  at  $80^\circ \text{C}$ .  $P_{\text{H}_2} = 0.8 \text{ bar}$ .

mately  $130 \text{ mV}$  - above this value, the electrochemical oxidation of nickel begins [24]. Only in the characteristic of the material not oxidized by air can indications for this be determined on the basis of the slight bending of the curve. The rise of each straight line represents the individual polarization resistance  $\Delta\eta / \Delta i$  of the electrodes and is therefore a measure of the quality of the catalyst employed. Fig. 11 shows that the content of nickel hydroxide has a considerable effect on the capacity of Raney nickel catalysts. The  $\eta$ - $i$  characteristics become increasingly flatter up to hydroxide contents of approximately  $5\%$ , corresponding to a decrease in polarization resistance or an improvement in the electrodes. At higher values of the  $\alpha$  nickel hydroxide content, an increase in the polarization resistance is determined again. A better survey on this relationship is obtained when the current density is considered as a function of the  $\alpha\text{-Ni(OH)}_2$  content at constant polarization. This is presented in Fig. 12 for a constant polarization of  $100 \text{ mV}$ . The curve shows a marked and sharp maximum at a content of  $5.1\% \alpha\text{-3Ni(OH)}_2 \cdot 2 \text{ H}_2\text{O}$ . The curve drops rapidly with higher and lower values. Especially in the range of approximately  $3\text{-}4\% \alpha\text{-3Ni(OH)}_2 \cdot 2 \text{ H}_2\text{O}$  there is a very strong dependency of the flow density on hydroxide content, the extremely slight scattering of the values in this range is noticeable, however, such that the sharp rise in the curve appears sufficiently certain. A quantitative consideration of the diagram produces the result that it is possible through a suitably controlled air oxidation of the Raney  $\text{NiTi}_2$  powder to increase the capacity of the catalyst material to 3 to 4 times the value of non-depyrophorized material.

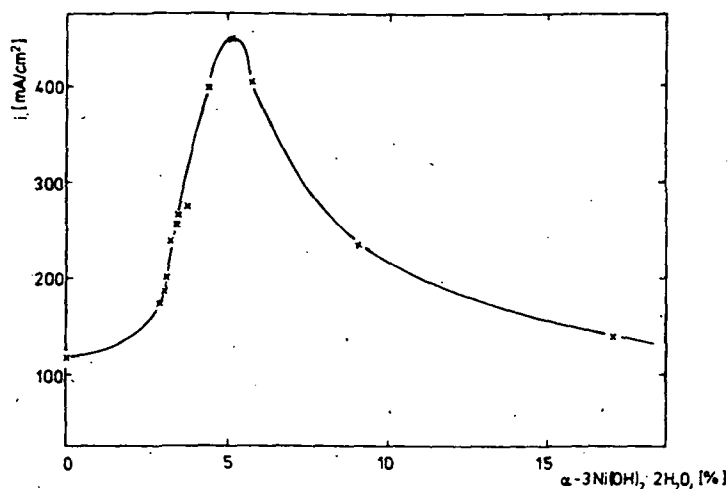


Fig. 12: Effect of  $\alpha\text{-Ni(OH)}_2$  on the Current Density of Air-Oxidized Raney  $\text{NiTi}_2$  Catalysts with Constant Potential of 100 mV (left-hand ordinate). Right-hand ordinate: Values of the Polarization Resistance determined from the  $\eta$ - $i$  characteristics.  $T = 80^\circ \text{C}$ .

The stationary current-voltage characteristics are only a general measure for quality of the catalyst employed, however, not generally permitting more precise statements on the individual partial steps of the hydrogen oxidation to be catalyzed. In many catalysts, the so-called passage reaction proves to be the partial step determining rate. This deals with the discharging reaction, i.e. the passage of the electron from the disassociated hydrogen at the catalysts surface to the conduction tape of the catalyst metal. It is possible that the  $\text{Ni(OH)}_2$  has a similar effect on this passage reaction as the alloyed titanium, also present in oxidized form [12.14]. The kinetics of the passage reaction are determined by the passage resistance  $R_d$  or equivalently from the exchange current  $i_0$  [12, 30, 31]. It applies that:

$$\left(\frac{di}{d\eta}\right)_{\eta \rightarrow 0} = \frac{F}{RT} i_0 = \frac{1}{R_d}$$

$R$  = general gas constant  
 $F$  = Faraday constant  
 $T$  = temperature [K]

[32].

From this equation it is possible to determine  $i_0$  from the initial rise of the  $\eta$ - $i$  characteristic, when other polarization may be neglected in relation to the passage polarization. This method is not suitable for porous electrodes, however, because the diffusion polarization is not negligible. Therefore, instantaneous measurement methods for determining the exchange current density are often employed.

### 2.4.3. Measurement of the Exchange Current Density According to the Method of Potential Jump

The theoretical basis of this method for determining the exchange current has already been treated in detail by Ewe [32] and Richter [12]. For this reason, a complete derivation of the equation of determination for the exchange current will not be presented here, only indicating the results necessary for further considerations. In this case, the greatly simplified equivalent circuit diagram of a supported porous electrode, presented in Fig. 13, serves for illustration.

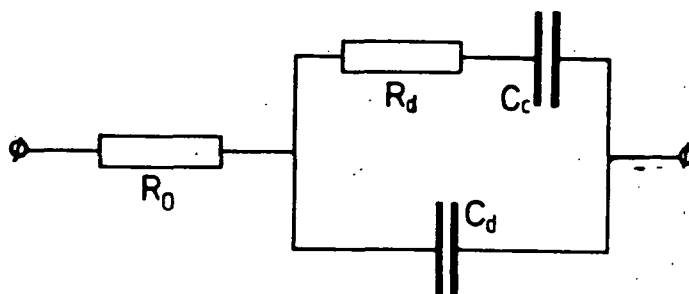


Fig. 13: Equivalent Circuit Diagram of a Porous Gas-Diffusion Electrode.

Here:

$R_0$  = the pure ohmic resistance between Luggin capillary and catalyst surface on the electrolyte side with the addition of the contact resistances at the nickel nets and pressure plate

$C_d$  = double-layer capacity

$C_c$  = chemical absorption capacity

$R_d$  = passage resistance.

It can be seen that the equivalent circuit diagram only describes those electrode reactions correctly which are stationary and do not require any subsequent supply of hydrogen for maintaining a stationary flow. The potential jump method employed for the exchange current measurement fulfills these requirements and may be described satisfactorily using these equivalent circuit diagram.

The electrode is maintained potentiostatically on a potential selected between 0 and 130 mV in an immersed condition, until the current produced by the capacitor recharging has become negligible. A subsequent jump in potential by the amount of  $\Delta U$  (generally 10 mV) causes an exchange in current in the electrode, limited at time  $t = 0$  by the resistances  $R_0$  and  $R_d$ ,



The compensation of  $R_0$  is carried out by a feedback coupling circuit; the voltage proportional to the cell current produced at  $R_k$  is amplified by the operational amplifier  $V_1$  and fed back at the desired voltage input of the potentiostat. The degree of feedback  $k$  can be adjusted by the adjustable amplification. In the case of  $k = 1$ ,  $R_0$  is completely compensated. This is shown by the fact that the arrangement is located at the beginning of vibrations. Amplification is then reduced to the extent that the vibration just reaches a threshold. The correct adjustment of compensation for  $R_0$  may be regulated with the aid of an oscilloscope. The monostable multivibrator constructed by the three gates  $N_1$ ,  $N_2$ ,  $N_3$  provides a rise in potential free of thumping in addition to the highest possible flank rise (greater than 50 nsec.). The amount of the potential jump between 0 and 10 mV may be varied with  $P_1$ . The duration in time of the voltage jump is determined by the RC member of the monoflop at approximately 10 sec.

The cell current produced by the jump in potential is recorded after logarithmic amplification through  $V_2$  on a y-t recorder such that  $y(t) = \lg(I(t))$  is obtained directly as measurement curve. Fig. 15 presents several measurement curves of an electrode with 20 mg/cm<sup>2</sup> air-oxidized Raney NiTi<sub>2</sub> at 20° C and various potentials.

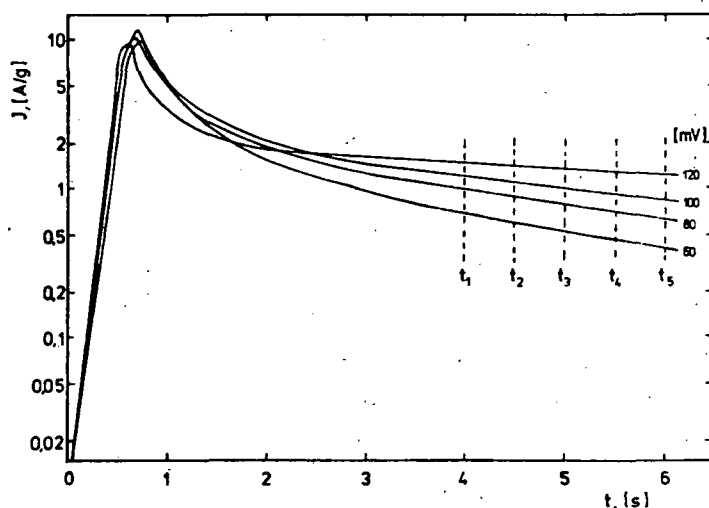


Fig. 15: Logarithmic Current-Time Functions of a Raney NiTi<sub>2</sub> Electrode at 20° C after a Potential Jump of 10 mV for Determining the Exchange Current Density for Various Potentials.

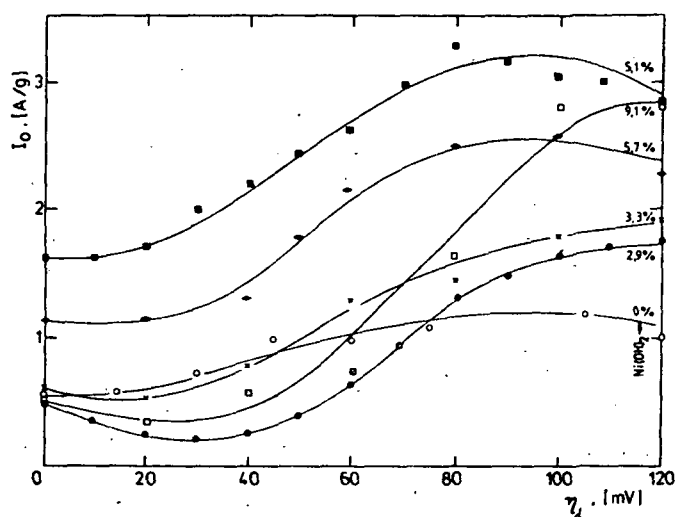
It can be seen that the exchange of the double-layer capacity is reduced after approximately 3.5 sec. and the curve converts into a straight line determined by the time constant  $\tau = R_d \cdot C_c$ . In order to exclude errors in the graph when extrapolating this straight line to the time  $t = 0$  (the

slightest changes in rise have a strong effect on the value of the current density because of the logarithmic division of the ordinate), the course of the curve after  $t = 4$  sec. was adapted according to the method of the smallest error squares to the function

$$\ln(I(t)) = -\frac{t}{R_d C_c} + \ln\left(\frac{\Delta U}{R_d}\right)$$

and the value determined for  $t = 0$ . The computer program was designed such that only the five  $I(t)$  values had to be inserted for the value  $t_1 \dots t_5$ . The exchange current densities are presented in Fig. 16 for several electrodes with various  $\text{Ni(OH)}_2$  contents as a function of polarization. All measurements were carried out in an immersed condition (electrodes without excess gas pressure) at room temperature. The individual measurement points are separated by a time period of about 10 minutes in order to permit the exchange current of capacities to drop to negligible values.

/31



/32

Fig. 16: Exchange Current Density of Raney  $\text{NiTi}_2$  Catalysts with Different Contents of  $\alpha\text{-Ni(OH)}_2$  as a Function of the Potential at  $20^\circ \text{C}$  and  $20 \text{ mg/cm}^2$  Catalyst Occupation.

In all these catalysts samples, a monotonous rise in the exchange current with the potential in the interval of 30-100 mV can be recognized, while the exchange current density in several catalyst samples drops again to values around 75 % of the maximum value at higher potential values. The following simple estimation should clarify whether the hydrogen storage capacity of the Raney nickel is possibly too small for the considerable exchange currents, so that the drop in the exchange current can



be explained at higher potentials.

The change amount  $Q$  converted in a voltage jump solely on the basis of the passage reaction amounts to [15]:

/33

$$Q = \frac{I_0 \Delta U \cdot F}{RT} \int_{t=0}^{\infty} e^{-\frac{t}{R_d C_c}} dt = - \frac{I_0 \Delta U \cdot F \cdot R_d C_c}{RT} e^{-\frac{t}{R_d C_c}} \Big|_0^{\infty}$$

where:  $\Delta U = 10 \text{ mV}$ ,  $T = 293 \text{ K}$

The value for  $R_d C_c = \tau$  may be determined directly from Fig. 15. Since the capacitor discharges in this diagram are presented in a logarithmic form, results directly as the negative rise of the individual curves in the linear portion ( $t \geq 4 \text{ sec.}$ ). The value  $\tau = 16 \text{ sec.}$  is taken for  $\eta_d = 120 \text{ mV}$  from Fig. 15 for  $R_d C_c$  while the exchange current of the most active catalyst (curve represented by blacked-in squares) is situated at about  $3 \text{ A/g}$  for this potential range. Therefore, a change amount results for the passage reaction of

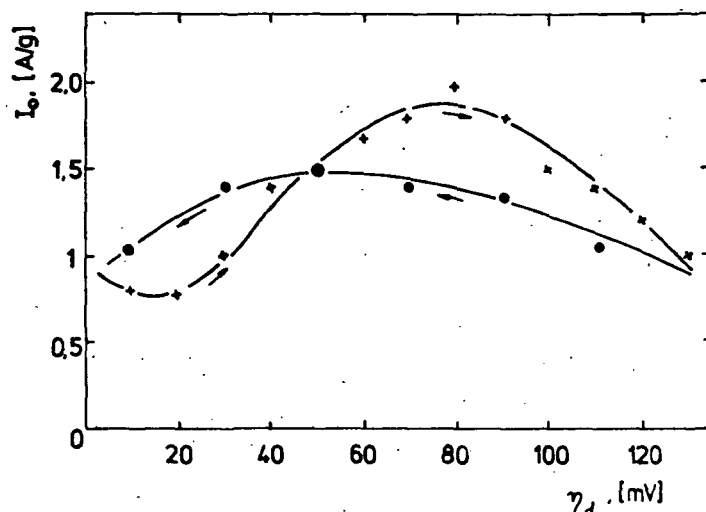
$$Q = \frac{I_0 \cdot \Delta U \cdot F \cdot \tau}{R \cdot T} \approx 19 \frac{\text{As}}{\text{g}}$$

According to the first Law of Faraday, approximately  $0.2 \text{ mmol}$  of adsorbed atomic hydrogen  $A_{ad}$  per gram of nickel must be discharged for this purpose, resulting in a molar ratio of  $\text{Ni:H}_{ad} = 86:1$ . Under the assumption that approximately every sixth nickel atom is a surface atom, it results that for an exchange current of  $3 \text{ A/g}$  an  $H_{ad}$  must be positioned at every 15th nickel surface atom in order to apply this measurement method. This value is far below the value indicated in literature for the hydrogen storage capacity of Raney nickel of one hydrogen atom per nickel surface atom [34]. Although this value from the literature refers to measurements near the hydrogen potential, it may be assumed that sufficient adsorbed hydrogen is present at the catalyst surface even for higher exchange current densities with positive potentials, such that a lack of hydrogen may be excluded as a reason for the reduction in the exchange current at higher potentials.

/34

Another explanation is supported by measurements undertaken by Shumilova and Bagotzky [35], proving that the nickel surface already forms a coating of  $\text{OH}^-$  groups after approximately  $+ 0.1 \text{ V}$  against hydrogen Rev. It may be assumed that the catalyst surface is partially passivized by a great adsorption of  $\text{OH}^-$  groups, thereby effecting a rise in the passage resistance, expressed in the drop in the exchange current. However, this  $\text{OH}^-$  coating may not be confused with nickel oxides and hydroxides produced by air oxidation. These are difficult to reduce in comparison, while the collection of  $\text{OH}^-$  groups may be reversed with decreasing potential values. Fig. 17 shows an exchange current density measurement, returning the measurement step-wise to the hydrogen potential after achieving the potential of  $130 \text{ mV}$ . It can be seen that the

initial value in the hydrogen potential is reached again in spite of a marked hysteresis, explained by the complete reduction of the  $\text{OH}^-$  ions collected above +100 mV.



/35

Fig. 17: Exchange Current Density of Air-Preserved Raney  $\text{NiTi}_2$  as a Function of the Potential at  $20^\circ \text{C}$  and  $20 \text{ mg/cm}^2$  Catalyst Occupation. x = measurement value of the potential branch increasing step-wise from 0 mV to 130 mV. o = measurement values of the potential branch decreasing step-wise from 130 mV to 0 mV.

The different shape of the exchange current density curves makes it difficult to compare the individual electrodes directly. Since the measurements become uncertain at high polarization because of the  $\text{OH}^-$  collections, on the one hand, but the range of higher current density is especially of interest, on the other hand, a comparison of the exchange current density curves appears logical in the range of  $\eta_d \approx 80 - 100 \text{ mV}$ .

Fig. 18 shows this exchange current density determined at  $\eta_d = 80 \text{ mV}$  and  $100 \text{ mV}$  as a function of the  $\alpha\text{-Ni(OH)}_2$  contents with polarization as the parameter. A strong effect of the nickel hydroxide is also demonstrated up to values of about 4-6 percent by weight  $\alpha\text{-Ni(OH)}_2$  in the exchange current density as in the instationary  $\eta\text{-i}$  characteristic. In this range, a considerable increase in activity of the catalyst is determined with increase in hydroxide. The catalyst with 5.1 %  $\text{Ni(OH)}_2$  even shows an increase in the exchange current around 300 % in comparison to the non-air-oxidized material. In contrast, hydroxide portions above 6 % do not provide any improvement in catalyst characteristics, but rather the exchange current drops with increase in

/36

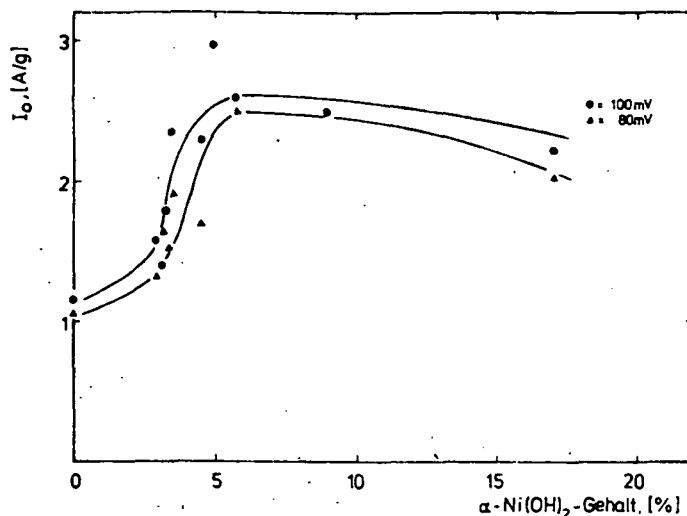


Fig. 18: Exchange Current Density at 80 mV and 100 mV for Raney NiTi<sub>2</sub> Catalysts as a Function of the Ni(OH)<sub>2</sub> Content at 20° C

the Ni(OH)<sub>2</sub> portion slowly to values around 200 % of the initial value; however, no similar steep drop is determined at higher hydroxide contents in comparison to the stationary current densities attainable (Fig. 12), and the shape of the curve can be described more by a saturation behavior above 6 % Ni(OH)<sub>2</sub>. This relationship is expressed more clearly when the passage resistance  $R_d$  also characteristic for the passage reaction is plotted as a function of hydroxide content as in Fig. 19 in place of the exchange current density.

This representation shows a steep drop in the passage resistance of 22 [mΩ · g] to about 10 [mΩ · g] in the range of 0-6 % α-Ni(OH)<sub>2</sub> and from there approximately a constant course around 10 [mΩ · g].

These results quantitatively confirm the assumption expressed by other authors [36] that nickel hydroxide may effect a considerable improvement in the passage reaction.

#### 2.4.4. Estimation of the Effect of Nickel Hydroxide on Diffusion Polarization

The polarization measured at the stationary n-i characteristics results from several sequential reaction steps in hydrogen oxidation. In a simple model, the passage reaction and the diffusion of the hydrogen to the location of the reaction may be considered as the two most important processes determining rate. This model, describing supported powder electrodes in

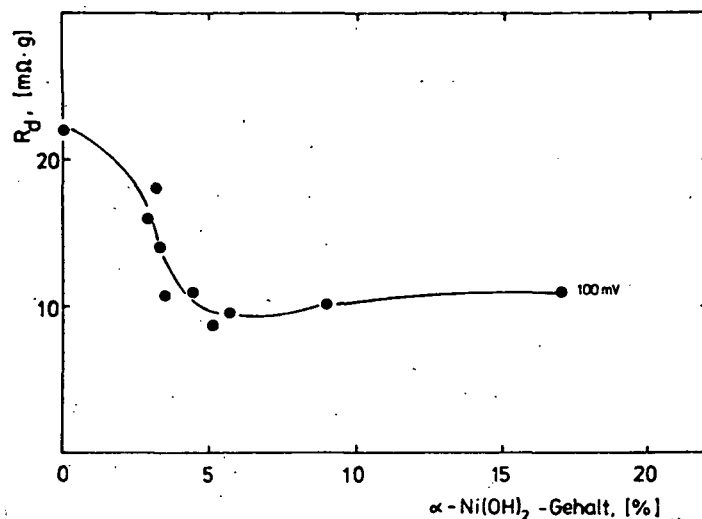
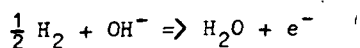


Fig. 19: Relationship of the Passage Resistance and  $\alpha$ -Ni(OH)<sub>2</sub> Contents of Raney NiTi<sub>2</sub> Catalysts at a Potential of 100 mV and 20 °C.

a good approximation will be explained briefly with Fig. 20. The gross reaction of oxidation of the gaseous molecular hydrogen to H<sub>2</sub>O with the release of an electron per hydrogen atom in accordance with



is divided into several partial reactions, more or less determining rate. For example, the H<sub>ad</sub> atom adsorbed as an atom at the location of reaction is discharged in the passage reaction, but only molecular hydrogen is supplied from the gaseous side. The passage reaction is therefore preceded by at least three partial steps: the dissolving of molecular H<sub>2</sub> in the electrolyte, the diffusion of the dissolved H<sub>2</sub> in the pores and the dissociative adsorption at the catalyst surface:  $\text{H}_2 \rightarrow 2 \text{H}_{ad}$ .

A further reaction mechanism occurs in parallel with the hydrogen dissolved in the electrolyte being adsorbed disassociatively at another point differing from the location of reaction, preferably in the area of the triple phase boundary at the pore mouth and moved by diffusion from there as an H<sub>ad</sub> atom on the pore surface to the location of the passage reaction. Both diffusion processes, the volume diffusion in the electrolyte of the pore and the surface diffusion of the hydrogen taking place at the pore walls, occur in Raney nickel catalysts, in which case it may be assumed according to reports by Schmitt [15] that the surface diffusion has an advantage in pore radii  $r < 500 \text{ \AA}$ . Since the average pore radius of Raney NiTi<sub>2</sub> catalysts is far less than 500 Å, the major portion of hydrogen

/39

/40

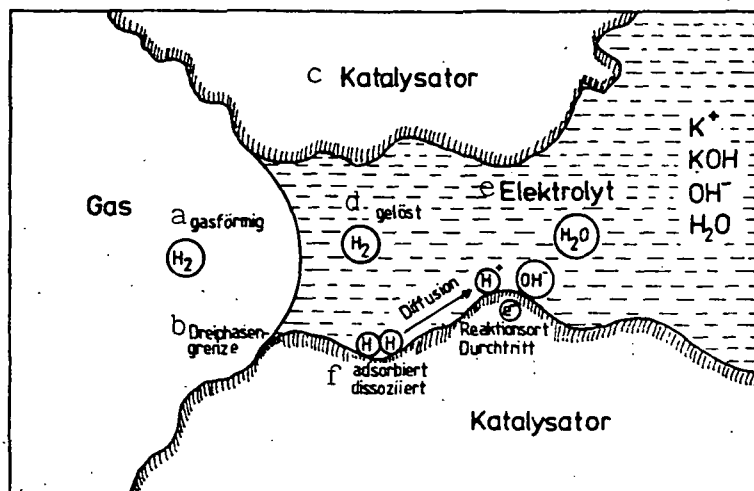


Fig. 20: Simple Model of the Reaction Sequence during Anodic Oxidation of Hydrogen.

Key: a. gaseous  
 b. triple-phase boundary  
 c. catalyst  
 d. dissolved  
 e. electrolyte  
 f. adsorbed  
 disassociated

transport to the location of reaction probably is carried out via the surface diffusion at the pore wall surfaces. As a result of the finite rate of diffusion processes, the diffusion polarization  $\eta_{diff}$  is produced additionally to the passage polarization  $\eta_d$ , producing the total polarization  $\eta_t = \eta_d + \eta_{diff}$  insofar as all other partial reactions may not be considered determining factors for rate. This assumption is justified for Raney nickel catalysts, as the corresponding calculations of Mund and Ewe demonstrate [37, 38].

With the previous results, it is now possible to undertake an estimation of diffusion inhibition as a function of  $Ni(OH)_2$  contents. A correction in the exchange current must first be carried out, however, since the  $\eta$ - $i$  characteristic was measured at  $80^\circ C$ , but the exchange current density at  $20^\circ C$ . It follows for the exchange current from theory of hydrogen discharge

$$I_o = \frac{1}{R_d} \frac{RT}{F}$$

i.e., when  $R_d$  exhibits no dependency on temperature, the exchange current densities at various temperatures should behave as does the quotient of the temperatures:

$$\frac{(I_0)_{T_1}}{(I_0)_{T_0}} = \frac{T_1}{T_0}$$

In order to test this relationship experimentally, exchange current density measurements were taken with an electrode at 20° C and 80° C. The electrode with 3.3 %  $\alpha$ -Ni(OH)<sub>2</sub> was selected for this purpose, exhibiting a relatively small exchange current density at 20°C and, in addition, not demonstrating any very large drop in the exchange current at high potentials caused by the OH<sup>-</sup> coating. The results of these measurements are presented in Fig. 21.

/41

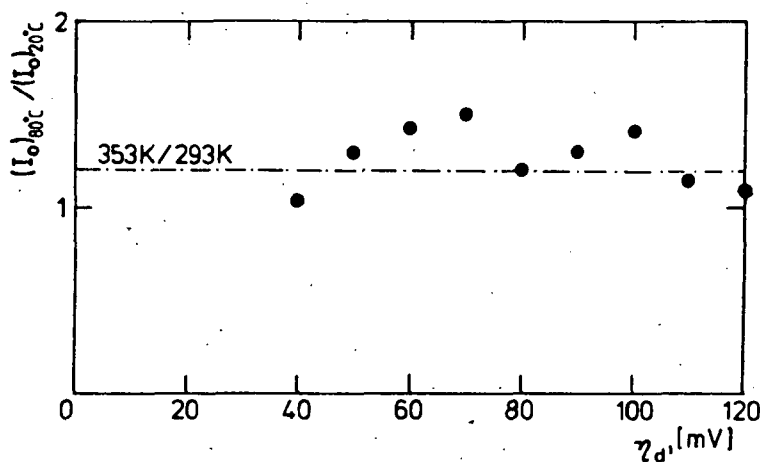


Fig. 21: Quotient of the Exchange Current Density Values at 80° C and 20° C Dependent on the Potential of a Raney NiTi<sub>2</sub> Electrode with a 3.3 % Content of  $\alpha$ -Ni(OH)<sub>2</sub>.

The relationship of the measured exchange current density at 80° C and 20° C is plotted on the ordinate. The dotted line indicates the relationship of both temperatures [K]. The measurement points are situated within the error tolerances near the theoretical expected value of  $\frac{353\text{K}}{293\text{K}} = 1.2$ . On the whole, it

/42

is demonstrated that the exchange current density values may be converted for a simple estimation:

$$I_0|_{80^\circ\text{C}} = 1.2 \cdot I_0|_{20^\circ\text{C}}$$

It applies for the current density determining the passage reaction:

$$i = I_0(\eta_d) \cdot \left( e^{\frac{\alpha F \eta_d}{RT}} - e^{-\frac{(1-\alpha) F \eta_d}{RT}} \right)$$

with  $I_0$  = exchange current density,  $\alpha$  = passage factor.  
It applies for nickel catalysts that  $\alpha \approx 0.5$ , simplifying the equation to

$$(*) \quad i = I_0(\eta_d)^2 \cdot \sinh\left(\frac{F}{2RT} \eta_d\right)$$

When the current density value determined from Fig. 12 for a total polarization  $\eta = \eta_{diff} + \eta_d = 100$  mV is inserted (see Table 2.2.), the value pair  $(I_0, \eta_d)$  may be determined, taking into consideration

$$I_0|_{80^\circ} = 1,2 \cdot I_0|_{20^\circ}$$

from the exchange current density measurements (Fig. 16), fulfilling the equation (\*). The diffusion polarization is therefore obtained at

$$\eta_{diff} = 100 \text{ mV} - \eta_d$$

The individual portions of diffusion and passage polarization for the total polarization of 100 mV determined in this manner are presented together with the individually achievable current densities.

/43

Table 2.2.

$\alpha\text{-Ni(OH)}_2, [\%]$	0	2,9	3,2	3,5	5,1	5,7	9,1	17
$i [A/g]  _{100mV}$	4	5,8	6,7	8,5	15	13,4	7,9	4,1
$\eta_d [mV]$	76	81	78	81	83	90	85	56
$\eta_{diff} [mV]$	24	19	22	19	17	10	17	44

The effect of  $\alpha\text{-Ni(OH)}_2$  on hydrogen diffusion at the catalyst surface may be estimated from Fig. 22. In this case, the percentual portion of the passage polarization (upper curve) and diffusion polarization (lower curve) is indicated as a function of the  $\alpha\text{-Ni(OH)}_2$  content. Without attempting to over-emphasize this simple estimation, the results still confirm the expectation that the diffusion of hydrogen is inhibited with

increasing content of disturbances at the catalyst surface, so that the portion of diffusion polarization increases, while the passage resistance decreases.

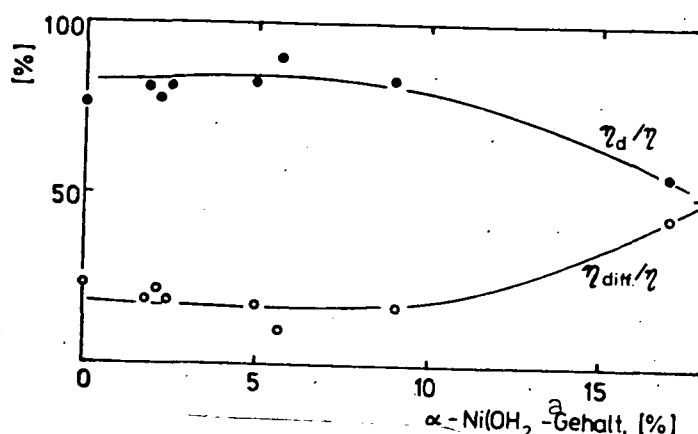


Fig. 22: Percentual Division of the Total Polarization of 100 mV into Diffusion and Passage Polarization as a Function of the  $\alpha\text{-Ni(OH)}_2$  Content of the Catalysts.

Key: a. content

#### 2.4.5. Discussion

The measurements undertaken up to now have clearly shown the strong effect of  $\alpha\text{-Ni(OH)}_2$  on the catalytic activity of the Raney nickel. It was possible to show that catalysts with 5-6 %  $\text{Ni(OH)}_2$  content permit three to four times the current density with the same polarization in comparison to non-air-oxidized material. This improvement in the  $\eta$ -i characteristic is attributed to a strong reduction in the passage resistance, as can be seen from the measurements of the exchange current. A further increase in the  $\text{Ni(OH)}_2$  content (above 6 %) causes only a slight reduction in exchange current, but has a clearly negative effect on the characteristics. Apparently, local, active passage centers are created by the  $\alpha\text{-Ni(OH)}_2$  covering with a preference for discharging the adsorbed hydrogen atoms. The passage polarization also is reduced with the increase in these centers, until the passage centers are situated so close to one another that their increased activity is expanded to the entire catalyst surface. The further increase in hydroxide content then no longer results in a substantial increase in activity.

If we now observe the effects of the hydroxide content on the diffusion of the hydrogen, first the volume diffusion must be separated from the surface diffusion. The nickel hydroxide content probably has no effect on the volume diffusion of the dissolved hydrogen insofar as the hydroxide crystals do not become so large that they block entire pores. In contrast, however, a considerable effect of the  $\alpha\text{-Ni(OH)}_2$  content may be



expected on the surface diffusion. The  $\alpha$ -Ni(OH)<sub>2</sub> coating located at the catalyst surface causes much disturbance at the nickel surface and is an obstacle to diffusion of the adsorbed atomic hydrogen at the surface of the pore walls. Since the surface diffusion far exceeds volume diffusion in Raney NiTi<sub>2</sub> catalysts according to the estimations of Schmitt, Mund and Ewe [15, 37, 38], an increase in hydroxide causes an increase in diffusion inhibition.

In summary, the effect of  $\alpha$ -Ni(OH)<sub>2</sub> on the stationary  $\eta$ -i characteristic may be described as follows. The creation of active passage centers on the catalyst surface is responsible for the increase in catalytic activity with the increase in the content of Ni(OH)<sub>2</sub> up to about 6 %, while the drop in current density at higher concentrations of Ni(OH)<sub>2</sub> may be attributed to the prevention of surface diffusion and the accompanying increase in diffusion polarization.

/46

## 2.5. Behavior During Continuous Operations

In order to evaluate the quality of a catalyst, the long-term behavior of the catalytic activity in addition to the  $\eta$ -i characteristics and the exchange current density is of decisive importance. Since large capacities require increased temperature and positive potentials, these two parameters are of special interest, because both accelerate the catalyst aging. All long-term experiments were therefore carried out at 80° C; the current load was selected such that the highest capacity catalysts had a noticeable initial polarization, on the one hand, while the potential of the samples with less activity at the same current load were not to substantially exceed 100 mV initially, on the other hand, to secure an operating time of several hundred hours. A load of 4 A/g resulted as a favorable value. The catalyst occupation amounted to 30 mg/cm<sup>2</sup>. With this occupation and grain fraction of less than 50  $\mu$ m, the electrode is only one grain layer thick so that an even load on the entire sum of catalyst employed may be assumed. The design of the electrodes was identical to that of the  $\eta$ -i characteristics. Fig. 23 shows the measurement results of the galvano-static long-term experiment for several air-oxidized Raney NiTi<sub>2</sub> catalysts in comparison to non-air-oxidized Raney NiTi<sub>2</sub>.

/47

In Fig. 23, polarization is plotted as a function of operating duration with the Ni(OH)<sub>2</sub> content as parameter. All air-oxidized catalysts exhibit a rather high life span with the relatively hard operating conditions (80° C, 4 A/g), while the non-oxidized material already demonstrates a polarization around 150 mV after approximately 230 hours, i.e. it has achieved a range in which the electrochemical oxidation of the nickel and the accompanying destruction of the catalyst begins. Furthermore, it can be seen that the air-oxidized samples exhibit a range of constant polarization at the beginning of the experiment, increasing with the content of Ni(OH)<sub>2</sub> of the catalyst concerned. This observation is in agreement with the previously

/48

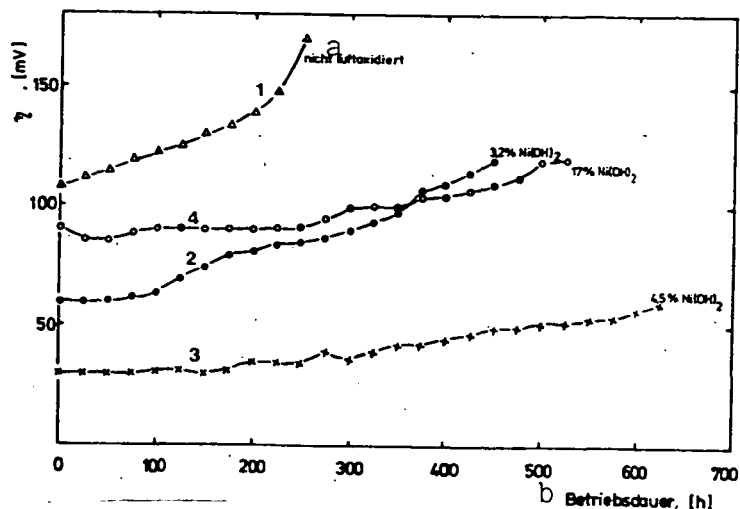


Fig. 23: Galvano-static Continuous Experiment with Non-Air-Oxidized (1) and Air-Oxidized (2-4) Catalysts at 80° C, 4 A/g and 30 mg/cm<sup>2</sup> Catalyst Occupation.

Key: a. non-air-oxidized  
b. duration of operations

expressed assumption [15] that the  $\alpha\text{-3Ni(OH)}_2 \cdot 2\text{H}_2\text{O}$ , effecting the improvement in catalyst, is reduced in the course of time in the presence of hydrogen. After this period, polarization increases monotonously in time as it does in the non-air-oxidized material, the aging rate being comparable on an order of magnitude with that of the untreated Raney  $\text{NiTi}_2$ . As a result of the high catalytic activity and the resulting slight initial polarization, however, catalysts with approximately 4-6 %  $\text{Ni(OH)}_2$  exhibits greater life-spans at equal current loads. If curve (3) is extrapolated, for example, taking into consideration the increased aging rate of curve (1), a life-span of more than 1000 hours is still obtained. The entire increase in polarization produces 30 mV for curve (3) after 625 hours. The average value for aging rate therefore amounts to about 50  $\mu\text{V/hours}$ . In spite of this relatively low value, the direction for further studies on aging behavior of air-oxidized Raney catalysts can be seen in Fig. 23; a  $\text{Ni(OH)}_2$  content of about 5 % has a favorable effect on aging as a result of the low initial polarization, but it is unfortunately unstable. Further studies will therefore have to apply to stabilization of the remaining hydroxide, i.e. the replacement by the more stable nickel oxide.

### 3. Preservation through Air Oxidation with Subsequent Stabilization of the Oxide in a $\text{H}_2$ Flow at 300° C

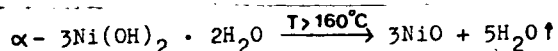
The Raney nickel, depyrophorized through controlled air oxidation and therefore preserved, is catalytically inactive

and must be reactivated, for example, in the electrode subjected to hydrogen pressure at 80° C in 6n KOH. It was shown in the previous section that approximately half of the hydroxide produced in oxidation during this reactivation is retained and effects an increase in catalytic activity. Unfortunately, the hydroxides are slowly reduced further when operating the electrodes in the vicinity of the hydrogen gas potential, thereby losing the increased activity of the catalyst.

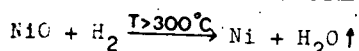
In the following, therefore, the possibilities for stabilizing the remainder oxide through tempering in the hydrogen flow will be examined.

### 3.1. Mechanisms of Reduction through Hydrogen and Experimental Studies of this Phenomenon

The  $\alpha$ - $3\text{Ni}(\text{OH})_2 \cdot 2\text{H}_2\text{O}$  produced in air oxidation decomposes at temperatures of 160° C into NiO and  $\text{H}_2\text{O}$  with the simultaneous release of the water of crystallization:



The rough crystallized NiO produced in this manner is very stable thermally, the melting temperature of NiO indicated at 1990° C [39], so that a cleavage of the NiO is not possible solely through the effect of temperature. It is possible, however, to reduce the nickel oxide at least partially to nickel at temperatures above 300° C through hydrogen:



The decomposition of nickel hydroxide is therefore attained by tempering the air-oxidized Raney nickel at 350° C in the hydrogen flow, producing very stable NiO and simultaneously a partial reduction in the nickel oxide at the NiO surfaces. Furthermore, a recrystallization of the Raney nickel with a strongly defective structure (see electron grid microscope exposures, section 3.3.1.) occurs, dependent on tempering time at this tempering temperature - approximately one-third of the melting temperature of nickel. After the conclusion of this tempering process, the catalyst treated in this manner is again pyrophorous and must be subjected to a second regulated air oxidation at lower temperature. In this case,  $\alpha$ -nickel hydroxide is reformed because of the hydrogen adsorbed at the nickel surface, on the one hand, and the reduced nickel is partially re-oxidized to NiO, on the other hand, with the resulting combination dependent on the execution of tempering. The purpose and aim of this subsequent treatment of the air-oxidized material is to replace the catalytically very active  $\alpha$ - $3\text{Ni}(\text{OH})_2 \cdot 2\text{H}_2\text{O}$ , unfortunately not stable in continuous operations, with the much more stable NiO under the assumption that the NiO has effects

/50

comparable to the  $\alpha$ -hydroxide on the catalytic activity. An attempt is undertaken through variation in tempering times to affect the ratio of  $\text{Ni}:\text{NiO}:\text{Ni}(\text{OH})_2$  to produce catalysts through optimal treatment, permitting long operating times in addition to high catalytic activity.

/51

The same equipment is employed for air oxidation with several alterations for the practical execution of stabilization in the  $\text{H}_2$  flow (Fig. 1). Fig. 24 presents the additional components of the total set-up important for tempering.

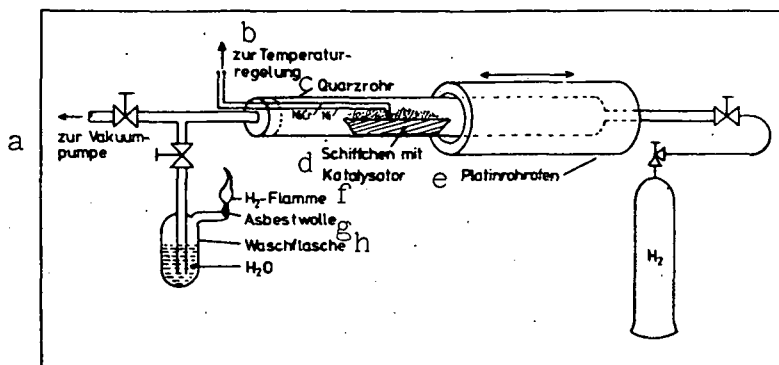


Fig. 24: Arrangement for Tempering the Air-Oxidized Raney- $\text{NiTi}_2$  Catalyst in the Hydrogen Flow.

- Key:
- a. to the vacuum pump
  - b. to temperature control
  - c. quartz tube
  - d. shuttle with catalyst
  - e. platinum tube furnace
  - f. flame
  - g. asbestos woll
  - h. rinsing flask

The catalyst material is introduced into the quartz tube in a shuttle, over which a platinum tube furnace may be pushed. A  $\text{NiCr-Ni}$  thermal element serves for temperature control and regulation. During the heating process and tempering hydrogen slowly passes through the quartz tube with several  $\text{cm}^3/\text{sec}$ . The exiting hydrogen is combusted. The rinsing flask filled with water is necessary for safety to prevent the flame from moving back into the equipment.

/52

All tempering times given in the following studies were measured from time at which the catalyst powder had achieved a temperature of  $250^\circ \text{C}$  during heating.

### 3.2. Effect of Tempering Time on the $\eta$ -i Characteristics and the Exchange Current Density

Previous measurements showed that the catalytic activity of the Raney  $\text{NiTi}_2$  depends greatly on the  $\text{Ni(OH)}_2$  content. The  $\text{Ni(OH)}_2$  content is also altered through subsequent tempering of the air-oxidized catalysts, such that a noticeable effect of the tempering time may be expected on the  $\eta$ -i characteristic and on the exchange current. The individual catalyst samples with differing contents of  $\text{Ni(OH)}_2$  were divided into several individual samples, tempered for 2.5 to 30 minutes in a hydrogen flow and subsequently subjected once again to a controlled air oxidation; thereafter, the measurements of the  $\eta$ -i characteristics, the exchange current density and long-term trials were undertaken. The effect of tempering time on the  $\eta$ -i characteristics is presented in Figs. 25-28. All measurements were carried out in 6N KOH at 80° C and excess hydrogen pressure of 1 bar. The catalyst occupation amounted to a unified 30 mg/cm<sup>2</sup>.

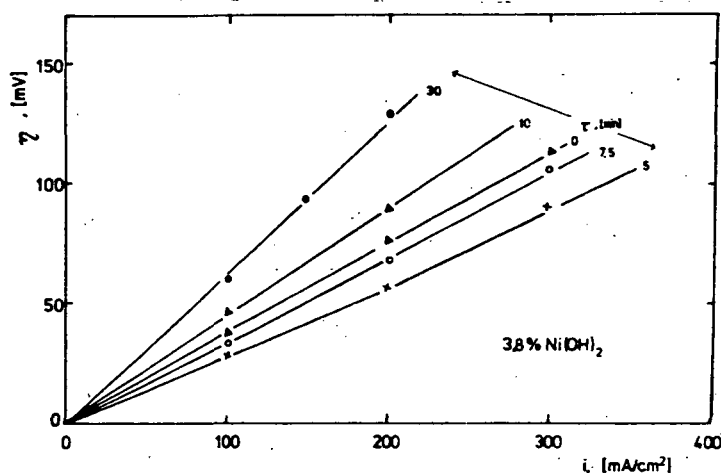


Fig. 25:  $\eta$ -i Characteristics of Air-Oxidized Raney- $\text{NiTi}_2$  Catalysts with 3.8 %  $\text{Ni(OH)}_2$  Content of the Untempered Initial Material and Tempering Time  $\tau$  as Parameter.

In all four figures, several representative characteristics are plotted with tempering time as parameter. The characteristic designated with tempering time  $\tau = 0$  represents the characteristics of the appropriate initial material of the individual families of characteristics. The basic materials were selected such that they exhibit the clearest possible differences with respect to the  $\alpha$ - $\text{Ni(OH)}_2$  content. It can be seen from Figs. 25-28 that all characteristics are almost straight lines with a rise varying more or less greatly with tempering time. In all families of curves, first a reduction in the rise corresponding to an improvement in catalytic characteristics is demonstrated with tempering time. At tempering times of more than 10 minutes, the characteristics of the families of curves become steeper with the low initial  $\text{Ni(OH)}_2$  contents than that of the appropriate initial material. In the curves with relatively high  $\text{Ni(OH)}_2$

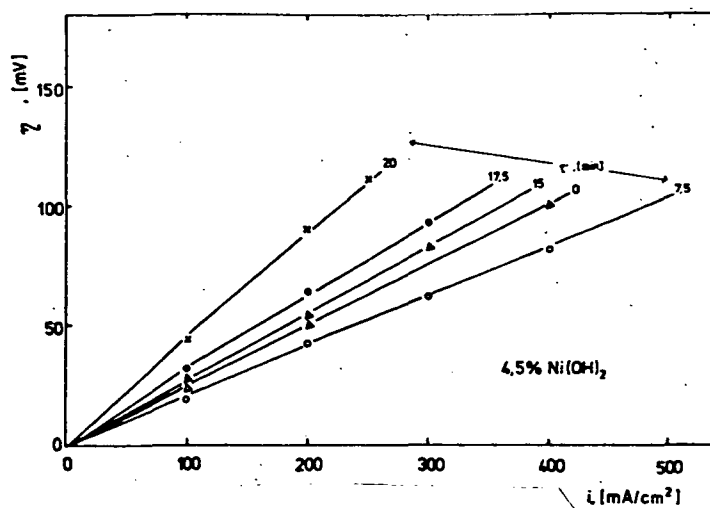


Fig. 26:  $\eta$ - $i$  Characteristics of Air-Oxidized Raney  $\text{NiTi}_2$  Catalysts with 4.5 %  $\text{Ni(OH)}_2$  Content of the Untempered Initial Material and Tempering Time  $\tau$  as Parameter.

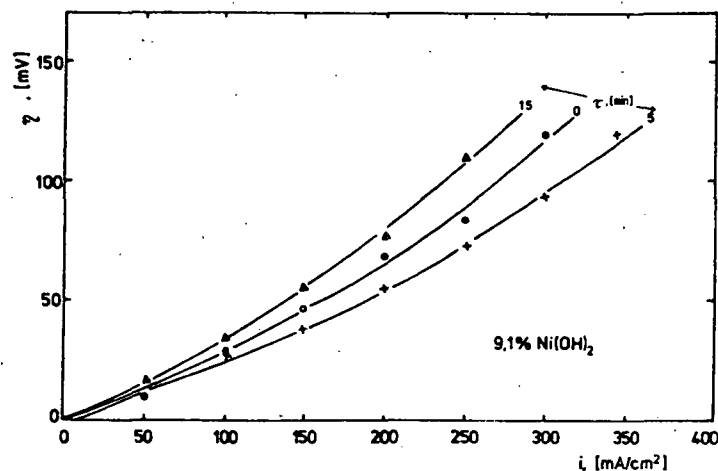


Fig. 27:  $\eta$ - $i$  Characteristics of Air-Oxidized Raney  $\text{NiTi}_2$  Catalysts with 9.1 %  $\text{Ni(OH)}_2$  Content of the Untempered Initial Material and Tempering Time  $\tau$  as Parameter.

contents of the initial material, even the samples tempered for 15 or 20 minutes demonstrate better properties than the untempered catalyst material.

In order to permit a direct comparison of all samples with one another, it is necessary to plot the relationship of the current density to the tempering time with constant polarization.

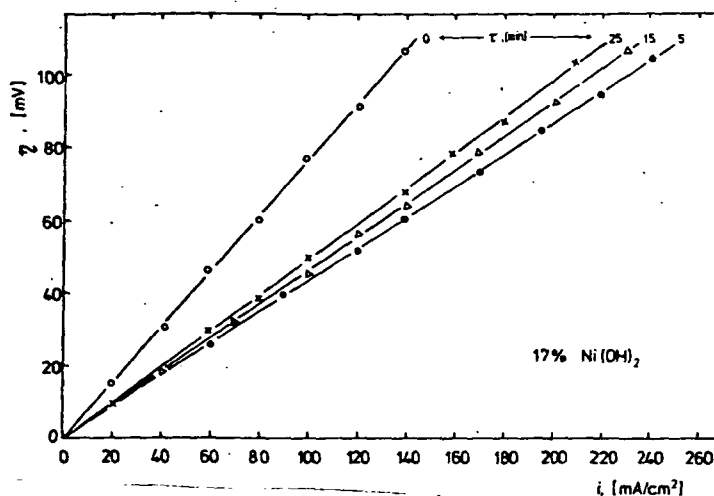


Fig. 28:  $\eta$ - $i$  Characteristics of Air-Oxidized Raney NiTi<sub>2</sub> Catalysts with 17.0 % Ni(OH)<sub>2</sub> Content of the Untempered Initial Material and Tempering Time  $\tau$  as Parameter.

In Fig. 29, all results of Figs. 25-28 are compiled for a polarization of 100 mV. The curve a in Fig. 29 additionally shows the behavior of the samples with an initial Ni(OH)<sub>2</sub> content of 3.25 % with characteristics not separately plotted since they also represent almost straight lines and therefore do not exhibit any fundamental differences to the given characteristics. Parameter is the Ni(OH)<sub>2</sub> content of the initial material. It is noted that in all catalyst samples with the exception of that with 3.25 %  $\alpha$ -Ni(OH)<sub>2</sub>, tempering in the hydrogen flow between 5 and 10 minutes causes a considerable increase in current density. The highest rate in rise with approximately 75 % in comparison to the untempered material is exhibited by the catalyst sample with 17 % nickel hydroxide, but this also has the lowest initial value with approximately 130 mA/cm<sup>2</sup> at 100 mV. Even in the material with the highest initial current density value of 400 mA/cm<sup>2</sup>, however, an increase in current density of about 20 % may be attained through a 7.5 minute tempering time. Longer tempering times than 10 minutes cause a more or less clear drop in the current density in all samples to values around or below 200 mA/cm<sup>2</sup>.

Moreover, Fig. 29 demonstrates the qualitative relationship between the initial content of the nickel hydroxide, the position and shape of the current density maxima. Apparently, the maximum of current density, found in the samples with the lowest content of Ni(OH)<sub>2</sub> of 3.25 % at  $\tau \approx 0$ , shifts with increasing hydroxide content of the initial materials to higher tempering times up to very high values of the hydroxide content of 17 % in the curve having almost constant current density values after a marked increase in current density caused by a tempering time of 5-10 minutes and the curve passes through a further flat maximum in the range of 10 min.  $< \tau < 25$  min.

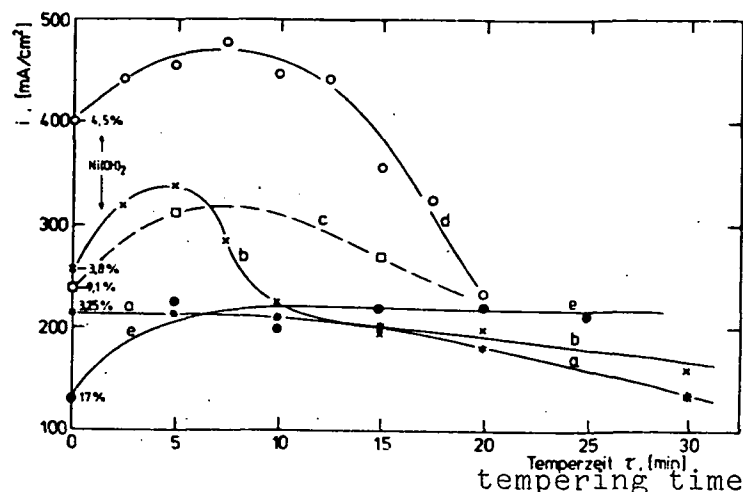


Fig. 29 : Current Density at a Polarization of 100 mV as a Function of Tempering Time in a Hydrogen Flow with the  $\text{Ni}(\text{OH})_2$  Content of the Untempered Catalyst as Parameter. The measurements were Carried out with  $30 \text{ mg/cm}^2$  Catalyst Occupation in 6n KOH at a Temperature of  $80^\circ \text{C}$ .

On the whole, the result of the measurements is that the tempering of the catalyst material in the hydrogen flow following air oxidation leads to a considerable improvement in the catalytic activity of the Raney  $\text{NiTi}_2$  insofar as the air-oxidized initial material does not have an insufficient content of  $\alpha\text{-Ni}(\text{OH})_2$  ( $\geq 3.8\%$ ). The attainable percentual improvements in catalytic activity through tempering in comparison to untempered initial materials are higher in the samples (by about 80 % for curve e) having lower current density values than in the catalysts with an initial state already permitting higher current densities on the basis of the favorable  $\text{Ni}(\text{OH})_2$  content.

In order to provide a survey on the effect of individual parameters studied on the catalytic activity of the Raney  $\text{NiTi}_2$ , an attempt is made in Fig. 30 to present the individual measurements together in a quasi-three dimensional representation.

/58

The current density is indicated on the z axis at  $\eta = 100 \text{ mV}$ , 1 bar hydrogen pressure,  $30 \text{ mg/cm}^2$  catalyst occupation and  $T = 80^\circ \text{C}$ , simultaneously to be considered as a measure for catalytic activity. The y axis indicates the  $\text{Ni}(\text{OH})_2$  content of the untempered initial material and the x axis the tempering time at  $300^\circ \text{C}$  in the hydrogen flow. The curve in the z-y plane at  $x = 0$  is identical to Fig. 12 ( $i = f(\text{Ni}(\text{OH})_2 \text{ content})$ ). The curves in the z-y plane at  $y = 3.25\%$ ,  $3.8\%$ ,  $4.5\%$ ,  $9.1\%$  and  $17\%$  correspond to those of Fig. 29. Although this quasi-three dimensional image is not especially suitable to supply quantitative determinations of current density as a function of both parameters of tempering time and initial content of nickel

/59



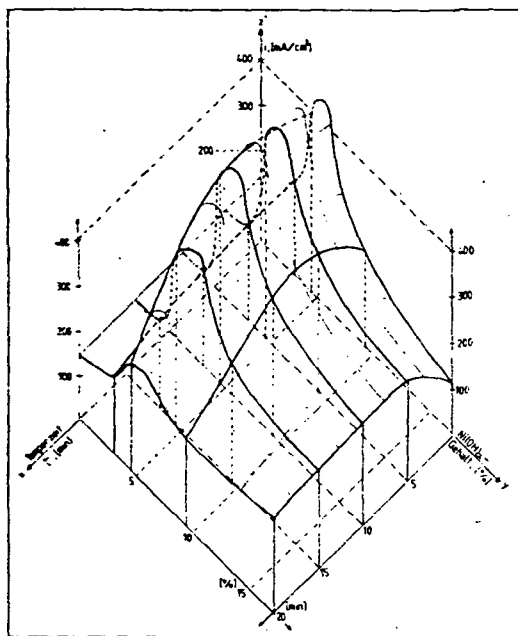


Fig. 30: Quasi-Three Dimensional Representation of the Current Densities Achieved with Raney  $\text{NiTi}_2$  Catalysts at 100 mV Polarization, 30  $\text{mg/cm}^2$  Occupation and  $80^\circ \text{C}$  as a Function fo the  $\text{Ni(OH)}_2$  Content and Tempering Time.

hydroxide, it does provide a survey on the wide range of variation in catalytic activity of Raney  $\text{NiTi}_2$  catalysts. Simultaneously, it also becomes clear that the desireable range with very high capacity of the catalyst is only very narrow. Optimal relationships are apparently only provided when air-oxidized Raney  $\text{NiTi}_2$  catalysts with a  $\alpha\text{-Ni(OH)}_2$  content around 5 % is subjected to a subsequent treatment through tempering in a  $\text{H}_2$  flow for 5 - 10 minutes (at 4.5 %  $\text{Ni(OH)}_2$ , 7 1/2 minutes).

In section 2.4., a reference was made to knowledge of the exchange current describing the passage reaction being necessary for a complete evaluation of the activity of electrochemical catalysts. Therefore, where possible, measurements of exchange current density were also carried out with all samples having the stationary  $\eta$ -i characteristics measured as a function of tempering time in the hydrogen flow. In all cases, electrodes were employed with 20  $\text{mg/cm}^2$  catalyst material. The measurements were carried as described in section 2.4.3. at  $20^\circ \text{C}$  in 6N KOH without excess gas pressure. With respect to the shape of the exchange current density curves, similar relationships resulted to those in the measurements of the untempered materials. After an initial rise in exchange current in the potential range

of 40-90 mV, the curves become increasingly flatter until the exchange current slowly drops again at potentials above 100-110 mV. The exchange current density curves in the potential range of interest of 50-130 mV are provided in Fig. 31 for a series of tempered materials with tempering times of 0 min. (untempered initial material) up to 25 min.

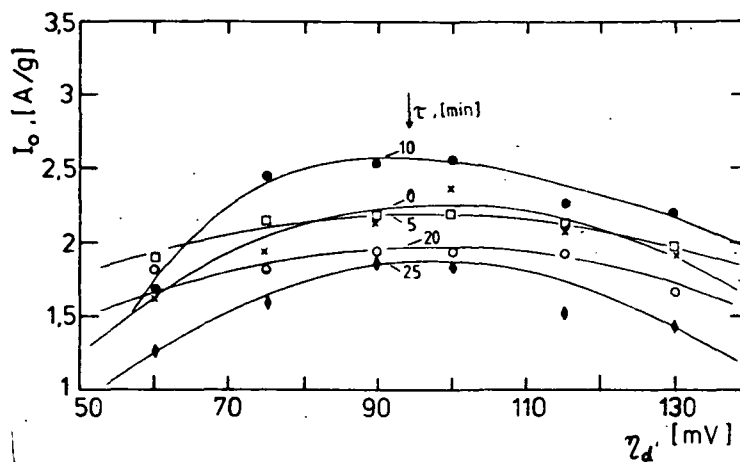


Fig. 31: Exchange Current Density of Raney  $\text{NiTi}_2$  Catalysts at 20° C as a function of Potential with Tempering time as Parameter.

The sequence described above can be seen in all curves. It is noticeable that the qualitative relationship of exchange current density and potential is almost identical for all catalysts. The effect of tempering leads to a parallel shift in the curves to higher or lower exchange current values with the maximum exchange current being achieved in the range around 100 mV. Therefore, it suggests itself to observe the effect of tempering time by comparing exchange current densities at 100 mV. The exchange current densities for four representative catalyst series are presented in Fig. 32 at 100 mV as a function of tempering time. The catalysts were selected such that the initial material of one series (curve a) exhibits a high initial  $\text{Ni(OH)}_2$  content (17 %), the curve (b) has an initial  $\text{Ni(OH)}_2$  content near the maximum catalytic activity with 4.5 %, while curves (c) and (d) have only a low initial  $\text{Ni(OH)}_2$  content around 3 %. The measurements show that tempering at 350° C in the hydrogen flow does not have any especially large effects on the passage reaction, even with tempering times up to 30 minutes does the exchange current drop at most to 0.6 of the value of the initial exchange current density (d). An improvement in the passage reaction through tempering in comparison to the untempered material can be noted best in the sample series with high initial  $\text{Ni(OH)}_2$  content (curve a), while all other catalysts show smaller exchange current densities after the subsequent treatment in the hydrogen flow. The clear, but not large drop in exchange current is noticeable, however, in the curves (b-d) in those samples tempered up to 5 minutes. In contrast, the

/61

/62

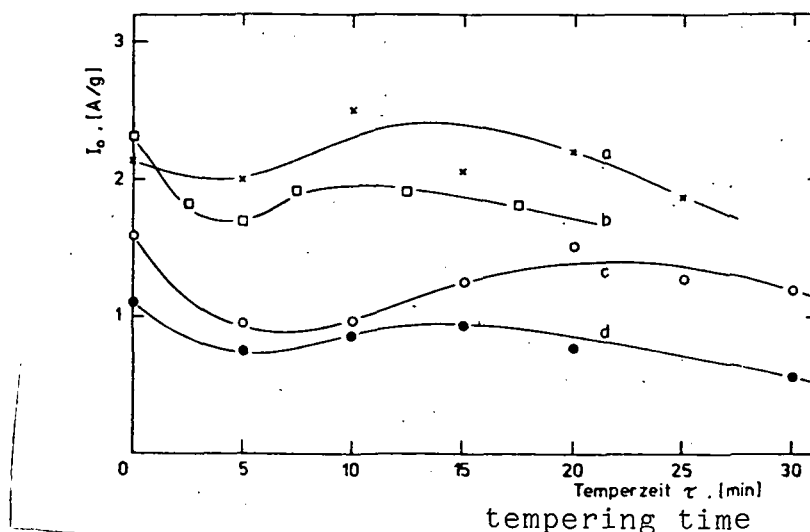


Fig. 32: Exchange Current Density at a Potential of 100 mV for various Catalyst Series as a Function of Tempering Time. The Parameter is the  $\text{Ni}(\text{OH})_2$  content of the Untempered Material.

exchange current again increases to comparable values of the untempered material with greater tempering times.

The drop in current density with shorter tempering times may be explained plausibly. Since the nickel hydroxide is decomposed when tempering the catalyst, the amount of the hydroxide decomposing into  $\text{H}_2\text{O}^\uparrow$  and  $\text{NiO}$  depending on the duration of tempering time, it can be expected that the  $\alpha\text{-Ni}(\text{OH})_2$  decreases with increasing duration of subsequent treatment in the hydrogen flow, even if  $\alpha\text{-Ni}(\text{OH})_2$  is formed in the subsequent second controlled air oxidation as a result of the hydrogen adsorbed at the catalyst surface. It can be seen from section 2.3.4. (Fig. 18), that a reduction in hydroxide content results in a decrease in exchange current density insofar as the initial  $\text{Ni}(\text{OH})_2$  content does not exceed a value of about 6 %. This demand applies to curves (b-d) with an initial  $\text{Ni}(\text{OH})_2$  content clearly below 6 %. A reduction in hydroxide therefore has a negative effect on the passage reaction. In contrast, curve (a) behaves differently with the exchange current density remaining relatively constant up to tempering times of about seven minutes. This behavior can also be explained with the aid of the results from Fig. 18. The curve a describes the measurement of a catalyst series with high initial  $\text{Ni}(\text{OH})_2$  content (17 %). It can be seen from Fig. 18 that the reduction in hydroxide content from 17 % down to values around 7 % does not have any noticeable effect the exchange current density. This explains the lack of a clear current density minimum at about 5 minutes for curve a in Fig. 32.

All four curves now demonstrate a slight rise in exchange current densities for higher tempering times in spite of the expected decrease in hydrogen content. It is necessary to seek

the cause for this behavior in the production of NiO when the hydroxide decomposes into NiO and H<sub>2</sub>O such that the nickel oxide, as already suspected earlier, exhibits comparable catalytic properties similar to  $\alpha$ -Ni(OH)<sub>2</sub>.

On the whole, the effect of tempering on the exchange current density of air-oxidized Raney NiTi<sub>2</sub> catalysts can be designated as relatively slight. An initial reduction in exchange current with increasing tempering time, attributable to the reduction in the  $\alpha$ -3Ni(OH)<sub>2</sub> content of the catalyst is apparently compensated almost completely in longer tempering times in the range of 7-10 minutes by the additional production of NiO.

### 3.3. Structural Studies with Preserved and Stabilized Raney NiTi<sub>2</sub> Catalysts

/64

#### 3.3.1. Effect of Tempering on the $\alpha$ -Ni(OH)<sub>2</sub> Content

The considerations in the previous section were based essentially on the assumption that a subsequent treatment of the air-oxidized catalyst material in hydrogen atmosphere at approximately 350° C leads to a reduction in the hydrogen content of individual samples. In order to confirm this assumption quantitatively, the Ni(OH)<sub>2</sub> contents of several samples of various initial catalysts tempered for various amounts of time were determined as indicated in section 2.4. In Fig. 33, the relationship of Ni(OH)<sub>2</sub> to tempering time is given for an initial Ni(OH)<sub>2</sub> content of 17 %. The curve demonstrates one exponential function as is also expected theoretically. A simple calculation may clarify this. The percentual alteration dp of the Ni(OH)<sub>2</sub> content should be proportional to the time interval dt and proportional to the available amount p of the hydroxide under the assumption that the rate of decomposition of Ni(OH)<sub>2</sub> is constant in time with constant temperature, such that it must apply with the proportionality constant a:

$$-dp = a \cdot p \cdot dt$$

This known differential equation has the solution  $p(t) = p_0 e^{-at}$  with the boundary condition  $p(t=0) = p_0$ . This exponential function, however, only describes the decomposition of the hydroxide as a function of tempering time, but does not take into consideration the fact that  $\alpha$ -Ni(OH)<sub>2</sub> is reformed in the subsequent, second controlled oxidation. This may be taken into consideration in a first approximation through the addition of a further constant  $p_e$  in accordance with

$$p(t) = p_0 e^{-at} + p_e$$

It appears justified to describe the new formation of the hydroxide with a constant  $p_e$  insofar as the amount of hydrogen adsorbed at the nickel surface exclusively determines the amount of the newly produced hydroxide, because the water is completely

/66

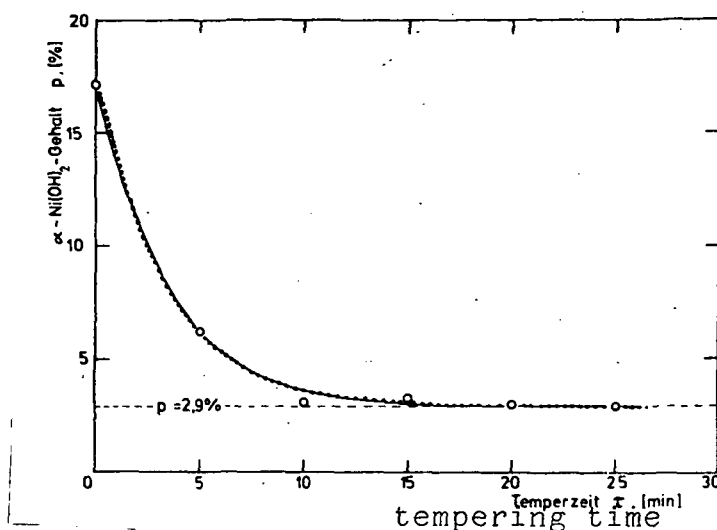


Fig. 33:  $\text{Ni(OH)}_2$  Content of Raney  $\text{NiTi}_2$  Catalysts as a Function of Tempering Time at  $350^\circ \text{C}$  in an Hydrogen Atmosphere. Solid Line = Measurement Curve; Dotted Line = with the Constants  $a = 0.3 \text{ min}^{-1}$  and  $p_e = 2.9 \%$  Calculated Course of the Curve.

removed from the catalyst powder at very long tempering times at  $350^\circ \text{C}$ .

The constants result through adjustments in calculation of the equation to the measurement values in Fig. 33:

$$a = 0.3 \text{ min}^{-1} \quad \text{and}$$

$$p_e = 2.9 \%.$$

The curve calculated with these values is presented in Fig. 33 as a dotted line. It becomes clear that this equation describes the measurement results very well with the given constants. Both curves (Figs. 33 and 34) asymptotically approach a lower limit value for the  $\text{Ni(OH)}_2$  content, apparently the minimum value even with extended tempering, situated around 2.9 %. Precisely this value also represented the lower limit in the untempered catalysts with varying  $\text{Ni(OH)}_2$  contents, even catalysts, dried for 24 hours at  $135^\circ \text{C}$  before air oxidation and therefore no longer containing any moisture, had  $\text{Ni(OH)}_2$  contents around 3 % after air oxidation. This minimum hydroxide content may only be explained with the production of  $\text{H}_2\text{O}$  through oxidation of the hydrogen adsorbed at the nickel surface, even for catalyst powders extensively free of water.

The course of hydroxide content is presented in Fig. 34 once again with tempering time for another catalyst series in order to confirm the results. In this case the initial material has only 4.5 %  $\text{Ni(OH)}_2$ , therefore situated very near the constant

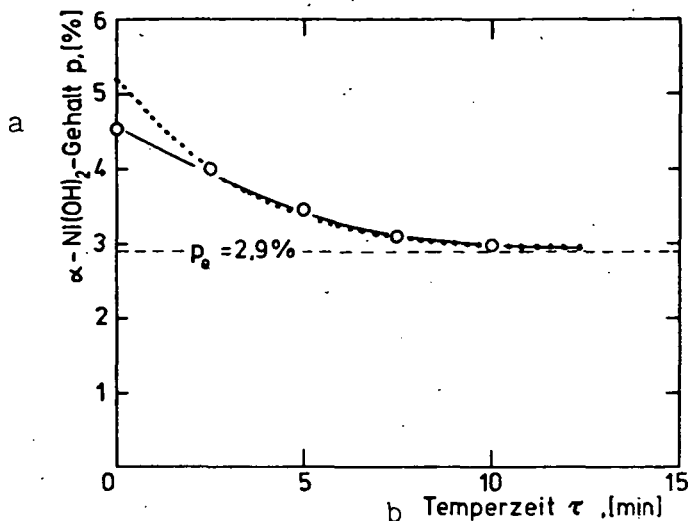


Fig. 34: Relationship of the  $\text{Ni(OH)}_2$  Content and Tempering Time of a Catalyst Series with Initial Content of 4.5 %  $\text{Ni(OH)}_2$ . The curve calculated with the same constants  $a$  and  $p_e$  as in Fig. 33 is represented as a dotted line.  
Key: a. content      b. tempering time.

final value of about 3 %. The curve also approaches this value with long tempering times. The dotted line in Fig. 34 again represents the curve adjusted through calculations of  $p(t) = p_0 e^{-0.3t/\text{min}} + 2.9\%$  with the same constants  $a$  and  $p_e$ . In this case, the measurement results also agree well with the calculated course.

In connection with the measurements of the  $\text{Ni(OH)}_2$  content as a function of tempering time, the knowledge of  $\text{NiO}$  content also appears important. Unfortunately, however, there is no practical method for determining the  $\text{NiO}$  content precisely, as is provided by the decomposition of the hydroxide. Since  $\text{NiO}$  may be reduced, however, at temperatures of more than  $300^\circ\text{C}$  in an hydrogen atmosphere, as previously described, an attempt was made to determine at least the reducible portion of the  $\text{NiO}$  as a function of tempering time. For this purpose, the  $\text{Ni(OH)}_2$  content had to be determined first, as is customary, in the catalyst under investigation, since additional  $\text{NiO}$  is produced in this decomposition, to be subtracted subsequently from the total amount of  $\text{NiO}$  determined. The  $\text{NiO}$  content was determined in analogy to the measurements of the hydroxide content through thermogravimetric measurements via the weight loss as a result of the oxygen released in the reduction. Forming gas of the composition  $\text{N}_2:\text{H}_2 = 3:1$  was employed for the measurements carried out at  $350^\circ\text{C}$  for safety reasons with a pressure of 1 bar, corresponding to a partial hydrogen pressure of 250 mbar. Under these conditions, the sample was left until a constant weight was achieved (approximately 20 hours).

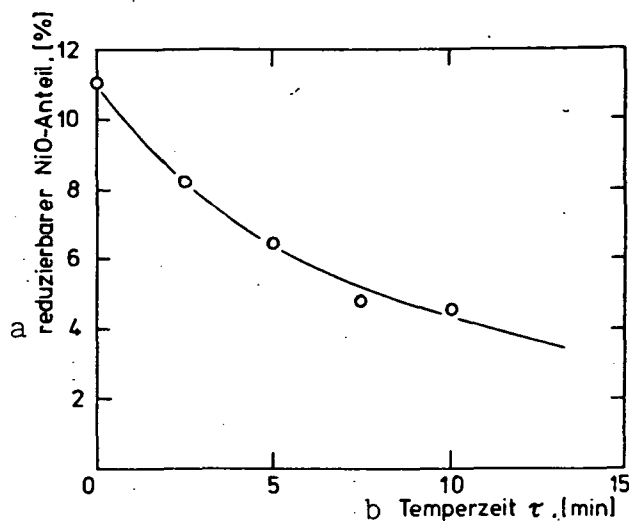


Fig. 35: Portion of NiO in Air-Oxidized Raney NiTi<sub>2</sub> Catalysts Reduced in a Hydrogen Atmosphere at 350° C as a Function of Tempering Time. Nickel Oxide Portion in Relation to Total Nickel Mass.  
Key: a. reducible NiO Portion  
b. tempering time

The measurement results are presented in Fig. 35. The reducible portion of the NiO present on the catalyst surface falls monotonously with the increase in tempering time. The behavior, surprising at first glance, confirms the idea when examined more closely, however, that more stable, coarser crystallized NiO is produced in tempering. Apparently, the portion of the less stable nickel oxide is reduced during tempering in the hydrogen flow in favor of the more stable NiO crystals, very difficult to reduce. The measurements of the reducible portion of NiO may not be considered as a proof of the production of stable NiO crystals, but the results fit into this model with no contradiction, therefore at least supporting it. Moreover, the accompanying spectral photometric measurements point to the fact that the total portion of NiO is not substantially altered by tempering.

### 3.3.2. Electron-Grid Microscope Exposures of Preserved Raney NiTi<sub>2</sub> Powders

Electron grid microscope exposures were prepared for several samples of Raney nickel catalysts tempered for differing amounts of time to find further explanation for the effects of tempering on the characteristics of these catalysts. It was necessary to apply an approximately 0.1  $\mu\text{m}$  thick gold layer via evaporation to the powder samples to make even the non-conducting nickel oxides and hydroxides visible.

Fig. 36 (a - l) shows the results of these studies. Exposures are presented for sample series with tempering times of 0 minutes (untempered material), 2.5 minutes, 7.5 minutes and 10 minutes. The three enlargement factors of 480, 2000 and 10,000 were chosen for all samples to provide a good survey over a wide range of the catalyst up to detail exposures of the individual catalyst grain.

The effect of tempering on the Raney nickel may already be seen in a comparison of the exposures at 480x enlargement. An increasing proportion of more coarse grains is ascertained on the order of magnitude of about 50  $\mu\text{m}$  with increasing tempering time. The result may be attributed to a recrystallization of the initially highly porous nickel with strongly defective structure as well as to recrystallization processes of the nickel oxides and nickel hydroxides.

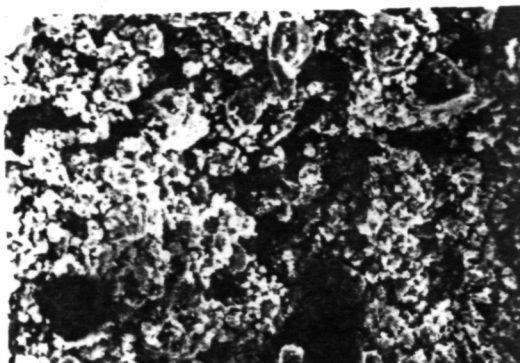
In addition to this increase in the coarse crystals in the range of 50  $\mu\text{m}$ , a numerical reduction in the finer crystals is observed. This becomes especially marked in the exposures with an enlargement of 2000s. The exposure of the untempered sample shows mainly fine crystal grains with a diameter of less than 10  $\mu\text{m}$ , apparently covering the surface of larger grains (larger than 30  $\mu\text{m}$ ). The surface covering of fine crystals is reduced with increasing tempering time and the resulting coarse grains partially show completely smooth surfaces. It is noticeable that the decrease in the smallest crystals is greatest at tempering times up to 2 1/2 min., while the alteration is not as clear above this point; nevertheless, the growth of the coarse crystals may be observed during the entire period of 10 min. It may therefore be concluded that the growth of the larger crystals may be based on recrystallization of nickel, while the fine crystalline surface covering of the powder grains is probably nickel hydroxide, reduced during the first minutes of tempering in agreement with the preceding measurements. The exposures at an enlargement of 10,000x also support this argument. Figs. 36c and 36f show a layered crystalline structure, typical for hydroxides. For comparison, Fig. 36m shows an electron grid exposure of pure  $\alpha\text{-3Ni(OH)}_2 \cdot 2\text{H}_2\text{O}$  in a 10,000 enlargement with a layered structure similar to that in Fig. 36c and 36f.

The powder samples examined are not reactivated catalyst material, because a previous reactivation in 6n KOH was not possible for technical reasons related to the electron grid microscope, but the electron grid microscope exposures still provide a clear view into the structural changes in the highly porous  $\text{NiTi}_2$  powder during tempering in a hydrogen atmosphere.



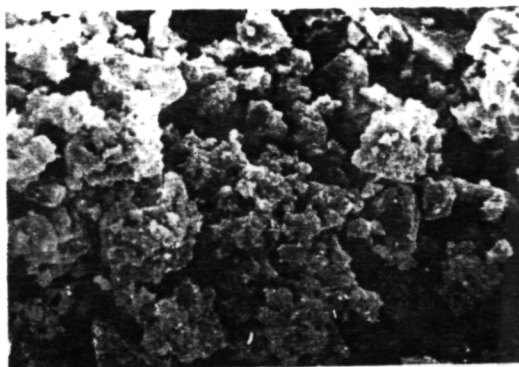
50  $\mu\text{m}$

a) 480-<sup>a</sup>-fache Ver-  
größerung



10  $\mu\text{m}$

a  
b) 2000-<sup>a</sup>-fache Ver-  
größerung



1  $\mu\text{m}$

a  
c) 10000-<sup>a</sup>-fache Ver-  
größerung

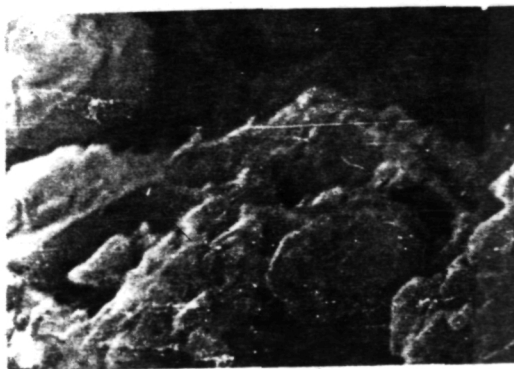


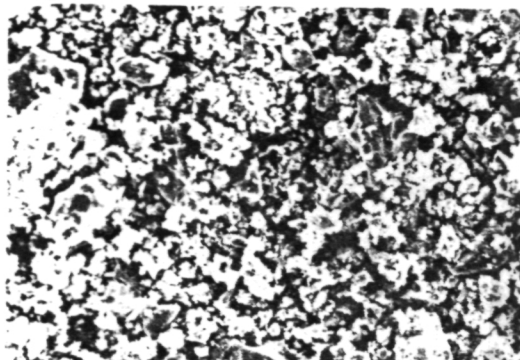
Fig. 36 (a-c): Electron Grid Microscope Exposures of  
Untempered Air-Oxidized Raney  $\text{NiTi}_2$  Catalyst  
Powder.

Key: a. fold enlargement.

50  $\mu\text{m}$

a

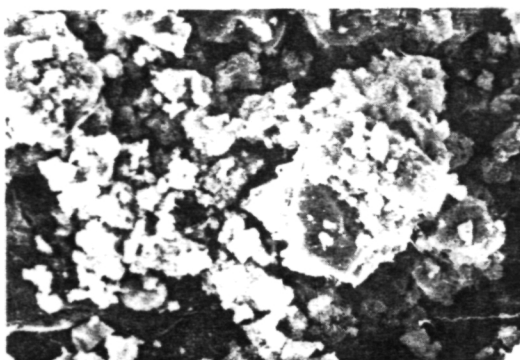
480- fache Ver-  
größerung



10  $\mu\text{m}$

a

2000- fache Ver-  
größerung



1  $\mu\text{m}$

10000- fache Ver-  
größerung

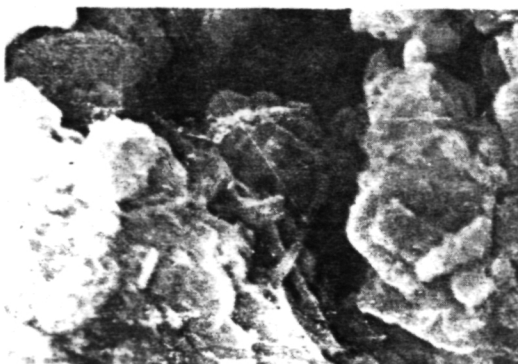
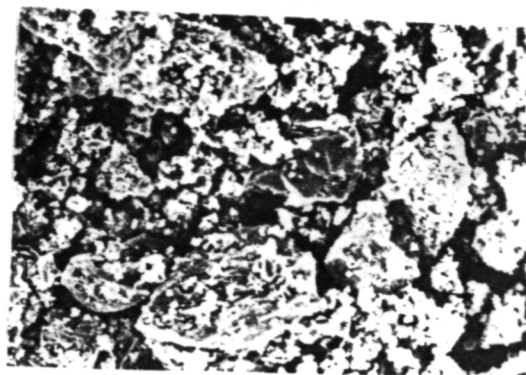
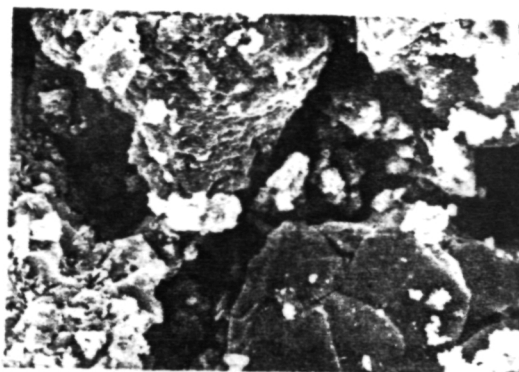


Fig. 36 (d-f): Electron Grid Microscope Exposures of  
Raney  $\text{NiTi}_2$  Catalyst Powder Tempered for 2.5  
Minutes in a Hydrogen Flow and Reoxidized in Air.  
Key: a. -fold enlargement.

50  $\mu\text{m}$   
a  
g) 450- fache Ver-  
größerung



10  $\mu\text{m}$   
a  
h) 2000- fache Ver-  
größerung



1  $\mu\text{m}$   
a  
i) 10000- fache Ver-  
größerung

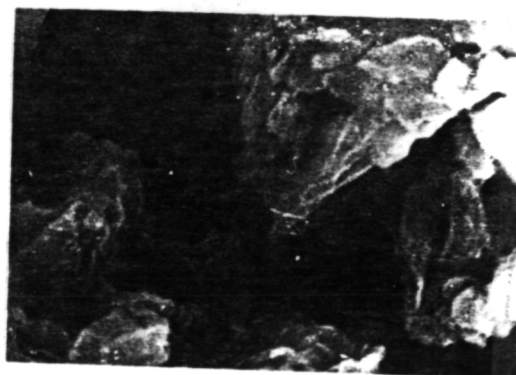

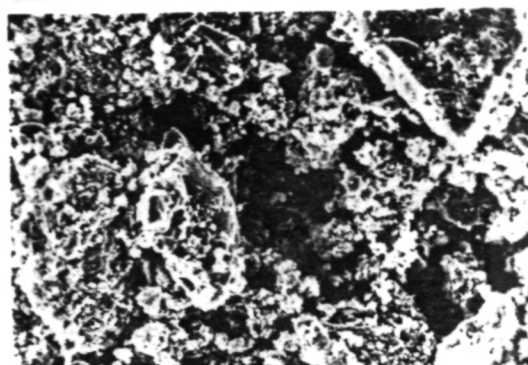

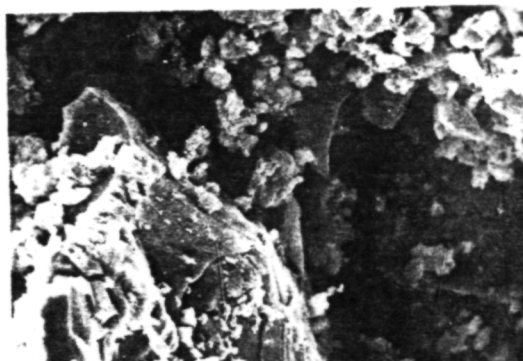


Fig. 36 (g-i): Electron Grid Microscope Exposures of  
Raney  $\text{NiTi}_2$  Catalyst Powder Tempered for 7.5  
Minutes in a Hydrogen Flow and Reoxidized in Air.  
Key: a. -fold enlargement.

 50  $\mu\text{m}$   
 a  
 j) 480- fache Ver-  
 größerung



 10  $\mu\text{m}$   
 a  
 k) 2000- fache Ver-  
 größerung




 1  $\mu\text{m}$   
 a  
 l) 10000- fache Ver-  
 größerung



Fig. 36 (j-l): Electron Grid Microscope Exposures of  
 Raney  $\text{NiTi}_2$  Catalyst Powder Tempered for 10  
 minutes in a Hydrogen Flow and Reoxidized in Air.  
 Key: a. -fold enlargement.

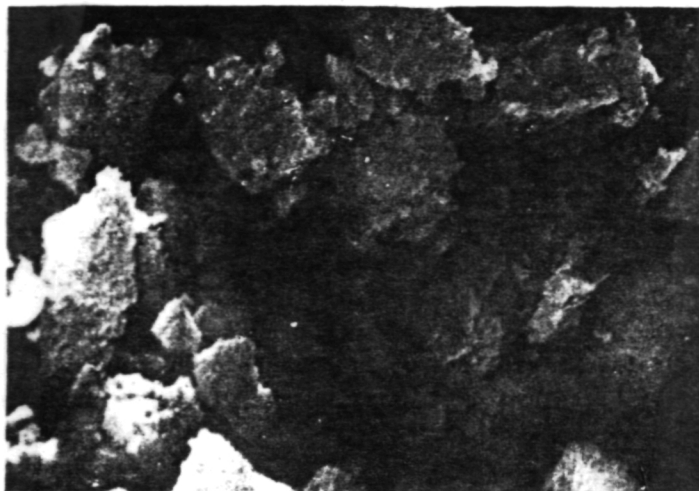


Abb. 36m REM-Aufnahme von reinem  $\alpha$ -3Ni(OH) $_2$  · 2H $_2$ O mit 10.000-facher Vergrößerung

Fig. 36 (m): Electron Grid Microscope Exposure of Pure  $\alpha$ -3Ni(OH) $_2$  · 2 H $_2$ O in a 10,000x enlargement.

### 3.3.3. BET Surface and Pore Structure of Raney NiTi $_2$ Catalysts as a Function of Tempering Time

The high catalytic activity of Raney catalysts is the result, for the most part, of the very large inner surfaces. This is understood as the total amount of the surfaces of all individual grains of the catalyst powder. The inner or specific surface therefore represents one of the more important structural parameters of porous gas diffusion electrodes in addition to pore distribution and will be studied in the following with preserved and tempered Raney NiTi $_2$  powders. The isothermal gas adsorption of an inert gas at the boiling temperature at the surface of the material to be examined has proven a suitable investigation method for this purpose [40]. Nitrogen is often employed as adsorbing agent, since it may be considered inert at the boiling point of 77 K. The inner surface of the adsorbed material may be determined from the increase in weight during adsorption and the knowledge of the spatial requirements of an adsorbing molecule according to the method of Brunauer, Emmet and Teller (BET) [41, 42].

#### 3.3.3.1. Fundamentals on the BET Measurements of Surface Determination, Experimental Arrangement and Measurement Results

Adsorption of the inert gas may be described in certain limits,  $0.05 < \rho < 0.3$ , by the BET straight line:

$$y_g = c_1 g + c_2$$

under the prerequisite that only the first monomolecular layer is bound by the specific surface forces in the multiple-layer adsorption of the inert gas at the surface of the adsorbing agent, while adsorption and desorption of all further layers proceed as for pure liquids. In the equation above (p. 50),  $\rho = p/p_s$  is the relative pressure ( $p_s$  = saturation vapor pressure of the inert gas) and  $c_1, c_2$  are constants, determined from the BET straight lines, for example by a compression calculation.  $y_0$  is obtained from the adsorption isotherms in accordance with BET theory:

$$y_0 = \frac{S}{m_a(1-\rho)}$$

with the mass  $m_a$  of the adsorbed gas, such that the BET equation assumes the form:

$$(m_a(1-\rho))^{-1} = c_1 + c_2(\rho^{-1})$$

From the BET theory, it follows further for the amount of gas  $m_m$ , covering the surface of the adsorbing agent in a monomolecular layer:

$$m_m = (c_1 + c_2)^{-1}$$

The inner surface of the sample may be calculated from this equation and from the spatial requirement  $F_m$  of a molecule being adsorbed (for nitrogen,  $F_m = 16.2 \text{ \AA}^2$ ) [40,43].

$$\theta = m_m N_L F_m / (M \cdot G)$$

where  $N_L$  = Loschmidt number,  $M$  = molecular weight of the adsorbed material and  $G$  = weight of the adsorbing sample.

The experimental studies were carried out in a gassorption-gravimetric of the Sartorius company. The entire set-up of the equipment is presented as a diagram in Fig. 37. The measurement equipment contains two electronic scales of the same design in principle with the scale designated by (1) serving as pressure scale via the measurement of the difference in lift of two lifting objects, while scale (2) is employed for determining the weight of the sample under study. The gas pressure in the equipment may be altered with the aid of a closed-loop circuit automatically in about 100 pressure steps via the pressure scale in the range  $0 \leq p \leq 1$  bar.

During the measurements, the measurement signals of both scales proportional to pressure and sample weight are recorded simultaneously.

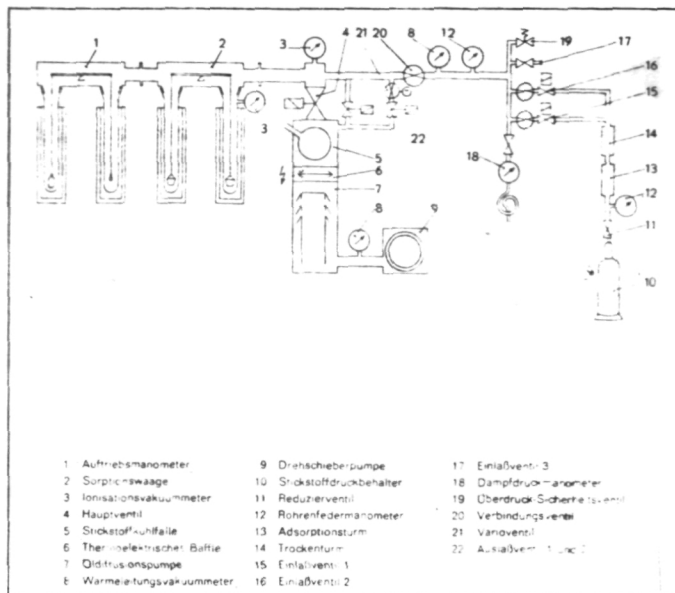


Fig. 37: Diagram of the Gravimetric Adsorption Automatic Equipment.

- Key:
1. lift manometer
  2. adsorption balance
  3. ionization vacuum meter
  4. main valve
  5. nitrogen cooling trap
  6. thermoelectric baffle
  7. oil diffusion pump
  8. heat conduction vacuum meter
  9. rotary push pump
  10. pressurized nitrogen container
  11. reducing valve
  12. bourdon tube manometer
  13. adsorption column
  14. drying column
  15. inlet valve 1
  16. inlet valve 2
  17. inlet valve 3
  18. vapor pressure manometer
  19. pressure safety valve
  20. connecting valve
  21. variovalve
  22. outlet valves 1 and 2

The catalyst samples were reactivated before beginning measurements as usual in 6N KOH at 80° C for 24 hours with hydrogen gas, then rinsed free of alkalis and subsequently introduced into a balance dish of the weight scale while still moist. A piece of solid nickel with approximately the same weight serves as counterweight in order to exclude lifting errors to the greatest possible extent. The surface of the counterweight of several mm<sup>2</sup> may be neglected in relation to the BET surface of the

samples situated around  $10\text{--}100\text{ m}^2/\text{g}$ . The moist sample powder had to be dried before recording the adsorption isotherms at about  $130^\circ\text{C}$  until the weight remained constant, then the sample is thermostated by immersing the glass supports of the weight balance into boiling nitrogen at  $77\text{ K}$ . In contrast, the temperature of the pressure balance is maintained at  $0^\circ\text{C}$  to remain in the validity range of the ideal gas law. Thereafter, the increase and decrease in weight of the sample is measured in steps from  $p = 0$  bar up to the saturation vapor pressure and back to a vacuum. A typical adsorption and desorption isotherm at  $77\text{ K}$  is shown in Fig. 38.

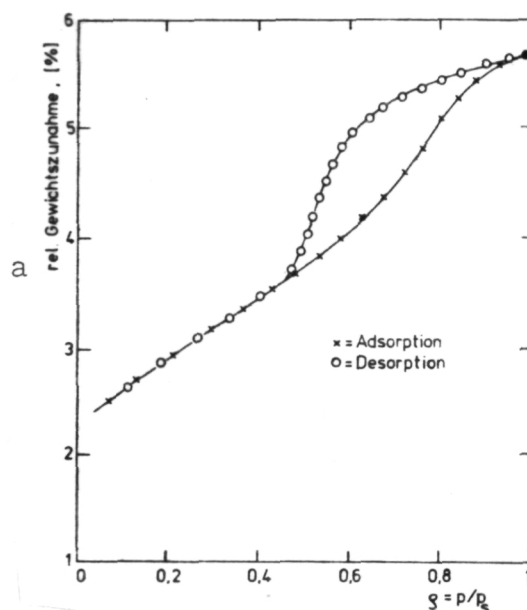


Fig. 38: Adsorption and Desorption Isotherms of a Raney  $\text{NiTi}_2$  Sample at  $77\text{ K}$ .  
Key: a. relative increase in weight.

The percentual increase and decrease in weight of the sample is plotted against the relative pressure  $\rho = p/p_s$ . It can be seen that the adsorption and desorption isotherms coincide in the range of  $0 < \rho < 0.4$ . The inner area of the sample is determined within this range of  $\rho$  via the BET function. The hysteresis occurring at higher relative pressures between the adsorption and desorption branch is a typical indication for sample porosity, while the shape provides information on the type of pore structure. Several remarks are presented on this subject later in connection with the determination of pore distribution.

Since the amount of material adsorbed  $m_a$  is determined via the difference  $m_a = m_p - m_0$  ( $m_p$  = weight of the sample at pressure  $p$ ,  $m_0$  = weight of the sample in a vacuum), it is necessary to determine  $m_0$  precisely for calculating the BET area. In order



to avoid errors through possible chemical adsorption of the first adsorbate layer on the nickel surface,  $m_0$  is determined from the desorption branch at  $p = 0$ . The evaluation of all adsorption measurements was carried out with the computer program prepared by Schmitt [15].

The results of the calculations of the BET area for two catalyst series with an initial  $\text{Ni}(\text{OH})_2$  content of 4.5 % and 17 % is presented in Fig. 39 as a function of tempering time. It can be seen that the initial values of the curves for the untempered samples have approximately the same value of about  $70 \text{ m}^2/\text{g}$  in spite of the very different content  $\text{Ni}(\text{OH})_2$ , a value also indicated by other authors for air-oxidized, non-tempered Raney  $\text{NiTi}_2$ , although with an unknown content of  $\text{Ni}(\text{OH})_2$  [36, 44]. In the tempered samples, the BET area increases slightly with increasing tempering time for both sample series up to a value of about  $\tau \approx 15$  minutes, then a reduction in the BET area is determined, more marked in the catalyst series with an initial content of 4.5 %  $\text{Ni}(\text{OH})_2$  than in the series with 17 % initial content of this nickel hydroxide.

/82

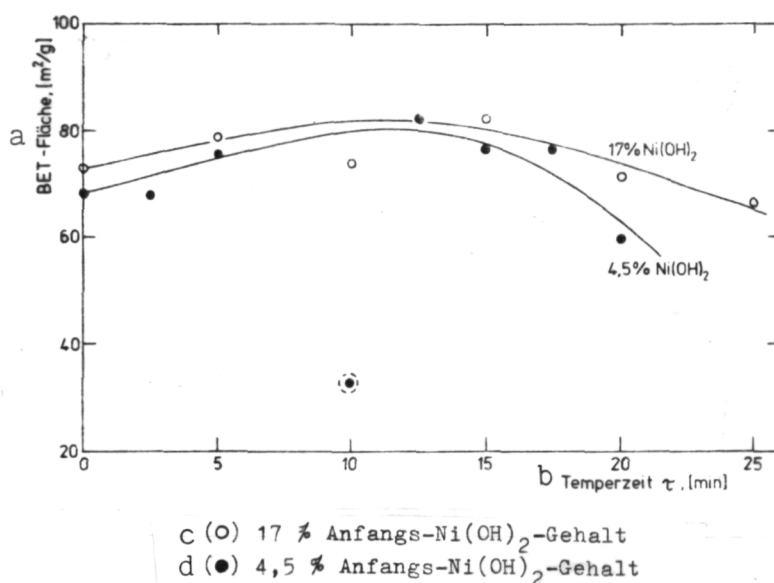


Fig. 39: BET Area of Raney  $\text{NiTi}_2$  Catalysts as a Function of Tempering time.

Key: a. area  
b. tempering time  
c. (o) 17 % initial  $\text{Ni}(\text{OH})_2$  content  
d. (●) 4.5 % initial  $\text{Ni}(\text{OH})_2$  content

The main portion of the inner areas of the catalyst powder is supplied by the so-called traditional pore system, i.e. by pores with radii in the range of  $15\text{-}30 \text{ \AA}$ . The widest pores are therefore still smaller than the finest hydroxide crystals by at least two orders of magnitude, as can be seen in the electron grid microscopic exposures (Fig. 36), such that no substantial contribution to the inner area of the catalyst may be expected

/83

from the outer areas of the hydroxide and NiO crystals; however, the gaps present between the layers of hydroxide containing nitrogen might contribute to the BET area. If the initial value of about 70 m<sup>2</sup>/g of the air-oxidized samples is compared, however, with the BET areas of freshly activated Raney-NiTi<sub>2</sub> (without nickel oxide and nickel hydroxide), situated at 100-120 m<sup>2</sup>/g [45], it must be concluded that the products of oxidation produced for conservation close a considerable portion of the transitional pores on the surface, i.e. lock them by hydroxide and nickel oxide growth in the pores, so that the oxide covering causes a reduction in the BET area on the whole. This explanation also clarifies the slight increase in BET area with increasing tempering time and the accompanying reduction in hydroxide content; apparently, in this process previously closed pores are released once again through the reduction of the  $\alpha$ -Ni(OH)<sub>2</sub> such that these again make a contribution in the inner area. This process is overlapped, however, by the recrystallization of nickel, detected by the electron grid microscope, effecting a correction in the disturbance points of the defective nickel structure and therefore partially a disappearance of the transitional pores. This situation explains the reduction in the BET area in longer tempering times.

Finally, it remains to be mentioned that the effect of tempering time on the inner surface of air-oxidized Raney-NiTi<sub>2</sub> catalysts is in agreement with the results of the other structural studies, but may be designated only as relatively weak on the whole. An exclusive relationship to the comparably considerable alterations in the electrochemical properties cannot be established as a result of the subsequent treatment in hydrogen atmosphere.

### 3.3.3.2. Determination of Pore Distribution

/84

In addition to the determination of the inner area of the sample material, the measurements of the physical gas adsorption and desorption also provide information on the type and distribution of pores in the grains of the catalyst in the range of 20 Å - 200 Å as well as porosity. Several theoretical models for determining the distribution of pore frequency are known from literature, differing with respect to the assumptions made on the adsorbate covering of the pore wall surfaces and the pore shape employed as a basis [46 - 49].

Only two types of the numerous possible pore shapes [50] are significant for Raney NiTi<sub>2</sub> catalysts, specifically cylindrical and spherical pores, where spherical shapes are understood as so-called bottle-neck pores, i.e. pores with a relatively large volume in comparison to a narrow opening at the catalyst surface. Theoretical considerations of these two pore models lead to the idealized adsorption and desorption isotherms in Fig. 40. A comparison with the curve measured under practical conditions (Fig. 38) shows that one type of sample is present in

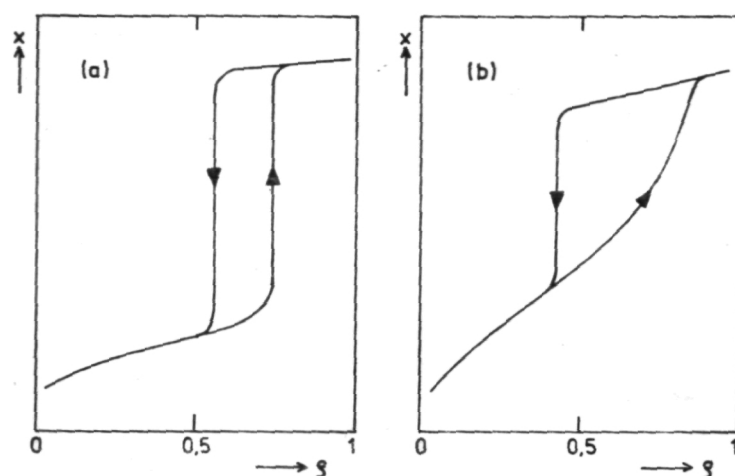


Fig. 40: Idealized Adsorption and Desorption Isotherms for  
a) Cylindrical Pores, b) Spherical Pores.

the catalysts examined, possibly considered as an intermediate form of cylindrical and spherical models, i.e. that both pore shapes exist adjacent to one another but apparently bottle-neck pores are in the majority. Since all measured isotherms can be compared in shape, the determination of precise type of pore is of subordinate significance. In the following, mainly the relative alteration in pore distribution under the effect of tempering will be discussed. The distribution of pore radii was determined with the numerical computer program prepared by Schmitt from the adsorption isotherms. Detailed considerations of the calculations are found in the literature indicated [15, 38, 51]. The results of the measurements of pore distribution of a catalyst series in Figs. 41 and 42. Fig. 41 shows the values calculated from the adsorption isotherms according to the cylindrical model, while the distributions calculated according to the spherical pore model are presented in Fig. 42. The differential pore volume  $\Delta V_p / \Delta r$  is plotted in each case over the pore radius  $r$ . Both for the cylindrical and for the spherical model, a shift in maximum pore frequency to larger pore radii is shown under the effect of tempering; while the most frequent pores in the non-tempered material have radii of less than 20 Å in the cylindrical model or less than 25 Å in the spherical model, the corresponding values for the most frequent pores are situated around 20 Å (cylinder) and 30 Å (sphere) for a tempering time of 10 minutes and at 25 Å or 35 Å, respectively, for the catalyst material tempered for 20 minutes. The shift to greater pore size as a result of tempering is also described through the alteration of the average pore radii, as can be seen in Fig. 43 from the lower curve (c) and the ordinate on the right hand. The average pore radius increases slightly with tempering time from 14 Å to values around 19 Å. The average

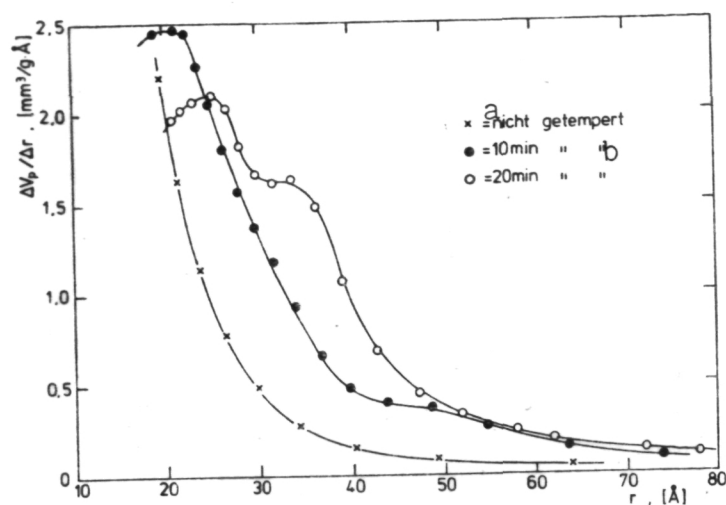


Fig. 41: Pore Distributions of Air-Preserved Raney NiTi<sub>2</sub> Catalysts according to the Cylindrical Model with Tempering Time as parameter.

Key: a. untempered  
b. tempered

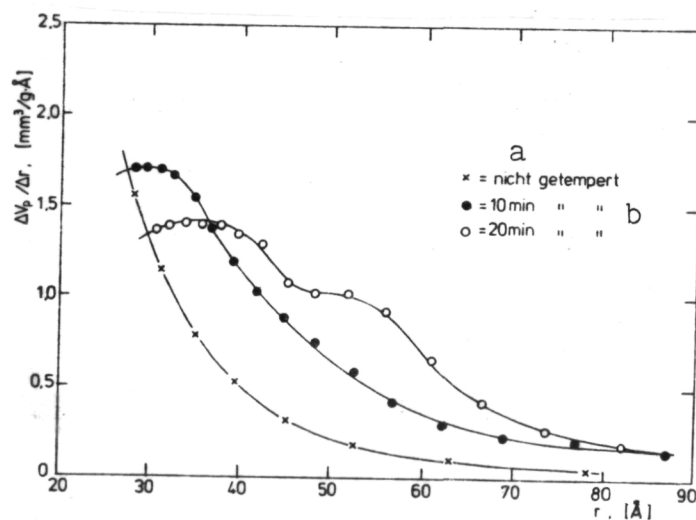


Fig. 42: Pore Distributions of Air-Oxidized Raney NiTi<sub>2</sub> Catalysts according to the Spherical Model with Tempering Time as parameter.

Key: a. untempered  
b. tempered

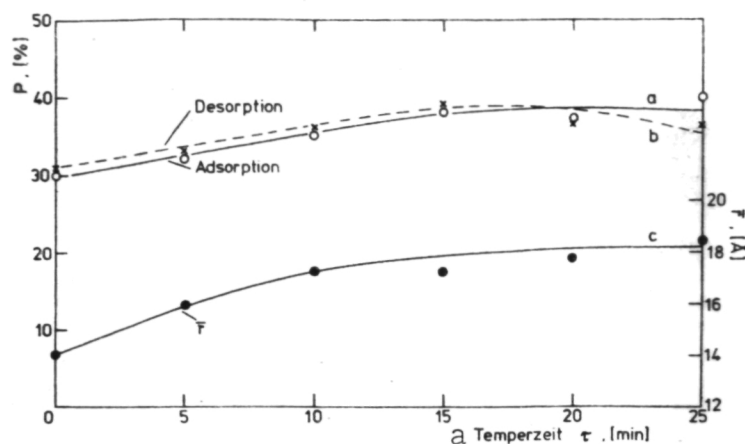


Fig. 43: Transition Porosity (left-hand ordinate, curves a,b) and Averaged Pore Radius (right-hand ordinate, curve c) as a Function of Tempering Time.

Key: a. tempering time

pore radius is determined from the total pore volume  $V_G$  filled with nitrogen in the vicinity of the saturation vapor pressure, the so-called Gurvitsch Volume, through the elementary geometrical relationships:

$$r_{\text{Zylinder}}^a [\text{\AA}] = \frac{2V_G [\text{cm}^3/\text{g}]}{O_{\text{BET}} [\text{m}^2/\text{g}]} \cdot 10^{-4}$$

$$r_{\text{Kugel}}^b [\text{\AA}] = \frac{3V_G [\text{cm}^3/\text{g}]}{O_{\text{BET}} [\text{m}^2/\text{g}]} \cdot 10^{-4}$$

Key: a. cylinder  
b. sphere

The values for cylindrical pores are given in Fig. 43, while the same sequence results for the spherical model, although all values must be multiplied by the factor  $r_{\text{sphere}}/r_{\text{cylinder}} = 1.5$ . The transitional porosity  $P[\%]$  may be determined from the Gurvitsch volume  $V_G [\text{cm}^3/\text{g}]$  with known density  $\delta [\text{g}/\text{cm}^3]$  of the adsorbing agent according to the definition

$$P[\%] = \frac{100[\%]}{1 + \frac{1}{\delta V_G}}$$

The porosity is dependent on tempering time (Figs. 43 a,b) in a course similar to that of the average pore radius; a slight

increase in porosity to a tempering time of approximately 15 minutes is observed, but from there on, P is slowly reduced once again. The maximum change in transitional porosity through the effect of tempering is situated at approximately 25 %.

### 3.3.4. Discussion

/89

The results of the structural studies with Raney NiTi<sub>2</sub> powders with respect to the effect of subsequent treatment of the air-oxidized catalysts in the hydrogen flow at 350° C demonstrate changes of all examined structural parameters. All results are compiled qualitatively in Table 2.1. to permit better evaluation of these changes.

The behavior of the structural parameters under the effect of tempering may be described essentially by two independent processes, with the most noticeable effect being the exponential reduction of  $\alpha$ -3Ni(OH)<sub>2</sub> · 2 H<sub>2</sub>O content with tempering time. In this case, it is possible to prove that a constant hydroxide content of about 3 % is achieved for long tempering times. The reduction in the hydroxide content may be related to the changes in the BET area and the traditional porosity such that the slight increase in the BET area and the enlargement in porosity may be attributed to an increase in the pores released, previously closed more or less by Ni(OH)<sub>2</sub> and therefore not contributing to the nitrogen adsorption. This process is expressed in the electron grid microscopoe exposures as a decrease in the smallest crystallites with a diameter of about 1  $\mu$ m, identified as  $\alpha$ -Ni(OH)<sub>2</sub> on the basis of the layered structure. Parallel to this process, however, recrystallization of the greatly defective catalyst may be mentioned as a second process. The electron grid microscopoe exposures show that this recrystallization has the most clear effect at tempering times of more than 7 - 10 minutes. The reduction in the BET area and porosity with long tempering times may be attributed to this process, since the number of pores, beginning with the smallest radii, becomes less as a result of recrystallization. As a further consequence of this "curing process," the studies of the pore frequency distributions and the averaged pore radii result in a shift of the most frequent pores to larger radii or increasing values of the average pore radii. Apparently, the NiO present on the catalyst surface is also subject to such a curing process. The measurements of the reducible portion of NiO, decreasing with increasing tempering time, can only be explained logically if it is assumed that coarse crystalline nickel oxide, difficult to reduce, is created from reducible NiO to an increasing degree through recrystallization processes insofar as the oxide content of the catalyst does not decrease on the whole during tempering, but this can be excluded by the accompanying spectral-photometrical measurements. It was therefore generally shown that the subsequent treatment of catalysts at 350° C in a hydrogen atmosphere has a stabilizing effect on the catalytically active surface oxides of nickel.

/91

Table 3.1.

/90

Tab. 3.1.

a Struktur- parameter	b Meßmethode	c qualitative Veränderung mit zunehmender Temperzeit ge- genüber dem nicht getemper- ten Ausgangsmaterial
d Ni(OH) <sub>2</sub> - Gehalt	e thermogravi- metrische Messung	f exponentielle Abnahme bis zu einem konstanten Endwert von ca. 3 %
<sup>d</sup> NiO-Gehalt	g Reduktion mit H <sub>2</sub>	h Abnahme des reduzierbaren Anteils, keine Veränderung des Gesamtanteils
i Kristall- struktur	j R E M	k Abnahme feinsten Kristallite (offenbar Ni(OH) <sub>2</sub> ) bis etwa 5 min, danach annähernd kon- stant. Entstehung größerer Nickelkörner durch Rekri- stallisation
l BET-Fläche	q Aufnahme von Gasad- sorptions- und Gasde- sorptions- Isothermen	m mäßiger Anstieg bis ca. 10 - 15 min Temperzeit, da- nach abfallend
n Porenvertei- lung		r Verschiebung der häufigsten Poren zu größeren Porenradien
o gemittelter Porenradius		s monotoner, schwacher Anstieg im Bereich 14 - 20 Å
p transitiona- le Porosität		t leichtes Anwachsen bis 15 min Temperzeit, danach konstant bzw. leicht ab- nehmend

Key:

- a. structural parameter
- b. measurement method
- c. qualitative change with increasing tempering time in comparison to the untempered initial material
- e. content
- d. thermogravimetric measurement
- f. exponential reduction to a constant final value of about 3 %
- g. reduction with hydrogen
- h. reduction of the reducible portion, no change in total proportion
- i. crystalline structure
- j. electron grid microscope

(See following page for continuation of key)



Key for Table 3.1., continued

- k. reduction in finest crystals (apparently  $\text{Ni}(\text{OH})_2$ ) to about 5 minutes, then almost constant. Production of larger nickel grains through recrystallization.
- l. BET area
- m. moderate rise to about 10 - 15 minutes tempering time, then dropping.
- n. pore distribution
- o. averaged pore radius
- p. transitional porosity
- q. exposure of gas adsorption and desorption isotherms
- r. shift in more frequent pores to larger pore radii
- s. monotonous, slight increase in the range of 14 - 20 Å
- t. slight increase to a tempering time of 15 minutes, then constant or slightly decreasing.

4. Long-Term Experiments with Air-Preserved And Hydrogen-Reduced Raney  $\text{NiTi}_2$  Catalysts

---

/92

In order to test the stabilizing effect of tempering in the hydrogen flow on the surface oxides of the catalysts, as recognized from the structural studies, various catalyst powders were introduced into the supported electrodes of customary half-cells (Fig. 9) by sedimentation and tested in galvanostatic constant operations. The catalyst occupation was selected at  $30 \text{ mg/cm}^2$  in order to obtain sufficiently thin electrodes and to insure an even load on the entire catalyst material employed. In order to compare the most possible prepared catalyst samples with one another, i.e. to employ them under the same conditions, the constant current density was selected such that clear deviations from the equilibrium rest potential could be measured, on the one hand, and, on the other hand, the polarizations of less active materials, corrected by the ohmic voltage drop, still remain less than 100 mV in order to achieve a minimum operating duration of about 500 hours with these electrodes. A constant current density of 4 A/g proved a favorable value under these prerequisites for carrying out all following long-term studies if not indicated otherwise. The results of two typical continuous trials are presented in Fig. 44 with air-oxidized Raney  $\text{NiTi}_2$  without tempering (upper curve) and with 5 minutes of tempering in a hydrogen flow (lower curve). The curves demonstrate a very different behavior, already providing information on the parameters to be studied and their effect on long-term slighter initial polarization is also possible as a result of clearly better continuous operation behavior, pointing to a stabilizing effect of tempering, while the effect of the much slight initial polarization is also possible as a result of higher activity of the tempered catalyst. The two parameters will be studied separately. Furthermore, that parameter can be seen in Fig. 44, understood in the following under the concept of "aging rate." The aging rate  $\mu$  represents the average hourly increase in polarization over the first 500 operating hours and is determined for all catalysts from the difference



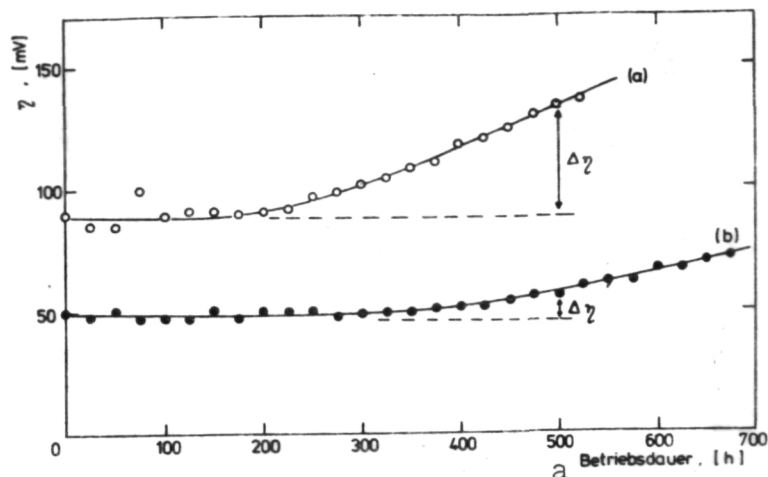


Fig. 44 : Galvanostatic Long-Term Experiment with Untempered (a) Raney  $\text{NiTi}_2$  Catalysts and Such Catalysts Tempered for 5 Minutes at 4 A/g in 6n KOH at 80° C.

Key: a. operating time

$\Delta\eta$  of the initial polarization and the polarization after 500 hours of operating time at

194

$$\mu = \frac{\Delta\eta}{500} \left[ \frac{\text{mV}}{\text{h}} \right]$$

#### 4.1. Long-Term Behavior of Raney $\text{NiTi}_2$ Catalysts as a Function of Operating Temperature

Almost all voltage losses by reaction inhibitions in the anodic hydrogen oxidation may be considerably reduced by increasing operating temperature. A reduction in long-term stability is also ascertained, however, at the same time as is this positive effect. Several electrodes of the same catalyst material were tested at various temperatures in long-term experiments (operating time up to 700 hours) to evaluate the relationship of aging rate and operating temperature more precisely. On the basis of the lower activity of the catalyst at low temperatures, the current density was selected at 2.7 A/g, deviating from the data given above. Fig. 45 shows the results of these studies in the temperature range of 40° - 90° C. The aging rate is indicated with a constant current load as a function of the electrolyte temperature. An almost exponential rise in the aging rate  $\mu$  can be seen with operating temperature of less than  $\mu\text{V/h}$  at 40° C to about 60 - 70  $\mu\text{V/h}$  for electrolyte temperatures around 90° C. The exponential relationship becomes even more clear in the customary semi-logarithmic plotting of  $T \sim \ln \mu$  in Fig. 46. A straight line is a good approximation of the measurement points. It can be seen from the rise

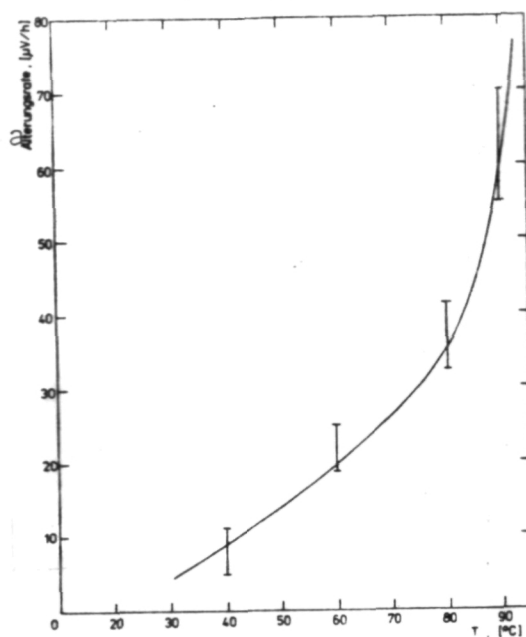


Fig. 45: Relationship of Aging Rate and Electrolyte Temperature with a Current Load of 2.7 A/g.  
Key: a. aging rate

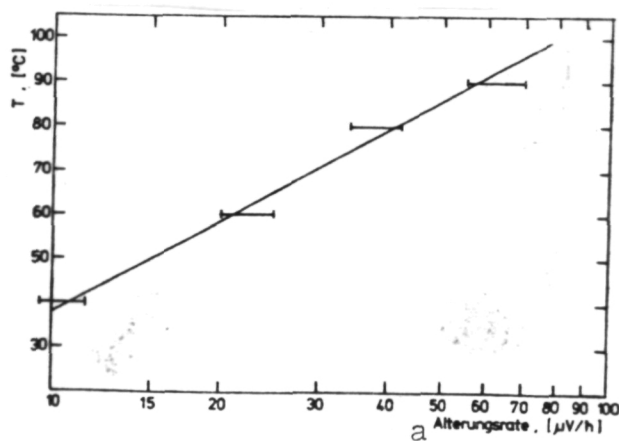


Fig. 46: Semi-Logarithmic Representation of the Relationship between Temperature and Aging Rate for Tempered Raney  $\text{NiTi}_2$  Catalysts.  
Key: a. aging rate

in the straight lines that the aging rate almost doubles with an increase in operating temperature of 20° C. According, procedures for reducing aging receive additional importance in the case of the operating temperatures employed at present of 80° C - 90° C in comparison to the 60° C of earlier fuel cell aggregates. The following long-term trials are therefore also exclusively concentrated on studies at an electrolyte temperature of 80° C.

/96

#### 4.2. Effect of Tempering Time on Long-Term Stability

For the following studies, several series of individual samples of an air-preserved catalyst material with a defined  $\alpha$ -Ni(OH)<sub>2</sub> content, tempered for differing amounts of time, were tested in galvanostatic long-term trials. The measurement results of three representative catalyst series are presented with 3.8 % (curve a), 4.5 % (curve b) and 17 % initial Ni(OH)<sub>2</sub> content (curve c). Because of a lack of space and for reasons of clarity, the potential course of the individual electrodes over operating time is dispensed with, but instead the aging rates gained in accordance with the definition in section 4. from the long-term experiments directly in relationship to tempering time. All three curves, as well as the measurements not provided here for other catalyst series have a common clear minimum of aging rate  $\mu$  at a tempering time around 5 min. It is noticeable that the relative deduction in aging rate, measured against the individual initial material, is more marked with increasing amount of the  $\alpha$ -Ni(OH)<sub>2</sub> content of the basic catalyst. For example, the aging rate is reduced in the catalyst series with a content of 17 % Ni(OH)<sub>2</sub> to 21 % of the value of the untempered initial material on the basis of a tempering time of 5 minutes, while the aging in the series with 4.5 % Ni(OH)<sub>2</sub> is reduced to 45 % and to 76 % of the initial value for a 3.8 % Ni(OH)<sub>2</sub>. The absolute values of the minimum values also drop with increasing content of the basic material of Ni(OH)<sub>2</sub> from 48  $\mu$ V/h (3.8 % Ni(OH)<sub>2</sub>) over 27  $\mu$  V/h (4.5 %) to the extreme low value of 15  $\mu$ V/h for the material with a initial Ni(OH)<sub>2</sub> content of 17 %, tempered for 5 minutes. Tempering times extending beyond 5 - 8 minutes again cause an increase in aging rates in all samples to the comparable values of the individual untempered catalyst or even exceed this value somewhat in very long tempering times.

From the drop in aging rate with short tempering times, it must be concluded that the subsequent treatment of the air-oxidized catalysts at 350° C in a hydrogen flow does indeed exert the desired stabilizing effect on the surface oxide of the catalyst, therefore contributing to a partial extension in life-span of Raney NiTi<sub>2</sub> catalysts. The reinitiation of the rise aging rate with longer subsequent treatment times points to a further aging mechanism. Since all samples tempered for longer than 5 - 8 minutes exhibit less activity and therefore higher polarization with equal load than the corresponding catalyst tempered optimally, the reason for the worsening in long-term behavior may be found in a dependency of aging rate on initial polarization. A quantitative clarification of these

/98

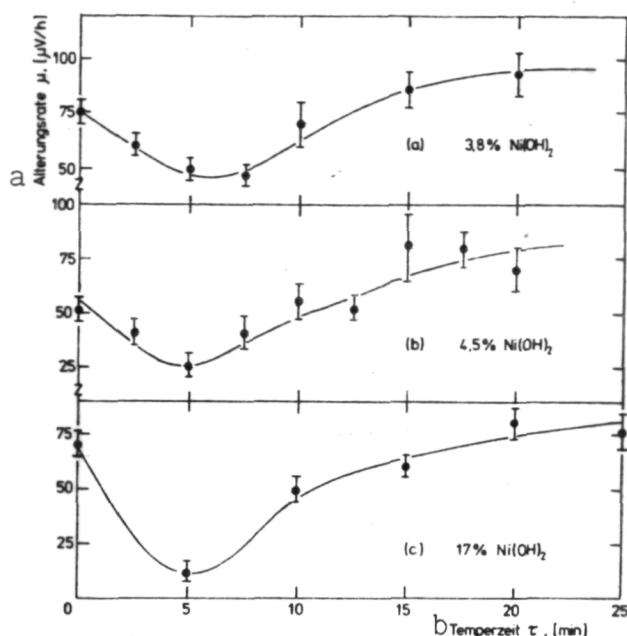


Fig. 47: Aging Rate of Raney  $\text{NiTi}_2$  Catalysts Tempered in a Hydrogen Flow with Different Initial Contents of  $\text{Ni(OH)}_2$  as a Function of Tempering Time.

Key: a. aging rate b. tempering time

relationships will be undertaken in the following section.

#### 4.3. Relationship of Aging Rate and Polarization

Polarization and tempering time may not be considered as independent parameters with respect to the effect on long-term behavior of Raney  $\text{NiTi}_2$  catalysts, but rather there is a functional relationship between the two via the activity of the catalysts so that measurements of polarization relationship on aging rate may only be undertaken at constant tempering time, i.e. only with electrodes of the same catalyst. Because of the determination that temperature remain constant ( $80^\circ \text{C}$ ) and catalyst occupation ( $30 \text{ mg/cm}^2$ ), the variation of the polarization in the fresh electrodes corrected by I-R portion is only possible via current density. Therefore, several identical electrodes with differing constant current densities were subjected to loads in long-term trials, and the measured aging rate correlated to the individual initial polarization of the fresh electrodes. Fig. 48 shows the results of these studies.

The aging rate rises from very low values (smaller than  $5 \mu \text{V/h}$ ) with polarizations of less than 20 mV slowly first, but then after a polarization of about 50 mV with greater acceleration, until it reaches more than  $250 \mu \text{V/h}$  at values

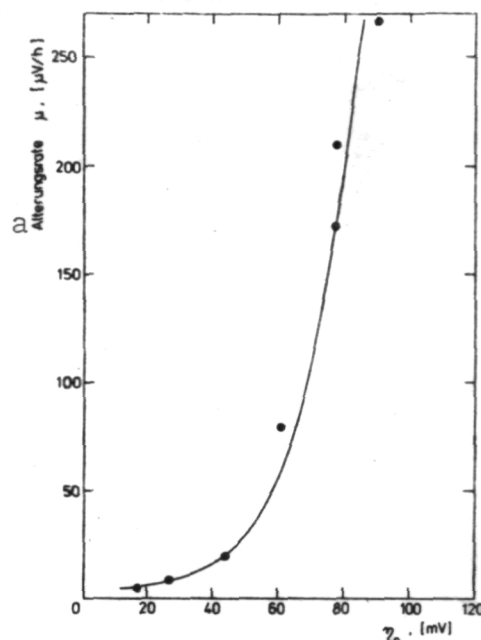


Fig. 48: Aging Rate of Tempered Raney  $\text{NiTi}_2$  Electrodes as a Function of Initial Polarization  $\eta_0$ .  
Key: a. aging rate

of more than 90 mV. The polarization of nickel electrodes may amount to a maximum of 130 mV, because the electrochemical oxidation of nickel begins above this value, but even with an initial polarization of 90 mV, a maximum life-span of about 100 hours may be expected. If the electrodes are operated, on the other hand, with current densities such that the polarization amounts to about 30 mV, operating times up to 10,000 hours may be achieved according to calculations with the resulting aging rate of 10  $\mu\text{V/h}$ . For a correct evaluation of the curves, however, it must be taken into consideration that the electrodes with a higher initial polarization have a corresponding higher output than those with lower polarization. In order to take this relationship into consideration, it is advantageous to take in consideration the time change in polarization resistance  $r_p$  as a function of the overload. For this purpose, the measured values of aging rate are divided by the current density of the individual electrode. Fig. 49 shows the result. Essentially, the same qualitative course of the curve as in Fig. 48 may be seen. However, the drastic increase in aging rate above a critical initial polarization of 50 mV is expressed much more clearly in the change in polarization resistance than by the course of aging rate in Fig. 48. The rate of alteration of resistance even demonstrates an almost constant range with an average value around  $80 \mu\Omega \text{ cm}^2/\text{h}$  for polarizations of less than 45 mV, then assuming the course of a straight line with the rise  $18 \mu\Omega \text{ cm}^2/(\text{h} \cdot \text{mV})$  after a very small transition range.

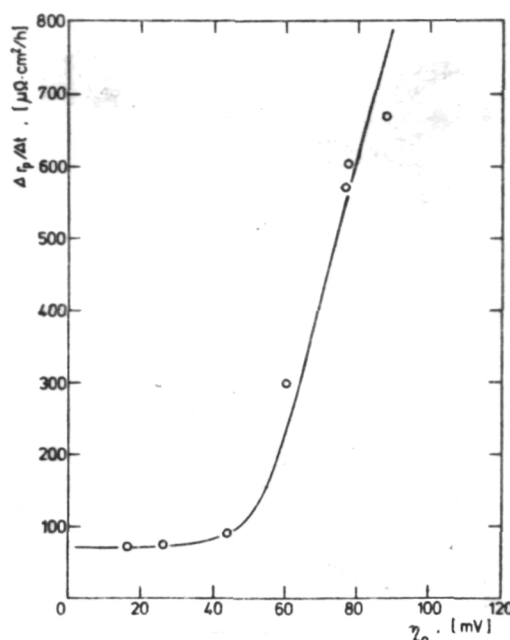


Fig. 49: Temporal Change in Polarization Resistance of  $r_p$  for Raney  $\text{NiTi}_2$  Catalysts as a Function of the Initial Polarization  $\eta_o$ .

Up to now, the measured values for aging behavior were related to the initial polarization  $\eta_o$  at  $t = 0$  of the freshly produced electrode. Since the potential of the electrode passes through all values of the initial polarization  $\eta_o$  up to the first oxidation stage of the nickel, however, during the long-term operations, the relationship of the alteration in polarization  $\partial \eta / \partial t$  and the overload at constant current density is of interest in the course of long-term operations. Therefore, the individual tangent at the curve of the course of potential was determined over operating time for several electrodes at various times and, accordingly, differing polarizations, and the tangent rise plotted against polarization. The curve presented in Fig. 50, representing these results, shows a course analogous to aging rate in relation to initial polarization. In accordance with the previous curves, a critical limit of polarization is ascertained in the vicinity of 50 mV. Below this value, aging rate remains in acceptable limits, but over this value it rises at an accelerated rate up to values of 200  $\mu\text{V/h}$  at a polarization of 90 mV. These measurements quite clearly confirm that the potential or the polarization of a Raney  $\text{NiTi}_2$  electrode exerts a decisive effect on the life-span to the catalysts.

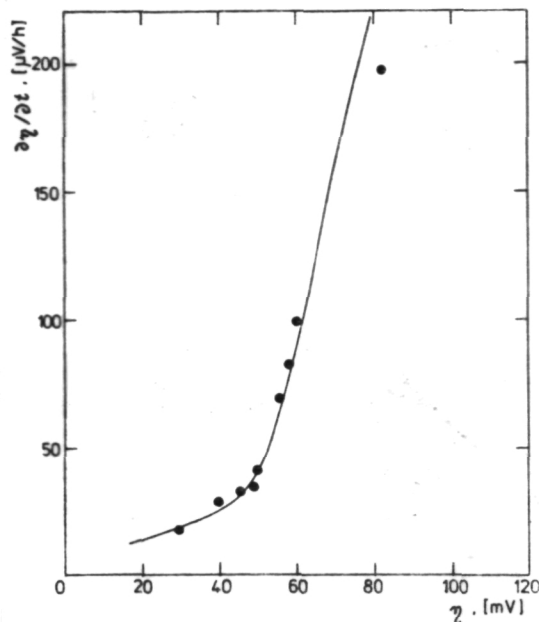


Fig. 50: Change in Polarization  $\partial\eta/\partial t$  as a Function of the Overload Occurring in the Galvanostatic Continuous Operations.

#### 4.3.1. Effect of Occupation Density of the Electrodes on the Long-Term Behavior of Raney NiTi<sub>2</sub> Catalysts

/103

Further long-term experiments were undertaken for completing the studies on aging mechanisms of NiTi<sub>2</sub> catalysts, varying the occupation density in the range 10-150 mg/cm<sup>2</sup> with constant current density of 80 mA/cm<sup>2</sup>. The material tempered for 5 minutes in the sample series with an initial Ni(OH)<sub>2</sub> content of 4.5 % was employed as catalyst. The measurement results in Fig. 51 show a clear drop in aging rate from 300  $\mu\text{V/h}$  at an occupation of 10 mg/cm<sup>2</sup> to about 20  $\mu\text{V/h}$  for 40 mg/cm<sup>2</sup> and approximately a constant course after this value up to occupations above 150 mg/cm<sup>2</sup>.

This strong dependency of aging rate on catalyst occupation, however, is only in the foreground; of course, a variation in polarization is combined with the alteration in electrode occupation at constant current load such that the dependency of aging rate on polarization is obtained implicitly in the present measurement curve. For this reason, the individual initial polarizations  $\eta_0$  are noted at the individual measurement values. When these values and the corresponding aging rates are compared with the course of curve in Fig. 50 and Fig. 48, it can be seen that all value pairs agree well with the indicated diagrams. It can therefore be concluded that the occupation density of electrodes does not have a direct effect on the aging of Raney NiTi<sub>2</sub>

/104

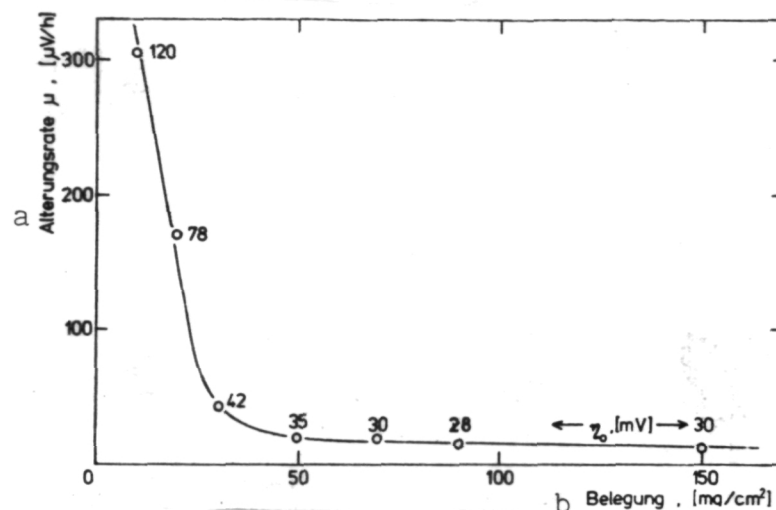


Fig. 51: Aging Rate of Raney NiTi<sub>2</sub> Catalysts as a Function of Occupation Density of the Electodes.

Key: a. aging rate b. occupation

catalysts, although this appears to be the case according to Fig. 51, but rather that the variation in polarization caused by the alteration in occupation mainly affects aging rate. Taking this manner of interpretation into consideration, the present measurement fits well into the studies made up to now on the dependency of aging on polarization and may be considered a further confirmation for these measurements.

#### 4.4. Discussion

The long-term experiments described with air-preserved and hydrogen-reduced Raney NiTi<sub>2</sub> catalysts have essentially produced three results. The aging rate of electrodes proved to be exponentially dependent on temperature in the range of 40 - 90° C as expected. It is noteworthy, however, that the low temperature range of about 20° C with a doubling of aging rate, clearly underlining the necessity for suitable procedures for reducing the aging rate with the present efforts of increasing operating temperatures.

A second result of the long-term experiment is that the subsequent treatment of air-oxidized catalysts in the hydrogen flow represents such a suitable procedure. It was possible to demonstrate that tempering in a hydrogen flow for 5 - 7 minutes may considerably reduce the aging rate in all catalysts with different Ni(OH)<sub>2</sub> content. The cause for this may be seen in the formation of stable surface oxides as were detected in the studies on structural parameters (section 3.), also much more difficult to reduce with negative potentials on the hydrogen

/105



anodes than the oxides produced by simple air oxidation.

Moreover, a further parameter was determined for aging with the aid of additional long-term experiments. The measurements produced a clear effect of polarization on aging rate such that it appears necessary to introduce the concept of a "critical polarization," with the aging rate low below this limit but rapid and accelerated at polarizations above this limit. This critical value was determined at 50 mV for the catalysts examined with an initial  $\text{Ni(OH)}_2$  content of 4.5 % after 5 minutes of tempering. Since the aging rate shows an extremely strong relationship to polarization for polarizations above the critical value, it is possible to consider this as the sole aging parameter and to attempt to explain the alteration in aging rate with tempering time over the differing polarizations of the individual catalysts. The experiments, however, demonstrate that even in electrodes with an initial polarization still far below 50 mV (Fig. 44, curve b) there is a clear minimum at 5 minutes. This behavior may only be explained with the effect of tempering time on the reducibility of surface oxides and therefore on aging rate.

/106

#### 5. Preservation of Raney $\text{NiTi}_2$ Catalysts by Air Oxidation with Subsequent Tempering in a Nitrogen Atmosphere at 300° C

/107

Although tempering air-oxidized Raney  $\text{NiTi}_2$  catalysts in a hydrogen flow may provide a considerable improvement in the long-term behavior of the catalyst, this relatively complicated procedure leads to considerations of simplifying the subsequent treatment by dropping one or more partial steps. This may be carried out, for example, by dispensing with the partial reduction of  $\text{NiO}$  to  $\text{Ni}$  through hydrogen, thereby no longer requiring any renewed air oxidation after concluding tempering. The catalyst must then be tempered in a vacuum or in a protective gas atmosphere instead of in the hydrogen gas to avoid uncontrolled oxidation of the powder. The protective gas atmosphere has the advantage of providing good heat conduction. Nitrogen was employed in the following studies, while other gases, not reacting chemically with the catalyst powder, are also useful.

#### 5.1. Execution of the Studies

Producing the individual catalyst samples tempered for various periods of time was carried out in analogy to the experiments on tempering in a hydrogen flow. The air-oxidized catalyst to be tempered was introduced into a quartz tube in a shuttle inserted into a platinum tube furnace with temperature control. During the heating phase, actual tempering and the cooling phase, subsequently purified nitrogen flowed through the quartz tube. By this means, it was possible to prevent diffusion of oxygen in the tube, on the one hand, and the water produced by the decomposition of the hydroxide was

/108

transported out of the tube, on the other hand. After conclusion of the tempering time, it was possible to bring the non-pyrophorous powder into the air, stir it there and utilize it for manufacturing electrodes.

Electrodes were manufactured with a  $30 \text{ mg/cm}^2$  catalyst occupation, used for recording  $\eta$ -i characteristics at  $80^\circ \text{C}$  and a  $p_{\text{H}_2} = 0.8$  bar after a reactivation of 24 hours in KOH at a temperature of  $80^\circ \text{C}$  in hydrogen atmosphere and then subjected to galvanostatic long-term tests with the same conditions as for the catalysts tempered in hydrogen.

## 5.2. Measurement Results

The  $\eta$ -i characteristics corrected by the I-R portion also proved to be almost straight lines with a rise depending to varying extents on tempering time in catalysts tempered in nitrogen. The representation of the individual characteristics may be dispensed with on the basis of the linear course, the data on current density at constant polarization (100 mV) being sufficient for describing the stationary characteristics.

Correspondingly, Fig. 52 shows the relationship of current density at constant polarization of 100 mV and tempering time of the catalysts. The untempered initial material ( $\tau = 0$ ) has an  $\alpha\text{-Ni(OH)}_2$  portion of 4.5 % and belongs to the most active catalyst material with  $400 \text{ mA/cm}^2$  at 100 mV. It can be seen in Fig. 52 that tempering in a nitrogen atmosphere at times of up to 5 minutes does not have any substantial effect on the activity of the catalysts, while beyond this point the current density is reduced somewhat with tempering time, dropping below  $300 \text{ mA/cm}^2$  at a tempering time of 20 minutes. This drop in current density may be attributed analogously to the measurements of the catalysts tempered in the hydrogen flow on the recrystallization of nickel and curing process of the catalyst with greatly defective structure. In contrast, a corresponding improvement in activity of the samples with short tempering times is not determined.

Immediately after measuring the  $\eta$ -i characteristics, galvanostatic long-term studies were carried out with the same catalysts at  $80^\circ \text{C}$  and a current load of 4 A/g for determination of the individual aging rate. The relationship of the aging rate of a catalyst series to tempering time is presented in Fig. 53. The aging rate increases monotonously over the entire range of the tempering time in the nitrogen flow with the aging rate almost doubling in the range up to 10 minutes tempering time from about  $50 \text{ }\mu\text{V/h}$  to about  $100 \text{ }\mu\text{V/h}$ , but then rising only slightly to about  $105 \text{ }\mu\text{V/h}$  with a tempering time of 20 minutes. No improvement in characteristics of the catalysts is noted in the subsequent treatment in a nitrogen atmosphere at  $300^\circ \text{C}$  even in the long-term studies.

/109

/110

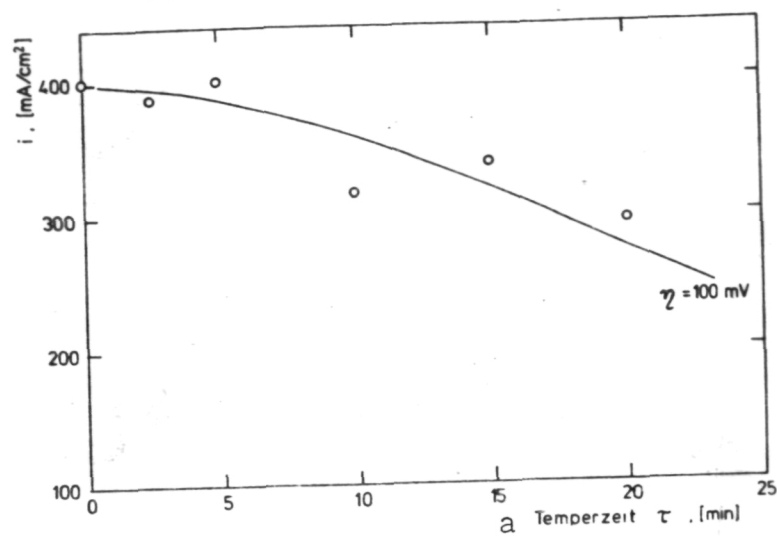


Fig. 52: Current Density with Constant Polarization of 100 mV as a Function of Tempering Time in a Nitrogen Atmosphere.

Key: a. tempering time

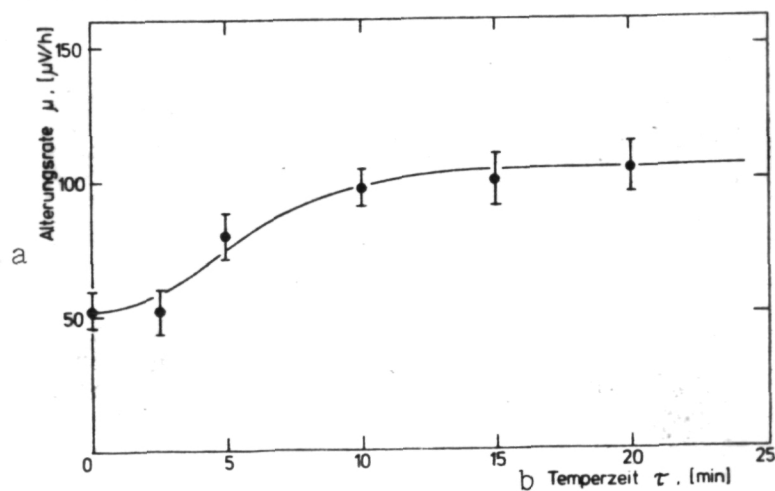


Fig. 53: Aging Rate of Raney  $\text{NiTi}_2$  Catalysts Tempered in Nitrogen as a Function of Tempering Time.

Key: a. aging rate b. tempering time

### 5.3. Discussion

/111

The application of protective gas ( $N_2$ ) in place of hydrogen when tempering Raney  $NiTi_2$  catalysts represents a simplification in preservation procedures insofar as no controlled air oxidation is required after tempering because the reduction of surface oxides is avoided during the subsequent treatment such that a rather problematic treatment step was no longer necessary. The measurement results show, however, that this procedure, simplified in comparison to tempering in the hydrogen flow, does not lead to any improvement in the characteristics with respect to activity and long-term behavior of the catalyst. Apparently, the reduction of the surface oxides and nickel surface in the hydrogen atmosphere, the resulting necessary air oxidation and the subsequent reformation of  $\alpha-Ni(OH)_2$  and  $NiO$  represent essential partial steps for the effects on the catalyst of stabilization and increase in activity. It is demonstrated that the thermal decomposition of the  $\alpha-Ni(OH)_2$  already present in an inert gas atmosphere does not exert this positive effect on the catalyst alone without a subsequent reformation of oxides, such that this procedure is clearly inferior to tempering in a hydrogen flow. For this reason, no further studies were carried out with air-oxidized catalysts tempering in an inert gas.

### 6. Measurements of Impedance

/112

Impedance measurements with electrochemical cells with sine-shaped alternating voltages have become a standard component of study methods in electrochemistry since the first studies of this type at the end of the previous century [32, 53] and are even applied now to actual battery and fuel cell electrodes [53 - 57]. Because modern, highly stable function generators with a frequency range for sine-shaped voltages extend up to  $10^{-3}$  Hz, impedance measurements may also be employed advantageously for gas diffusion electrodes of Raney catalysts. Since this measuring method permits conclusions about the kinetic processes at the phase boundaries of electrolyte/catalyst/reaction gas, it represents a welcome addition to the measurements of stationary and instationary methods of analysis of the  $\eta$ -i characteristics and the exchange current densities.

#### 6.1. Fundamentals of Impedance Measurements

Each electrochemical electrode may be considered as a complex  $Z$  with respect to the alternating current behavior, where  $Z$  may consist of a combination of pure ohmic, capacitive and also inductive partial elements, described in an equivalent circuit diagram by the electric analogs of resistance, capacity and inductivity. In accordance with the relation  $Z = [Z]e^{i\phi}$  the impedance  $Z$  of the electrode may be determined by measuring the amount  $[Z] = \frac{U_0}{I_0}$  and of the phase angle  $\phi$  between

$$\frac{U_0}{I_0}$$

the applied alternating current  $U = U_0 \sin(\omega t)$  and the resulting current  $I = I_0 \sin(\omega t + \phi)$  as a function of the circuit frequency  $\omega = 2\pi\nu$ . An attempt is now made, using the measured curves of the impedance amount  $[Z]$  and the phase angle  $\phi$  as a function of the circuit frequency  $\omega$ , to develop a suitable equivalent circuit diagram, approximating the measured values by calculation as precisely as possible, on the one hand, but limited, on the other hand, only to such circuit elements, practically representing the physical processes at the triple-phase boundary of the electrode. The combination of pure ohmic with capacitive elements proves sufficient [58] in the case of Raney  $\text{NiTi}_2$  catalysts in the equivalent circuit diagram.

/113

In addition to the ideal, loss-free capacities with the impedance  $Z_C = 1/i\omega C$ , capacities involving losses may also generally occur. In the simplest case, these losses may be taken into consideration by a resistance  $\hat{R}$  in a parallel circuit with the capacitor  $\hat{C}$ , where this partial impedance now amounts to  $\hat{Z}_C = \hat{R}/(1 + i\omega \hat{R}\hat{C})$  and the problem is returned to that of the ideal capacitor  $\hat{C}$ . Moreover, the introduction of a loss capacitor  $C^*$  with loss angle independent of frequency  $\frac{P\pi}{2}$ ; ( $0 \leq P \leq 1$ ) and the impedance  $Z_C^* = 1/C^*(i\omega)^{1-P}$  is ad-

vantageous in some cases [59]. Capacities are described by this method with a value apparently dependent on frequency in the form  $C^* = C/\omega^P$ . Recharging processes at electrochemical double layers or adsorption processes at electrodes are mentioned as example, having an insufficient penetration depth of the current threads into the pores at higher frequencies because of the porous structure of the catalyst, and then only including the extreme pore areas near the mouth of the pore, equated with an apparent reduction in capacity values. The possibility of such problems must be taken into consideration in the development of an equivalent circuit diagram and the evaluation of the impedance centers. Please see the literature [53, 60-63] for the treatment of further impedances not occurring in Raney  $\text{NiTi}_2$  catalysts (Young and Nernst impedance, etc.).

/114

## 6.2. Equivalent Circuit Diagram for Porous Raney $\text{NiTi}_2$ Electrodes

The impedance accessible to measurements for a supported, porous Raney  $\text{NiTi}_2$  electrode is the result of a variety of parallel and series circuits of impedances of the individual catalyst grains and pore sections. Under the assumption that the current load is distributed evenly along the entire catalyst material and that the relationship of the electrolytic diaphragm resistance of the powder filling against a measured impedance may be neglected (both is the case for this electrode), the sum of all individual impedances of the catalyst grains may be described by the impedance of the equivalent circuit diagram of a supported gas diffusion electrode as indicated in Fig. 54 [28,58]. In this case,  $R_0$  signifies the sum of the electrolyte resistance between catalyst filling and Luggin probe and contact resistances occurring on the gaseous side,  $R_1$  is the passage resistance and  $C_1$  the double-layer capacity. The parallel circuit

/115

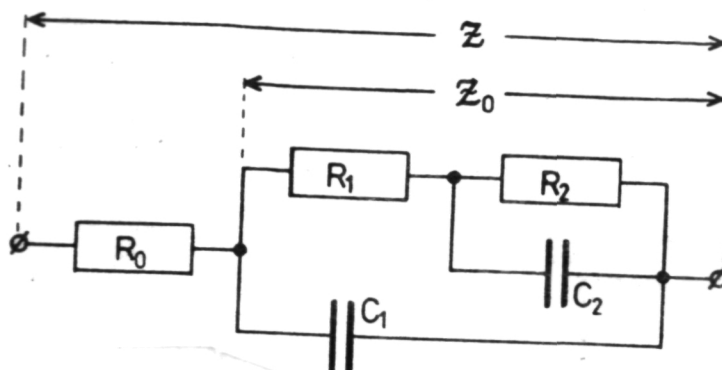


Fig. 54: Equivalent Circuit Diagram of a Supported Gas Diffusion Electrode.

of diffusion resistance  $R_2$  and chemical adsorption capacity  $C_2$  takes into consideration the subsequent supply of the hydrogen discharged at the triple-phase boundary through dissociative adsorption.

Generally, the elements of the equivalent circuit diagram indicated in Fig. 54 depend on the circuit frequency  $\omega$  of the applied alternating current; however, studies by Mund [56, 58] and estimations of the penetration depth of the alternating current into the catalyst pores by Schröder [51] show that the entire catalyst grain ( $< 50 \mu\text{m}$ ) is included in the measurement of alternating current at low frequencies ( $< 50 \text{ Hz}$ ) and the individual elements of the equivalent circuit diagram may be considered in a good approximation as independent of frequency. A simple procedure will be described later for the capacities  $C_1$  and  $C_2$ , permitting a test of the correctness of this assumption.

#### 6.2.1. The Impedance of the Supported Gas Diffusion Electrode

The complex impedance for the equivalent circuit diagram indicated in Fig. 54 is expressed as :

$$(1) \quad Z(\omega) = \left\{ \left[ (i\omega C_2 + \frac{1}{R_2})^{-1} + R_1 \right]^{-1} + i\omega C_1 \right\}^{-1} + R_0$$

After carrying out the calculations, the following is obtained:

$$(2) \quad Z(\omega) = \frac{R_1 + R_2 + i\omega R_1 R_2 C_2}{1 - \omega^2 R_1 R_2 C_1 C_2 + i\omega(R_1 C_1 + R_2 C_2 + R_2 C_1)} + R_0$$

Since  $\omega \rightarrow \infty$ ,  $Z(\infty) = R_0$  results for high frequencies, it is sufficient for further calculations to consider only that

portion  $Z_0$  of the impedance  $Z$ , describing the network of  $R_1$ ,  $R_2$ ,  $C_1$  and  $C_2$ . It is easy to verify that the following relationships apply:

$$(3) \quad |Z_0| = |Z| - R_0, \quad \text{Im } Z_0 = \text{Im } Z, \quad \text{Re } Z_0 = \text{Re}(Z - R_0) = \text{Re } Z - R_0$$

It follows from equation (2) by a separation into the real and imaginary portions

$$(4) \quad Z_0(\omega) = \Delta(\omega) (R_1 + R_2 + \omega^2 R_1 R_2^2 C_2^2) - i \Delta(\omega) \omega (\omega^2 R_1^2 R_2^2 C_1 C_2^2 + C_1 (R_1 + R_2)^2 + R_2^2 C_2) \\ \Delta(\omega) = \left\{ (1 - \omega^2 R_1 R_2 C_1 C_2)^2 + \omega^2 (R_1 C_1 + R_2 C_2 + R_2 C_1)^2 \right\}^{-1}$$

Since both the real and the imaginary portions may be calculated from the measured impedance and the phase angle  $\phi$  in accordance with the relationships

$$\text{Im } Z_0 = |Z| \sin \varphi \quad \text{und} \quad \text{Re } Z_0 = |Z| \cos \varphi - R_0$$

in principle there is a possibility of adapting the measured values as precisely as possible to the theoretical course of the real and imaginary portions by varying the network elements  $R_1, C_1$ , thereby determining  $R_1, R_2, C_1$  and  $C_2$ . The corresponding expressions for real and imaginary portions in equation (4) are still so complex, however, that a compensation calculation according to the method of the smallest error squares has hardly any chance of success with a justifiable amount of work. Therefore, an attempt must be made to simplify these expressions, at least for a partial area of the frequency spectrum examined. For low frequencies  $\omega \rightarrow 0$ , the results from equation (4) when neglecting all members, containing the circuit frequency in a higher order than  $\omega^2$ :

$$(5) \quad \text{Im } Z_0(\omega) \xrightarrow{\omega \rightarrow 0} \frac{\alpha \omega}{1 + \beta \omega^2} \\ \alpha = C_1 (R_1 + R_2)^2 + R_2^2 C_2 \\ \beta = C_1^2 (R_1 + R_2)^2 + R_2^2 C_2^2 + 2 R_2^2 C_1 C_2$$

Correspondingly, the results for low frequencies of the real portion are

$$(6) \quad \text{Re } Z_0(\omega) = \frac{R_1 + R_2 + \gamma \omega^2}{1 + \beta \omega^2} \quad \gamma = R_1 R_2^2 C_2^2$$

With these simplifications, it should be determined whether the real and imaginary portions correlate with one another in



the indicated manner for the area of low frequencies, i.e. whether they directly describe the impedance behavior of the network indicated in Fig. 54 for  $\omega \rightarrow 0$ . If the real and imaginary portion of a complex quantity are dependent on frequency, they are then connected via the Kramers-Kronig (K-K) relations [64, 65]. According to Meierhaege et al. [66], there is between  $R_S$  and  $C_S$  of an impedance  $Z_S = R_S - \frac{i}{\omega C_S}$ , where  $R_S$  represents the

sum of the ohmic portions and  $C_S$  that of the capacitive portions, the following relationship resulting from the K-K relations:

$$(7) R_S(\omega) - R_S(0) = \frac{2\omega^2}{\pi} \int_0^{\infty} \left( \frac{1}{x^2 C_S(x)} - \frac{1}{\omega^2 C_S(\omega)} \right) \frac{dx}{x^2 - \omega^2}$$

The circuit frequency  $\omega$  has the significance of a parameter in this case and  $x$  that of the variable frequency. Furthermore,  $R_S(\omega) = \text{Re } Z_0(\omega)$  and from equation (4)

$$R(0) = \lim_{\omega \rightarrow 0} \text{Re } Z_0(\omega) = R_1 + R_2.$$

when the imaginary portion of  $Z_S$  is compared with equation (50),  $C_S$  results at:

$$(8) C_S = \frac{1}{\alpha} \left( \frac{1}{\omega^2} + \beta \right)$$

inserted into (7), the result is

$$(9) \text{Re } Z_0(\omega) - (R_1 + R_2) = \frac{2\omega^2}{\pi} \int_0^{\infty} \left( \frac{\alpha}{1+x^2\beta} - \frac{\alpha}{1+\omega^2\beta} \right) \frac{dx}{x^2 - \omega^2}$$

and from this, after partially taking apart the fraction

$$(10) \text{Re } Z_0(\omega) - (R_1 + R_2) = - \frac{2\alpha\beta\omega^2}{\pi(1+\beta\omega^2)} \int_0^{\infty} \frac{dx}{1+x^2\beta}$$

Carrying out the integration and insertion of the limits results in:

$$(11) \text{Re } Z_0(\omega) - (R_1 + R_2) = - \frac{2\alpha\sqrt{\beta}\omega^2}{\pi(1+\beta\omega^2)} \text{arctg}(x\sqrt{\beta}) \Big|_0^{\infty} = - \frac{\alpha\sqrt{\beta}\omega^2}{1+\beta\omega^2}$$

and therefore:

$$(12) \text{Re } Z_0(\omega) = \frac{R_1 + R_2 + \omega^2((R_1 + R_2)\beta - \alpha\sqrt{\beta})}{1 + \beta\omega^2} = (R_1 + R_2) \frac{1 + \omega^2\left(\beta - \frac{\alpha\sqrt{\beta}}{(R_1 + R_2)}\right)}{1 + \omega^2\beta}$$



Therefore, it is demonstrated that equation (12) formally has the same form as (6), although the equality of

/119

$$(R_1 + R_2)\beta - \alpha\sqrt{\beta}$$

and  $\gamma$  is not directly proven; however, the numerical calculations of both expressions with the values determined for  $R_1$ ,  $C_1$  (section 6.4.2, 6.5.) demonstrate sufficient agreement. Furthermore, these calculations show that both  $\gamma/(R_1 + R_2)$  as well as

$$(\beta - \alpha\sqrt{\beta}) / (R_1 + R_2)$$

are small in comparison to  $\beta$ , so the equation (12) may be simplified further for  $\omega \rightarrow 0$  in an approximation

$$(13) \quad \operatorname{Re} Z_0(\omega) = \frac{R_1 + R_2}{1 + \omega^2 \beta}$$

### 6.2.2. Local Curve Representation

It has now become possible with equations (5) and (13) to determine the theoretical course of the local curve in the complex Gaussian numerical plane for low frequencies. By eliminating  $(1 + \beta\omega^2)$  from equations (5) and (13) and solving for the imaginary portion, the result for  $\omega \rightarrow 0$  is

$$(14) \quad -\operatorname{Im} Z_0(\operatorname{Re} Z_0, \omega) = \frac{\alpha \omega}{R_1 + R_2} \operatorname{Re} Z_0$$

Eliminating  $\omega$  with the aid of (13) leads to the local curve

$$(15) \quad \begin{aligned} \operatorname{Im} Z_0 &= f(\operatorname{Re} Z_0) \\ -\operatorname{Im} Z_0(\operatorname{Re} Z_0) &= \frac{\alpha \operatorname{Re} Z_0}{(R_1 + R_2)\sqrt{\beta}} \sqrt{\frac{R_1 + R_2}{\operatorname{Re} Z_0} - 1} = \\ &= \frac{\alpha}{(R_1 + R_2)\sqrt{\beta}} \sqrt{\operatorname{Re} Z_0 (R_1 + R_2 - \operatorname{Re} Z_0)} \end{aligned}$$

This is the form of the negative portion of an ellipse situated symmetrically to the real axis in the complex numerical plane with the axial relationship  $a/b = \alpha / (R_1 + R_2)\sqrt{\beta}$  and the points of intersection 0 and  $R_1 + R_2$  on the positive real axis for the impedance  $Z_0$  and with the points of intersection  $R_0$  and  $R_0 + R_1 + R_2$  for the impedance  $Z$ . The special case of the semi-circle is obtained by setting  $R_2$  approximately equal to zero, equivalent to the equivalent circuit diagram of the parallel circuits of passage resistance and double-layer capacity.

/120

### 6.3. Equivalent Circuit Diagram for Raney NiTi<sub>2</sub> Electrodes Without Hydrogen Diffusion

In the case of the electrode immersed in the electrolyte without hydrogen gas under excess pressure, no diffusion of hydrogen to the location of reaction is possible with the exception of a negligible diffusion from the electrolyte, and the diffusion resistance  $R_2$  in Fig. 54 approaches infinity. The alternating current behavior of the electrode may therefore be described by the impedance of the equivalent circuit diagram indicated in Fig. 55. For  $\omega \rightarrow \infty$ ,  $\tilde{Z}$  again assumes the value  $R_0$ , such that only impedance  $\tilde{Z}_0$  must be determined. The calculation of

$$(16) \quad \tilde{Z}_0 = [(i\omega C_2)^{-1} + R_1]^{-1} + i\omega C_1)^{-1}$$

after multiplication of the numerator with the conjugated complexes leads to

$$(17) \quad \tilde{Z}_0 = \frac{\omega R_1 C_2^2 - i(C_1 + C_2 + \omega^2 R_1^2 C_1 C_2^2)}{\omega^3 R_1^2 C_1^2 C_2^2 + \omega(C_1 + C_2)^2}$$

/121

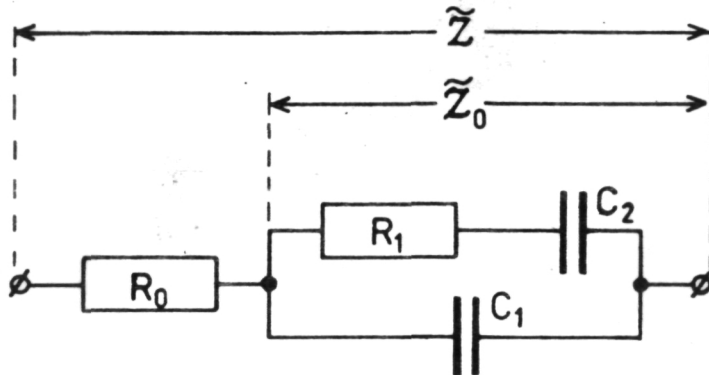


Fig. 55: Equivalent Circuit Diagram of a Supported Gas Diffusion Electrode without Excess Reaction Gas Pressure, i.e. with Pores Completely Filled by the Electrolyte.

From this, the result for the boundary transition  $\omega \rightarrow 0$  for the imaginary portion of  $\tilde{Z}_0$  is

$$(18) \quad \omega \rightarrow 0 : -I_m \tilde{Z}_0(\omega) = \frac{C_1 + C_2}{\omega(C_1 + C_2)^2} = \frac{1}{\omega(C_1 + C_2)}$$

The impedance measurements with immersed electrodes without excess hydrogen pressure therefore permit a determination of the sum of chemical adsorption and double-layer capacity in a simple manner. Moreover, equation (18) may be employed to determine whether  $C_1$  and  $C_2$  are independent of frequency in the validity range of equation (18). In the double logarithmic representation

$$\ln(I_m \tilde{Z}_0) = f(\ln \omega)$$

equation (18) produces a straight line with the rise  $m = -1$

$$\ln(I_m \tilde{Z}_0) = -\ln \omega - \ln(C_1 + C_2)$$

Loss capacities with the frequency relationship  $C^* = C\omega^{-p}$  ( $0 \leq p \leq 1$ ) lead in contrast to a straight line with the rise  $m = -(1-p)$  in the double logarithmic representation according to Grofov and Pekar [67].

/122

Fig. 56 presents the double logarithmic plotting

$$\ln(I_m \tilde{Z}_0) = f(\ln \nu)$$

for two Raney  $\text{NiTi}_2$  electrodes with catalyst occupation of  $10 \text{ mg/cm}^2$  without excess hydrogen pressure.

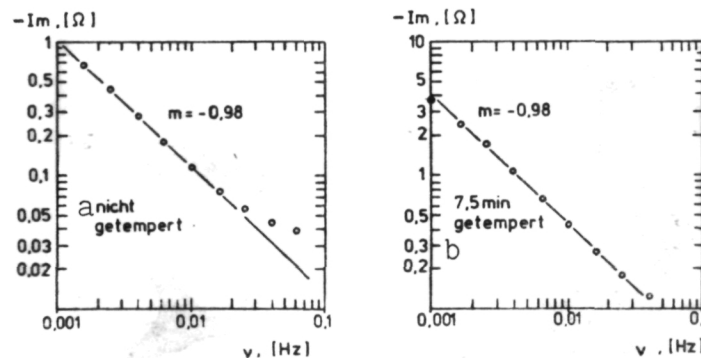


Fig. 56: Double Logarithmic Representation of an Untempered Raney  $\text{NiTi}_2$  Electrode and Such an Electrode Tempered for 7.5 Minutes without Excess Hydrogen Pressure.

Key: a. untempered b. tempered

It can be seen that the straight lines exhibit the rise  $m \approx -1$ , making the assumption of independence from frequency of the elements in the equivalent circuit diagram for low frequencies seem justified.

/123

#### 6.4. Description of the Experiment

The measurements of impedance were carried out with several Raney  $\text{NiTi}_2$  electrodes of the series with an initial  $\text{Ni(OH)}_2$  content of 4.5 % with an electrolyte temperature of  $80^\circ \text{C}$ , a catalyst occupation of  $10 \text{ mg/cm}^2$  and the potential of 50 mV against  $\text{H}_2$  rev. both in an immersed condition and with a slight excess hydrogen pressure (0.1 bar).

##### 6.4.1. Arrangement of the Measurement Equipment for Alternating Current Measurements

The arrangement of the measuring equipment, as it was employed for impedance measurements, is presented in Fig. 57. The working electrode AE of the electrochemical cell Z to be examined is maintained at a preselected desired potential in relation to the reference electrode RE with a potentiostat (type: Wenking 66 TS 1). In addition to an alternating current in the range of  $0 - 10 V_{\text{eff}}$  and  $10^{-3} - 10^{-4} \text{ Hz}$ , the internal desired voltage source of the potentiostat may be applied with the aid of the sine generator via the voltage separator  $P_1$  inserted in the potential measurement branch. The cell current produced by the desired voltage alteration causes a voltage difference proportional to the current at the resistor  $R_x$  with the same phase length and is registered optionally as the sine-shaped potential modulation with a 2-line recorder (Bryans 2600) for frequencies of less than or equal 1 Hz or with a lock-in amplifier (PAR, 124 A) for frequencies of greater than or equal 1 Hz.

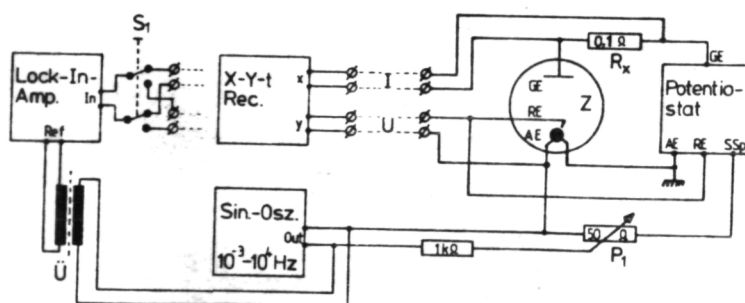


Fig. 57: Circuit Diagram of the Impedance Measuring Stand.

The reference signal necessary for the correct function of the lock-in amplifier is decoupled by the transmitter U at the sine generator and supplied to the reference input of the amplifier. The complicated function of the lock-in amplifier will be explained only in the components important for impedance measurements. The measurement signal reaching the input of the lock-in amplifier is displayed as effective value on the instrument after internal amplification; simultaneously, it is possible

to compensate reference and measurement signal to the same phase position with the aid of a built-in variable phase-shift circuit, while the calibration of the potentiometer provided for compensation permits the determination of phase difference between measurement and reference signals with an accuracy of 0.1 degree. The desired phase angle between  $U$  and  $I$  is obtained by the formation of difference in the phase differences of the current and voltage signal to the reference signal. Dividing the measured effective values provides the amount of impedance  $|Z| = \frac{U_{eff}}{I_{eff}}$ .

/125

The lock-in amplifier employed is designed for a frequency range of 0.2 Hz - 210 kHz, but the transmitter limits the lower frequency to 1 Hz, while parallel capacities have a disturbing effect on the electrode and lines above 10 kHz.

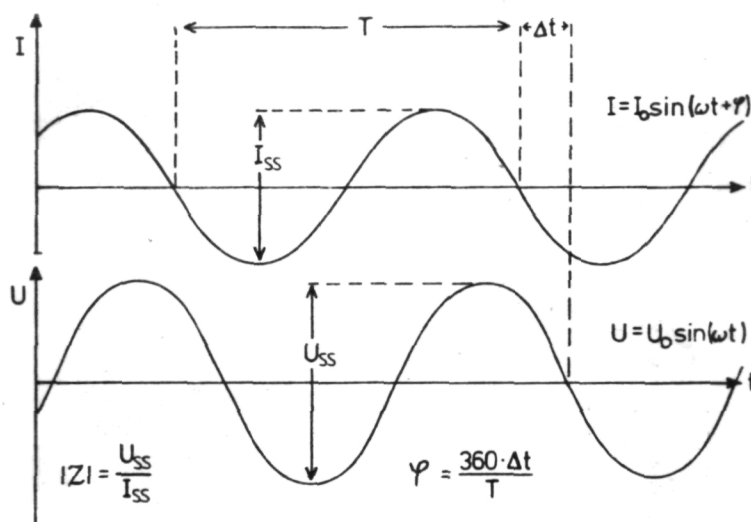


Fig. 58: Representation of the Course in Time of the Current (top) and Voltage Signals (bottom) Recorded Simultaneously with a 2-Line Recorder.

Below 1 Hz, a double-line recorder with variable time deflection serves a recording device for recording voltage and current signal synchronously as can be seen in Fig. 58. The difference in phase of both signals may be read directly at the zero passages of the sine oscillations shifted in time.  $\rho$  is obtained according to

/126

$$\varphi = \frac{360^\circ \cdot \Delta t}{T}$$

with  $\Delta t$  = difference in time of the zero passages,  $T$  = oscillation duration and the amount of impedance in accordance with

$$|Z| = \frac{U_{ss}}{I_{ss}}$$

The shift present in the  $t$  direction for both styluses amounting to about 3 mm is also taken into consideration in Fig. 58.

#### 6.4.2. Evaluating the Measurement Results

The real and imaginary portion are determined as a function of the circuit frequency  $\omega$  in accordance with the relation

$$\tilde{Z} = \text{Re } \tilde{Z} + i \text{Im } \tilde{Z} = |\tilde{Z}|(\cos \varphi + i \sin \varphi)$$

from the measurements of the impedance and phase cycle. A typical course of a real and an imaginary portion of a Raney NiTi<sub>2</sub> electrode may be seen in Fig. 59 with 10 mg/cm<sup>2</sup> catalyst occupation at a polarization of 50 mV, excess hydrogen pressure of 0.1 bar and temperature of 80° C. It can be seen that the interesting course of the curve is situated in the frequency range below 0.1 Hz, the maximum of the imaginary portion is even situated below 0.02 Hz. Accordingly, the equations (5) and (13) derived for small frequencies may be employed for evaluating the curves. The local curve representation in Fig. 60 confirms this situation again, clearly showing the theoretically derived elliptical course of the curve of  $\text{Im} = f(\text{Re})$  from equation (15). By comparing the theoretical curve according to equation (15) with the measured values, the values for  $R_0$  and  $\rho = R_1 + R_2$  are obtained directly from Fig. 60. When an adjustment of the theoretical curve is further carried out by varying the parameter of the measured values, for example according to the method of the smallest error squares [68, 69], for the imaginary and real portion [Fig. 59) taking into consideration equations (5) and (13), both parameters  $\alpha$  and  $\beta$  are obtained as the best approximation of the measured values. The equation system is then achieved with (5):

$$\begin{aligned} \alpha &= C_1(R_1 + R_2)^2 + C_2 R_2^2 \\ (19) \quad \beta &= C_1^2(R_1 + R_2)^2 + C_2^2 R_2^2 + 2R_2^2 C_1 C_2 \\ \rho &= R_1 + R_2 \end{aligned}$$

This system is underdetermined, such that a further determination equation must be found for solving the equation, obtained for example by measuring the impedance  $\tilde{Z}$  of the electrode without excess hydrogen pressure. According to equation (18), the imaginary portion of

for the range  $\omega \rightarrow 0$  assumes the form:

$$\text{Im } \tilde{Z}_0 = - \frac{1}{\omega(C_1 + C_2)}$$

/ 128

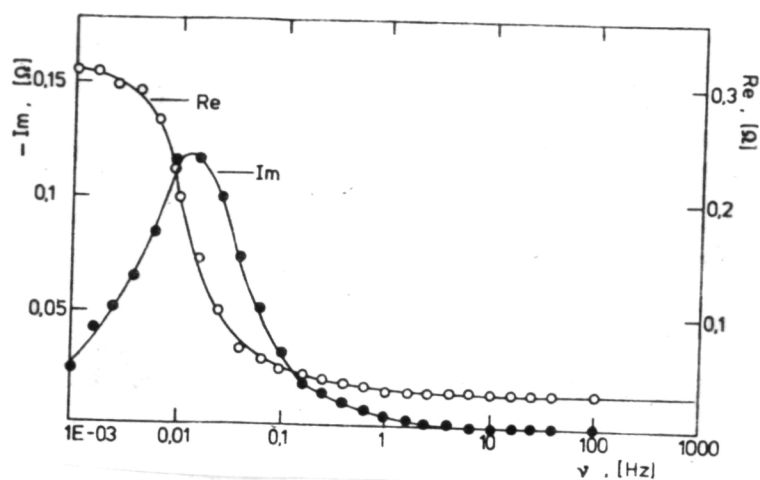


Fig. 59: Frequency Relationship of Real and Imaginary Portions of the Impedance in a Raney  $\text{NiTi}_2$  Electrode with  $10 \text{ mg/cm}^2$  Catalyst Occupation, 50 mV Polarization and 0.1 bar  $\text{H}_2$  Excess Pressure in 6n KOH at  $80^\circ \text{C}$ .

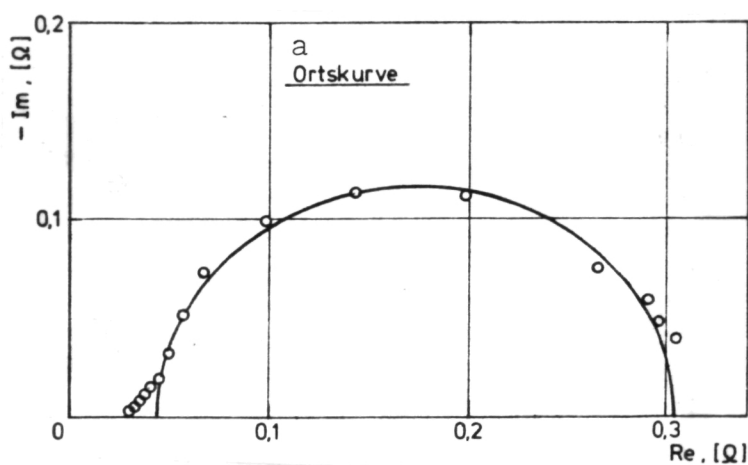


Fig. 60: Local Curve Representation of the Measured Values from Fig. 59.

Key: a. local curve.

Therefore, when the measured values for the imaginary portion are plotted against  $1/\omega$ , a straight line is obtained for low frequencies with the rise  $\varepsilon = -1/(C_1 + C_2)$ , thereby determining the equation system (19) and clearly solving it for  $R_1$ ,  $R_2$ ,  $C_1$  and  $C_2$ . By inserting the appropriate expressions, it can be easily verified that

$$(20) \quad \begin{aligned} C_1 &= \frac{\beta + \alpha/x}{\alpha + g^2/x} & C_2 &= -\frac{1}{x} - C_1 \\ R_2 &= \sqrt{\frac{\alpha - C_1 g^2}{C_2}} & R_1 &= g - R_2 \end{aligned}$$

Therefore, it has become possible to determine all network parameters in correspondence with Fig. 54 via the coefficients  $\alpha, \beta, \rho, \varepsilon$  gained from the impedance measurements.

/129

The courses of the curves of the real and imaginary portions are calculated in accordance with equation (4), i.e. without limitation to lower frequencies, and recorded with a digital plotter (Philips PM 8151) together with the values gained from the measurements in order to test the results gained by the evaluation procedure described with the aid of a small computer (Commodore PET 2001). The functions

$$\begin{aligned} |Z|(\omega) &= \sqrt{\text{Re}^2 Z_0(\omega) + \text{Im}^2 Z_0(\omega)} + R_0 \\ \varphi(\omega) &= \text{arctg} \left( \frac{\text{Im} Z(\omega)}{\text{Re} Z(\omega)} \right) \end{aligned}$$

to be calculated from equations (3) and (4) are also calculated with the resulting values for  $R_0$ ,  $R_1$ ,  $R$ ,  $C_1$  and  $C_2$  and recorded together with the measured values. The computer diagrams for an untempered and an air-oxidized Raney  $\text{NiTi}_2$  electrode tempered for 17.5 minutes are plotted in the figures 61 and 62 together with the measured values, representative for all measurements carried out. The diagrams show good to very good agreement with the experimental data both for the real and imaginary portion and for the amount of impedance and phase angle as a function of frequency. This agreement demonstrates that the simplifications undertaken in approximations were permissible and do not signify any decisive falsification in the evaluations.

#### 6.5. Effect of Tempering Time on the Network Parameters of Raney $\text{NiTi}_2$ Electrodes

/132

The impedance measurements were carried out with a series of samples of the air-oxidized catalyst with a  $\text{Ni}(\text{OH})_2$  content tempered for 2.5 to 17.5 minutes, and the network parameters were determined in the indicated manner. The alterations in the individual parameters are demonstrated in Figs. 63 and 64. The effect of tempering time on passage resistance  $R_d$  is most noticeable. This rises rapidly with increasing tempering time, achieving the five-fold value at a tempering time of 17.5 minutes



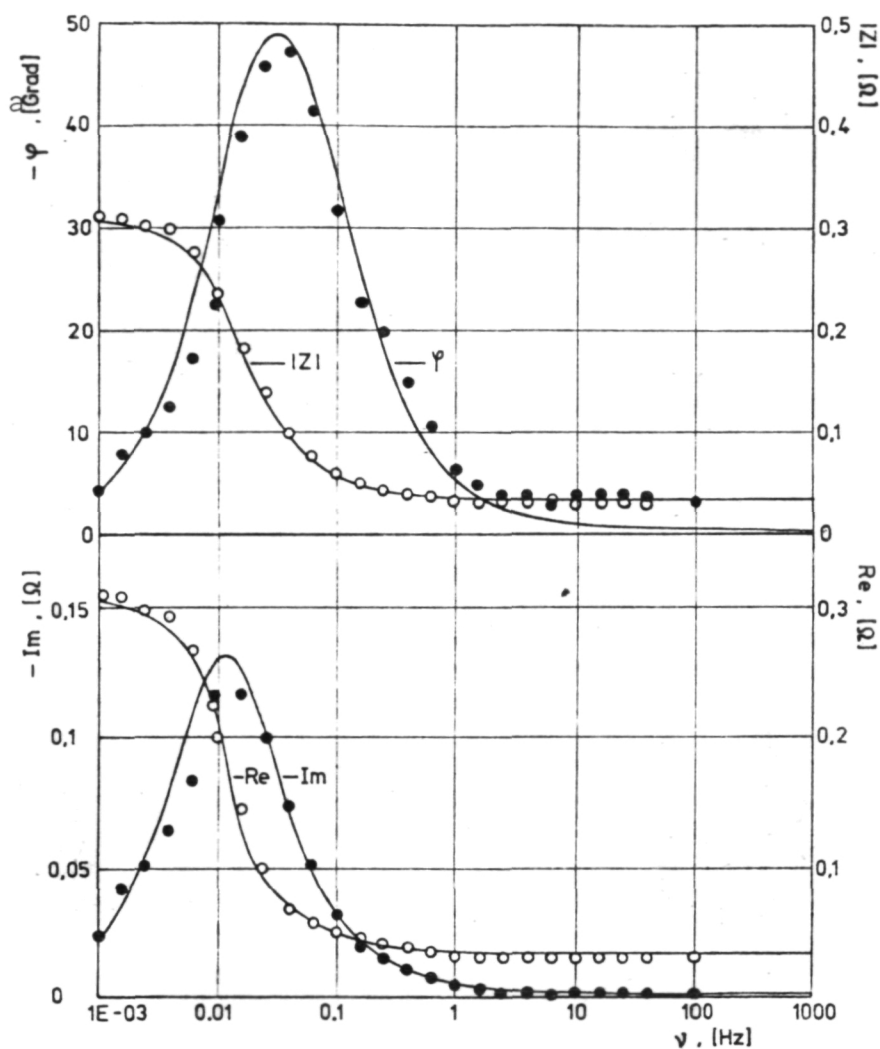


Fig. 61: Comparison of the Measured Values for the Amount of Impedance and Phase Angle (top) as well as Imaginary and Real Portions (bottom) with the Curves Calculated on a Theoretical Basis for an Electrode of 10 mg/cm<sup>2</sup> Untempered Raney NiTi<sub>2</sub>.

Key: a. degree

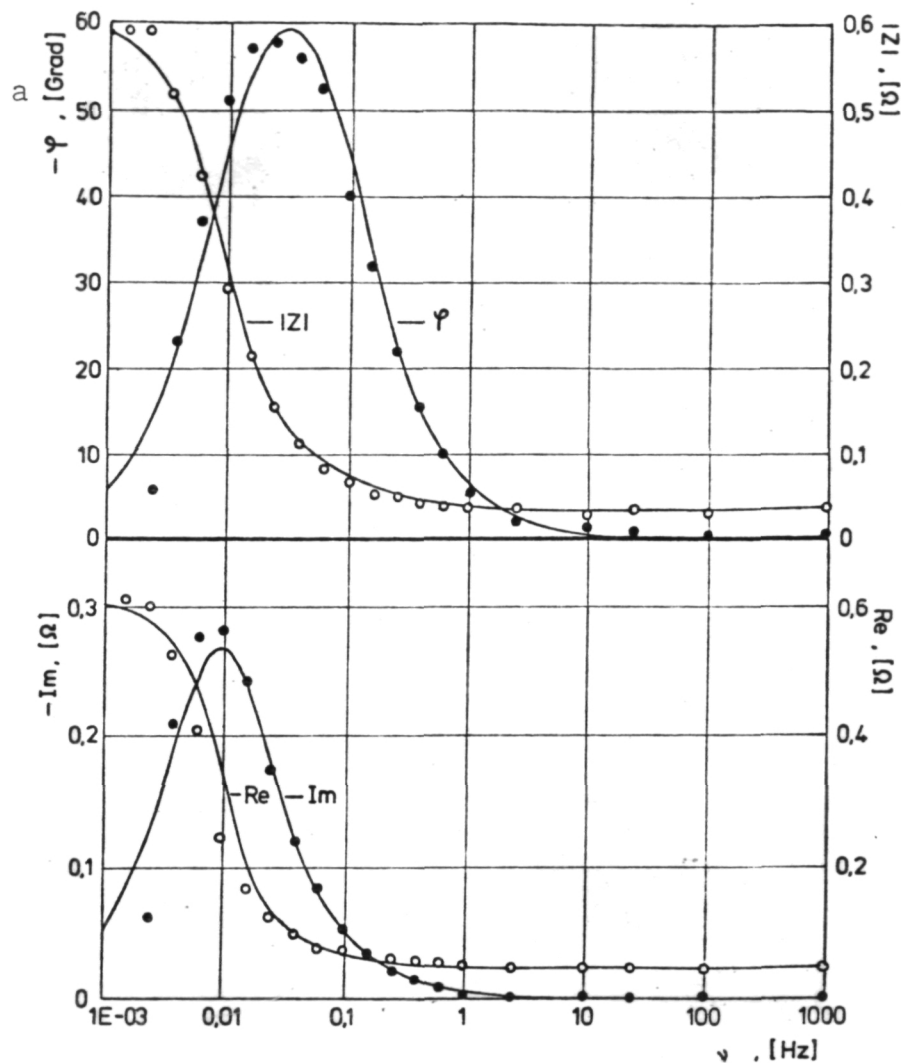


Fig. 62: Comparison of the Measured Values for the Amount of Impedance and Phase Angle (top) as well as Imaginary and Real Portions (bottom) with the Curves Calculated on a Theoretical Basis for an Electrode of 10 mg/cm<sup>2</sup> Raney NiTi<sub>2</sub> Tempered for 17.5 Minutes.

Key: a. degree

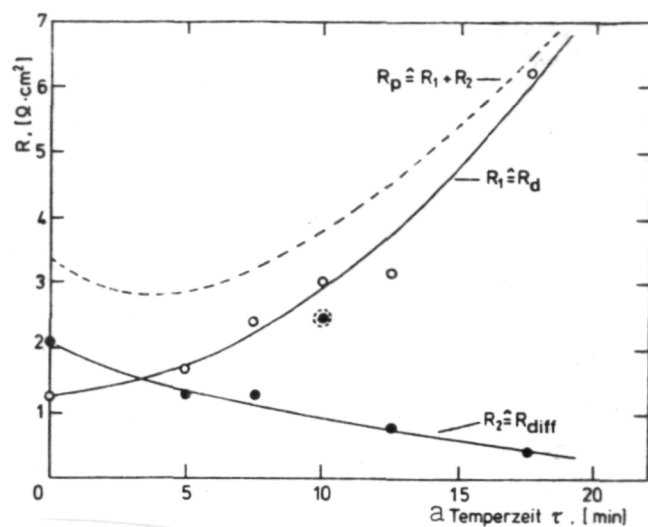


Fig. 63: Relationship of the Passage Resistance  $R_d$ , the Diffusion Resistance  $R_{\text{diff}}$  and the Polarization Resistance  $R_p$  as a Function of Tempering Time of Raney NiTi<sub>2</sub> Catalysts.

Key: a. tempering time

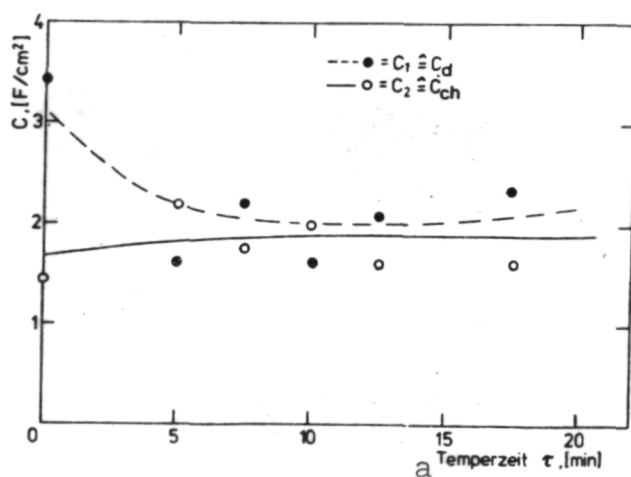


Fig. 64: Chemical Adsorption Capacity and Double-Layer Capacity as a Function of Tempering Time for Raney NiTi<sub>2</sub> Catalysts.

Key: a. tempering time

compared to the untempered material with a further increasing tendency. In contrast, the diffusion resistance  $R_{diff}$  exhibits the reverse behavior, as the diffusion resistance decreases monotonously with increasing tempering time to about 20 % of the initial value of the untempered material. The addition of  $R_d$  and  $R_{diff}$  represents the polarization resistance for direct-current loads. This course is drawn as the upper curve in Fig. 63. A minimum in polarization resistance results at a tempering time of about 4 minutes, with a clear rise in  $R_t$  after 6 minutes of tempering. This course agrees well qualitatively with the results obtained in section 3.2. from the stationary  $\eta$ - $i$  characteristics. A maximum in current density was also exhibited there at a tempering time of about 5 minutes with constant polarization corresponding to a minimum in the polarization resistance.

In contrast to the resistances  $R_1$  and  $R_2$ , no such clear dependency on tempering time was determined in both capacities. The chemical adsorption capacity  $C_{ch}$  is almost independent of tempering time at values between 1.5 and 2.1 F/cm<sup>2</sup>. Only for the double-layer capacity  $C_d$  was it possible to assume a course as indicated in Fig. 62 with a rapid drop in the double-layer capacity of about 3.5 F/cm<sup>2</sup> in the case of the untempered material to about 2.2 F/cm<sup>2</sup> with a tempering time of 5 minutes and, subsequently, a range of constancy up to tempering times around 17.5 minutes. However, the individual values for the double-layer capacity are scattered rather markedly such that this course shown as a dotted line in Fig. 62 may not apply with unconditional certainty.

/134

## 6.6. Discussion

The results of the impedance measurements demonstrate convincingly that it is possible to draw conclusions about the individual reactions occurring at the triple-phase boundary exclusively from the quantities accessible to the measurement, amount of impedance and phase angle, of a gas diffusion electrode under an alternating current load and to determine the quantities characterizing the individual reaction steps quantitatively. It was possible to demonstrate that the indicated equivalent circuit diagram prepared from these quantities for the porous electrode is a good approximation of the electrochemical processes of hydrogen oxidation with Raney NiTi<sub>2</sub> electrodes.

The center of attention in the impedance measurements, however, was situated in the studies on the effect of tempering time on the network parameters. In this case, it was demonstrated that the subsequent treatment of the catalysts at 350° C in a hydrogen flow produces a clear increase in the passage resistance. This may be explained in agreement with the measurements of the stationary  $\eta$ - $i$  characteristics and exchange current density with the reduction in the catalytically active  $\alpha$ -Ni(OH)<sub>2</sub> surface covering as a consequence of tempering.

Parallel to this process, a monotonous decrease in diffusion resistance was observed with increasing tempering time. This behavior may also be explained by earlier studies on the reduction of the nickel hydroxide preventing surface diffusion.

/135

The sum of diffusion and passage resistance represents the total polarization resistance of the electrode under a direct current load. With short tempering times, mainly the diffusion resistance determines the amount of polarization resistance corresponding to a higher proportion of diffusion polarization in the total polarization  $\eta$ . After long tempering times, in contrast, the passage resistance dominates, i.e. the passage polarization, while diffusion inhibition may be considered small in comparison.

Although the impedance measurements do not supply any such clear results from the scattering of measured values with respect to chemical adsorption and double-layer capacity as a function of tempering time, they still provide a good survey, on the whole, on the effect of tempering in a hydrogen flow on the electrode kinetics of Raney NiTi<sub>2</sub> catalysts. Furthermore, the results of the previous studies, such as effect of tempering time on exchange current density, on  $\eta$ -i characteristics and on the surface oxide covering are confirmed. Certainly the impedance measurements together with the studies carried out up to now such as BET measurements, electron grid microscope exposures, spectral photometrical and electrochemical studies have made it possible to gain especially good information on the reaction mechanisms of catalysts optimally suited for hydrogen oxidation and their production.

## 7. Summary

/136

It is known from earlier works that controlled air oxidation of Raney NiTi<sub>2</sub> catalysts may cause a considerable increase in catalytic activity, but this disappears again with extended operating time of the electrodes in galvanostatic continuous tests. Therefore, the object of the present report is to examine, on the one hand, the extent to which the surface oxides produced in air oxidation, especially nickel hydroxide, effect the considerable increase in activity of the catalyst and, on the other hand, to prepare a procedure for stabilizing the products of oxidation increasing the activity, thereby contributing to an increase in the life-span of Raney NiTi<sub>2</sub> catalysts.

In order to answer these questions, first the procedure of controlled air oxidation of Raney nickel catalysts is subjected to a precise examination. The special center of attention in this case is the quantitative analysis of nickel hydroxide. Accompanying x-ray studies show that only the  $\alpha$  modification of the nickel hydroxide  $\alpha$ -3Ni(OH)<sub>2</sub> · 2 H<sub>2</sub>O occurs in the air oxidation in addition to the NiO. Furthermore, measurements according to the principle of the differential-thermal analysis (DTA) show that  $\alpha$ -3Ni(OH)<sub>2</sub> · 2 H<sub>2</sub>O is almost completely decomposed

into NiO and H<sub>2</sub>O at temperatures above approximately 160° C with simultaneous release of the water of crystallization. The precise content of  $\alpha$ -Ni(OH)<sub>2</sub> of the air-oxidized catalyst samples may be determined on the basis of these results with the aid of thermal gravimetical and spectral photometrical measurements. The Ni(OH)<sub>2</sub> content of the catalysts employed for further studies varies between 2.9 and 17 percent by weight.

The measurements of the electrochemical properties of the Raney NiTi<sub>2</sub> catalysts show a considerable effect of the Ni(OH)<sub>2</sub> content. For example, the current density with constant polarization exhibits a clear maximum at a Ni(OH)<sub>2</sub> content of 5 - 6 percent by weight and is greater by the factor of 3 - 4 in this range than in non-air-oxidized samples or catalysts with a high Ni(OH)<sub>2</sub> content (< 10 percent by weight). The exchange current densities also increase greatly up to portions of Ni(OH)<sub>2</sub> around 5 %, but then remain almost constant with higher Ni(OH)<sub>2</sub> values.

/137

It can be concluded that the Ni(OH)<sub>2</sub> leads to a clear improvement in the passage reaction, but on the other hand, an excessive increase in hydroxide increasingly prevents surface diffusion of the hydrogen atoms to the location of reaction. A marked activity maximum is produced at 5 - 6 percent by weight of  $\alpha$ -Ni(OH)<sub>2</sub> by overlapping of both effects.

In a further section, preservation of Raney NiTi<sub>2</sub> catalysts through air oxidation is studied with subsequent stabilization in a hydrogen flow at 300° C. In this case, it was determined that tempering for about 5 minutes in a hydrogen flow increases the activity of the catalysts. Structural studies with the aid of the electron grid microscope and the BET area determination as well as determination of the Ni(OH)<sub>2</sub> content produced an exponential relationship of the  $\alpha$ -3Ni(OH)<sub>2</sub> · 2 H<sub>2</sub>O content and tempering time with an almost constant final value of about 3 percent by weight with very long tempering times.

Furthermore, the structural studies show that recrystallization processes occur in the surface oxides during tempering, having a positive effect on long-term stability of the catalytically active surface oxides. In order to test the stabilizing effect of tempering on the catalysts in an experiment, galvanostatic long-term tests are carried out with the air-oxidized, tempered samples. Tempering of 5 minutes in a hydrogen flow produces a reduction in aging rate in all examined Raney NiTi<sub>2</sub> catalysts with Ni(OH)<sub>2</sub> contents of about 3 to 17 %, while the best values of less than 15  $\mu$  V/h for a constant current load of 4 A/g are situated at an operating temperature of 80° C. On the whole, tempering in a hydrogen flow at 350° C proves a very good procedure for increasing the life-span and activity of Raney NiTi<sub>2</sub> catalysts.

/138

Finally, the results of the long-term tests give reason to introduce the concept of a "critical polarization," up to which the aging rate of the catalysts is relatively slight, but increases rapidly at higher polarization values. It may be

deduced from this fact and from previous results that optimal electrodes may be obtained for hydrogen oxidation when an air-oxidized Raney NiTi<sub>2</sub> catalysts is employed with a  $\alpha$ -Ni(OH)<sub>2</sub> content of 4 - 6 percent by weight, tempered in a hydrogen flow for about 5 minutes, and the catalyst occupation of the electrodes is such that the polarization at nominal load of the electrode does not exceed the critical value of 50 mV.

Since the surface oxides of nickel are partially reduced in the subsequent treatment in the hydrogen flow, this treatment requires a subsequent, repeated, controlled air oxidation, making the procedure relatively complicated. In order to simplify the process, therefore, an attempt is made to carry out tempering in a nitrogen atmosphere such that no reduction of nickel oxides may occur. The results with these nitrogen-tempered catalysts, however, show neither an increase in activity nor an improvement in long-term stability, leading to the conclusion that this procedure is inferior to hydrogen tempering, i.e. unusable.

/139

In a concluding section, alternating current measurements are carried out with porous Raney NiTi<sub>2</sub> electrodes. The theoretical observations on impedance measurements, preceding the studies, lead to the derivation of a formula for the local curve representation with the aid of an equivalent circuit diagram valid for Raney NiTi<sub>2</sub> electrodes, corresponding very well to the experimentally determined values in the informative frequency range of interest ( $10^{-3}$  to  $10^{-1}$  Hz). A procedure for evaluating the impedance spectra is given and a comparison of the theoretical with the measured impedance curves is carried out. This comparison produces a good agreement of measured and calculated, i.e. adjusted impedance curves, indicating the reliability of the quantities obtained for the passage and diffusion resistance as well as double-layer and chemical adsorption capacity.

Finally, the network parameters of the indicated equivalent circuit diagram is studied with respect to the effect of tempering in the hydrogen flow. A large increase in passage resistance and a clear decrease in diffusion resistance results with tempering time. A similar effect on chemical adsorption and double-layer capacity is not observed.

The alterations of passage resistance and diffusion resistance as a function of tempering time may be carried out in agreement with the structural studies on the reduction in the  $\alpha$ -Ni(OH)<sub>2</sub> content.

/140

It remains to be stated that the study undertaken here on a procedure for stabilizing preserved Raney NiTi<sub>2</sub> electrodes has led to a considerable increase in activity and especially to a respectable extension in life-span of the catalysts and, therefore, has supplied a further contribution for increasing the financial feasibility of H<sub>2</sub>-O<sub>2</sub> fuel cells.

## REFERENCES

- [1] Justi, E., Leitungsmechanismus und Energieumwandlung in Festkörpern [Mechanism of Conduction and Conversion of Energy in Solids], Vandenhoeck & Ruprecht, Göttingen, 1965, pp. 432-455.
- [2] Lindström, O., ASEA Journ. 37, no. 1 (1964).
- [3] BMFT (ed.), Study on "The Path to New Energy Systems," Part 3, Bonn, 1975.
- [4] Bockris, J. O'M., Energy - The Solar-Hydrogen Alternative, The Architectural Press, London, 1976.
- [5] Veziroglu, T.N. and W. Seifritz (ed.), Proceedings of the 2nd World Hydrogen Energy Conference, Zurich, Vol. 1 - 4, 1978.
- [6] Bockris, J.O'M. and E. Justi, Wasserstoff-Energie für alle Zeiten [Hydrogen Energy for all Times], Udo Pfriemer Verlag, Munich, 1980.
- [7] Justi, E., W. Scheibe and A. Winsel, DBP 1 019 361, 1954.
- [8] Wendtland, R., Brennstoff-Chemie 50, no. 2 (1969), p. 34.
- [9] v. Sturm, F. H. Cnoblock, H. Nischik and M. Marchetto, Abh. Sächs. Akad. Wiss. Leipzig 49, 169 (1967).
- [10] Jung, M. and H.v. Döhren, Metalloberfläche 25, no. 2, 42 (1971).
- [11] Pzhenichnikov, H, R. Burshtein, D. Lainer, N. Kagan, G. Melikova and F. Sabirov, USSR Patent 147616, 1961.
- [12] Richter, G., Third Intern. Symp. of Fuel Cells, Brussel, 1969.
- [13] Ewe, H., E. Justi and K. Stephan, Energy Conv. 13, 109 (1973).
- [14] Mund, K., G. Richter and F. v. Sturm, Electrochem. Soc. 124, no. 1 (1977).
- [15] Schmitt, A., Dissertation, Technical University in Braunschweig, 1973.
- [16] Gross, W., DWP 3718, 1953.
- [17] Kefeli, L.M. and S.L. Leltschuk, Berlin Akad. Wiss, USSR 83, 697 (1953).



- [18] Jung, M and H.v. Döhren, DBP 1 185 582, 1962.
- [19] Stölzel, Th. and H.J. Seifert, DWP 42, 101, 1964.
- [20] Douzek, F.B., SERAI Conference, Brussels, 1965.
- [21] Wendtland, R., "Preservation of Raney Nickel Catalysts for Fuel Cells," Technical Report, Varta Research and Development Center, Kelkheim, 1968.
- [22] Cairns, R.W. and E. Ott, J. Am. chem. Soc. 55, 527 (1933).
- [23] Bode, H., K. Demelt and J. Witte, Electrochim. Acta 11, 1079 (1966).
- [24] Heuer, J., Thesis for Diploma, Technical University in Braunschweig, 1970.
- [25] Dennstedt, W. and W. Löser, Electrochim. Acta 16, 429 (1971).
- [26] Kortüm, G., Lehrbuch der Elektrochemie [Textbook for Electrochemistry], Verlag Chemie GmbH, Weinheim/Bergstrasse, 1970.
- [27] Sturm, F.v., E. Weidlich and H. Nischik, Ingenieur Digest, 5, 52 (1966).
- [28] Selbach, H.-J., Thesis for Diploma, Technical University in Braunschweig, 1974.
- [29] Heuer, J. E. Justi and A. Kalberlah, Energy Conversion 13, 25-28 (1973).
- [30] Breiter, M.W., J. Phys. Chem. 68, 2249 (1964).
- [31] Sturm, F.V. and G. Richter, Electrochim. Acta 10, 1169 (1965).
- [32] Ewe, H., Dissertation, Technical University in Braunschweig, 1970.
- [33] Gerischer, H. and K. Staubach, Z. Elektrochemie 61, 789 (1957).
- [34] Ewe, H., Electrochim. Acta 17, 2267 (1972).
- [35] Shumilova, N. and V. Bagotzky, Electrochim. Acta 13, 285 (1968).
- [36] Ewe, H., E. Justi, A. Schmitt and H. Willgeroth, Batelle Information 11, 41 (1971).
- [37] Mund, K., 23rd Meeting of ISE, Stockholm, 1972.

- [38] Ewe, H., Paper presented for Professorial Chair, Technical University in Braunschweig, 1974.
- [39] D'Ans, J. and E. Lax, Taschenbuch für Chem. u. Phys. [Pocketbook for Chemistry and Physics], Springer Publishing House, 1949.
- [40] Gregg, S. and K. King, Adsorption, Surface Area and Porosity, Academic Press, London, 1967.
- [41] Brunauer, S., P.H. Emmet and E. Teller, Journal of the American Chemical Society 60, no. 2, 309-319 (1938).
- [42] Orr, C., Chem.-Ing.-Techn. 48, no. 8, 680-689 (1976).
- [43] McCleallen, A.C. and H.F. Harnsberg, Journal of Colloid and Interface Science 23, 577-599 (1967).
- [44] Ewe, H., E. Justi, W. Kalberlah and A. Schmitt, Energy Conv. 12, 1-8 (1972).
- [45] Ewe, H., E. Justi and A. Schmitt, Energy Conv. 14, 35-41 (1975).
- [46] Halsey, C.D., Journal of Chemical Physics 16, no. 10, 931-937 (1948).
- [47] Thomson, W.T., Philosophical Magazine 42, no. 282, 448-452 (1871)
- [48] Broekhoff, J.C.P. and B.G. Linsen, Physical and Chemical Aspects of Adsorbents and Catalysts, Academic Press, London/New York, 1-62, 1970.
- [49] de Boer, J. et al., Journal of Colloid Interface Sci. 21, 405 (1966).
- [50] de Boer, J., Colst. Research Soc., Proc. of the Symp. 10, 68 (1968).
- [51] Schröder, H.R., Dissertation, Technical University in Braunschweig, 1974.
- [52] Wien, M., Wied. Ann. 58, 27 (1896).
- [53] Warburg, E., Wied. Ann. 67 493 (1899).
- [54] Gerischer, H. and K.H. Vetter, Z. physik. Chem. 197, 92 (1951).
- [55] Euler, K.J., Electrochim. Acta, 17, 619-634 (1972).
- [56] Mund, K., Research report T 80 - 057, BMFT, Part 4, 1980.
- [57] Epelboin, I. and M. Keddam, J. electrochem. Soc. 117, 1052 (1970).

- [58] Mund, K., Siemens Forsch. u. Entwickl. - Report 4, no. 2, 68 (1975).
- [59] Müller, N., Dissertation, Erlangen-Nuremberg, 1980.
- [60] Göhr, H., Ber. Bunsenges. Phys. Chem. 85, 274-280 (1980).
- [61] Wabner, D.W., Dissertation, Munich, 1971.
- [62] Young, L., Trans. Faraday Soc. 51, 1250 (1955).
- [63] Göhr, H. and W. Meissner, Z. Phys. Chem. 93, 217 (1974).
- [64] Kramers, H.A., Phys. Z. 30, 522 (1929).
- [65] de L. Kronig, R., J. opt. Soc. Am. 12, 547 (1926).
- [66] Von Meirhaege, R.L., E.C. Dutoit, F. Cardon, W.P. Gomes, Electrochim. Acta 20, 995 - 999 (1975).
- [67] Grofov, B.M. and E. Pekar, Elektrokhimiyz 6, 547 (1970).
- [68] Zurmühl, R. Praktische Mathematik [Practical Mathematics], Springer Publishing House, 1957.
- [69] Bronstein, L.N. and K.A. Semendjajew, Taschenbuch der Mathematik [Pocketbook of Mathematics], H. Deutsch Publishers, Zurich/Frankfurt, 1969.
- [70] Römpp, H., Chemie Lexikon, [Encyclopedia of Chemistry], Franks'sche Publishing House, Stuttgart, 1966.